UNIVERSITÀ DEGLI STUDI DI PADOVA
DIPARTIMENTO DI INGEGNERIA INDUSTRIALE
Department Of Industrial Engineering

Corso di Laurea Magistrale in Ingegneria Energetica

TESI DI LAUREA

Design and specification for the construction of the cryogenic, electrical, and cooling penetrations for the DTT vacuum vessel

Relatore:
Prof. Sonato Piergiorgio

Laureando: Patrick Fanchin
Matricola: 2005716

Correlatore:
Dr. Ing. Mauro Dalla Palma

ANNO ACCADEMICO 2022-2023

Abstract

DTT is one of the largest superconducting Tokamak under construction with the mission to get scientific and technological proofs of power exhaust in prospect of the first nuclear fusion power plant [1, 2].
The 5.5MA maximum plasma current, 6T toroidal magnetic field at the plasma center, and 2.19m plasma radius make DTT a flexible and compact facility for testing D-shaped plasmas with different configurations of heat load spreading.
The mechanical systems of DTT are designed and integrated analysing interfaces consistently with machine operating states including plasma operation, disruptions, baking, possible seismic events, testing, and maintenance.
Multi-purpose ports are designed for the DTT vacuum vessel to house in each port a combination of more than one of the following three types of systems:
• diagnostics probing the plasma;
• auxiliary plasma heating systems (ECRH, ICRH, neutral beam injection with shielding plates in the port duct);
• services (divertor and first wall cooling tubes, vacuum pumping including cryolines, in-vessel coil feeders, cables for sensors embedded into the in-vessel components).
In particular, the use of multi-purpose ports introduces the need to integrate one port bellows (compensating relative displacements between the vacuum vessel and the cryostat) and more service bellows (compensating relative displacements between the services and the cryostat) in the same port.
The allocation of services, diagnostics, and auxiliary plasma heating systems is defined, but the design of supports and displacement compensation systems has to be developed.
Interfaces between the vessel ports and in-port systems have been analysed in order to address the structural integrity verification and the heat transfer analysis in particular during baking and plasma operation.
The design parameters resulting from this analysis and verification activity will be used to prepare suitable technical specifications for the procurement of the vacuum vessel and the cryostat of DTT.
The analysis has been carried out with *Ansys Workbench*, a commercial software that can be used for finite element method (FEM) analysis.
To the standard scenario (Plasma operation, baking, cryopump regeneration), the effect of two possible incident have been superimposed: the earthquake and the ingress of liquid inside the vacuum vessel.
It will be shown that important displacements might happen, in particular during baking/cryopump regeneration, and even more in the case of seismic event
The most solicited components are the water pipe (displacements up to 25.8mm from the original position) and the cryopump pipes (axial displacements up to 9.3mm).
However, further developments are needed, for example on the expansion loops: the stresses suffered by these pipes are too high for the selected material (stainless steel AISI316L), and so a review on their design is required.

Riassunto

DTT è uno dei più grandi Tokamak superconduttivi in costruzione e ha il compito di ottenere dati e prove scientifiche e tecnologiche sul rilascio di potenza termica in vista del funzionamento della prima centrale a fusione nucleare.
La massima corrente di plasma da 5.5MA, il campo magnetico toroidale da 6T al centro del plasma e il raggio del plasma di 2.19m rendono DTT una macchina flessibile e compatta per testare il plasma a forma di "D" con diverse configurazioni della distribuzione del carico termico.
I sistemi meccanici di DTT sono progettati e integrati analizzando le interfacce coerentemente con gli scenari operativi della macchina, che includono l'operazione con plasma, le disruzioni del plasma, il baking, gli eventuali eventi sismici, le fasi di test e le manutenzioni.
Sono state progettate diverse penetrazioni (port) per la camera a vuoto di DTT e ogni port ospita una combinazione di più di uno dei seguenti tre tipi di sistemi:
• sistemi di diagnostica del plasma;
• sistemi ausiliari per il riscaldamento del plasma (ECRH, ICRH, iniettore di neutri con pannelli schermanti alla parete del port);
• servizi (tubi di raffreddamento per divertore e prima parete, sistemi di pompaggio da vuoto compresi i tubi della criopompa, cavi d'alimentazione delle bobine all'interno della camera a vuoto, cavi per i sensori incorporati nei componenti all'interno della camera a vuoto).
In particolare, l'utilizzo di questi port multiuso introduce l'esigenza di integrare dei soffietti (per compensare gli spostamenti relativi tra servizi e criostato) al port stesso.
L'allocazione dei servizi, dei sistemi diagnostici e dei sistemi di riscaldamento ausiliario del plasma è definita, ma vanno realizzati i progetti dei supporti e dei sistemi di compensazione degli spostamenti.
Sono state analizzate le interfacce tra il port e i sistemi all'interno del port in modo da verificare l'integrità strutturale e gli scambi termici, in particolare durante il baking e l'operazione con plasma.
I parametri di progetto risultanti dall'analisi e dalle verifiche saranno usati per preparare delle specifiche tecniche per le forniture della camera a vuoto e del criostato di DTT.
L'analisi è stata realizzata utilizzando *Ansys Workbench*, un software commerciale utilizzabile per analisi con il metodo degli elementi finiti (FEM).
Agli scenari standard (operazione con plasma, baking, rigenerazione delle criopompe) sono stati sovrapposti gli effetti di due possibili eventi incidentali: il terremoto e l'ingresso di liquido all'interno della camera a vuoto.
Si mostrerà che possono avvenire deformazioni importanti, in particolare durante il baking/rigenerazione delle criopompe, e ancor di più in caso di eventi sismici.
I componenti più sollecitati sono il tubo dell'acqua (spostamenti fino a 25.8mm dalla posizione iniziale) e i tubi della criopompa (spostamenti assiali fino a 9.3mm).
Saranno comunque necessari altri sviluppi, per esempio proprio in questi percorsi di espansione: gli stress subiti da questi tubi sono troppo alti per il materiale selezionato (acciaio inox AISI316L), e dunque è richiesta una revisione nel loro disegno.

Contents

Chapter 1

Fusion energy

1.1 Introduction

In the last few years, the energy demand and the climate change have become two of the most urgent and severe problems for the society.
As the population keeps growing, having exceeded 8 billion people around the world, and as the technological progress spreads, the energy demand and the emissions of pollutants keep on growing too.
Moreover, the COVID-19 pandemic and the Ukrainian crisis have put even more on the spotlight the energetic problem. In particular, the Russian invasion in Ukraine had great impacts in the relationships between countries in Europe and in the world, as Russia was one of the largest natural gas exporting countries globally.
Otheri crises occurred in the past and all these situations underlined even more the needs to realise inexhaustible and accessible technologies to produce energy.
As about 40% of the CO_2 emissions come from the electricity and heat sector, a transition towards a zero-emission sector is likeable, if not necessary.
Recently, OECD countries have put lot of effort on the production of energy from renewable sources, such as solar photovoltaic and thermal, wind, hydroelectric and others.
Anyway, solar and wind energy production have shown some limitations that prevents them from being the only contribution in the future global energy mix. Hydroelectricity, on the other hand, can provide an important base load power production, but most of the sites for the production have been exploited, and so there isn't much room for a great increase in the energy production from this source.
That's why there is the need to find other valid options for the energy production without relevant emissions. In this sense, nuclear has always been a topic of great interest.
Many fission based power plants are in operation around the world, but they are still controversial for the population due to the risk of serious accidents and the problem of long-term radioactive waste.
Fusion based power plants could theoretically represent a real breakthrough in the future scenarios, as they would be able to generate a large amount of power to supply the base load demand with complete reliability and without the emission of greenhouse gases. There would still be some radioactive waste, but they would be much easier to handle since their life-time range would be in the order of 100 years.
However, nuclear fusion branch is still in research stage, and many years will be necessary before we can see commercial power plants producing electricity to the grid; this is due to the high technological complexity of the operation.
The feasibility of the production of a net amount of energy (producing more energy than the total amount of energy requested for the operation) will be investigated in ITER, an international project currently in construction in the south of France.
DEMO will be the successor project of ITER: it will aim to prove the commercial

feasibility of the energy production from fusion reactions.
The DTT (Divertor Tokamak Test) project fits into the program of *EUROfusion*; it will carry out scale experiments to find alternative for the divertor, so that it will suit as much as possible the foreseen conditions and solutions in DEMO.

1.2 Energy Outlook

World Energy Outlook is a very complete paper compiled by the International Energy Agency (IEA) which gives us any kind of information related to energy. It contains several data about production, consumption, emissions and much more.
Furthermore, IEA provides scenarios for the future, in order to evaluate the effects of some possible actions and interventions undertaken by the governments: with these information, it is possible to understand what is the roadmap to achieve a certain goal in the future, for example the limitation of the increase of the global temperature.
In the World Energy Outlook 2022, IEA introduces three different scenarios, explaining how and why they differ from each other, setting out the macroeconomic and demographic assumptions that underpin them as well as the outlook for energy and carbon prices and energy technology development. The three scenarios are:

- **Stated Policies Scenario (STEPS)**, which maps out a trajectory that reflects current policy settings, based on a detailed sector-by-sector assessment of what policies are actually in place or are under development by governments around the world.

- **Announced Pledges Scenario (APS)**, which assumes that all long-term emissions and energy access targets, including net zero commitments, will be met on time and in full, even where policies are not yet in place to deliver them.

- **Net Zero Emissions by 2050 (NZE) Scenario**, which sets out a pathway for the global energy sector to achieve net zero CO2 emissions by 2050, updating the landmark IEA analysis first published in 2021. While the first two scenarios are exploratory, the NZE Scenario is normative, as it is designed to achieve the stated objective and shows a pathway to that goal.

Electricity accounts for about 20% of the world's total final consumption of energy, but its share of energy services is higher due to its efficiency. It is central to many aspects of daily life and becomes more so as electricity spreads to new end-uses, such as electric vehicles and heat pumps. The electricity sector accounted for 59% of all the coal used globally in 2021, together with 34% of natural gas, 4% of oil, 52% of all renewables and nearly 100% of nuclear power. It also accounted for over one-third of all energy-related CO2 emissions in 2021.
Global electricity demand increases significantly in all the three scenarios by 2050. It rises from 24 700 terawatt-hours (TWh) in 2021 by about 80% in the STEPS, by 120% in the APS and by 150% in the NZE Scenario.
Renewable energy technologies currently provide close to 30% of electricity generation and are set for rapid growth in all scenarios, led by solar photovoltaics (PV) and wind. While renewables now represent the cheapest source of new electricity in most markets,

the pace of their expansion depends on the retirement or reuse of existing sources of electricity generation as well as on new capacity, and therefore still rests largely in the hands of policy makers.

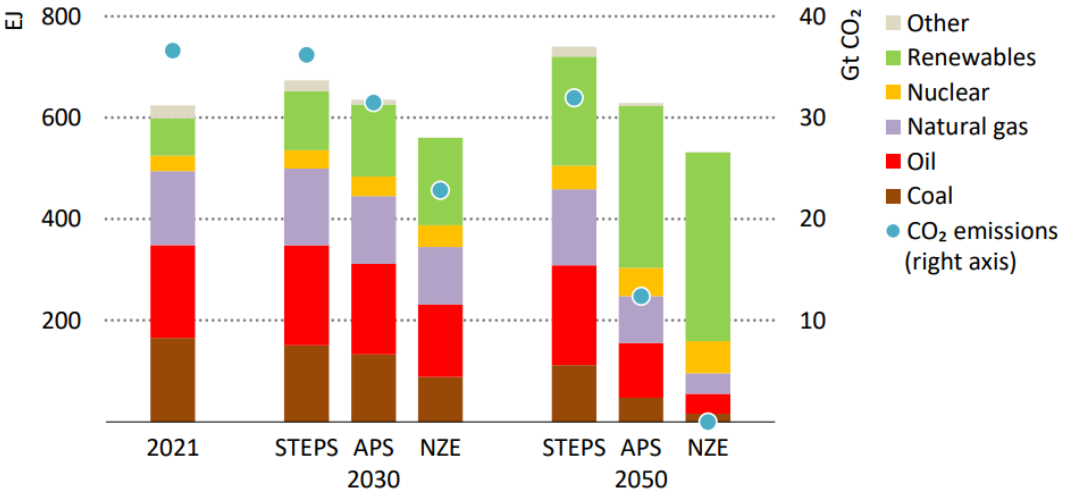

Figure 1.1. Total energy supply by fuel an CO_2 emission by scenario. Source: World Energy Outlook 2022 by IEA

The continued role of nuclear power in the electricity sector relies on decisions to extend the lifetime of existing reactors and the success of programmes to build new ones. In the STEPS, nuclear maintains its share of about 10% in total electricity generation. This requires the completion of 120 GW of new nuclear capacity over the 2022-30 period, as well as the addition of another 300 GW worth of new reactors (the equivalent of almost three-quarters of the current global fleet) between 2030 and 2050 in over 30 countries. In the APS, around 18 GW of new nuclear capacity is added per year over the outlook period, over a quarter more than in the STEPS, but the higher level of electricity demand in this scenario means that the nuclear share of the electricity supply mix remains at close to 10%. In the NZE Scenario, a wave of lifetime extensions in advanced economies in the 2020s helps limit global emissions, and an average of 24 GW of capacity added each year between 2022 and 2050 more than doubles nuclear power capacity by 2050. The nuclear share of the electricity mix, however, falls to 8% in 2050 due to very strong growth in electricity demand in the NZE Scenario.
However, as already mentioned, nuclear fission power plants are still controversial for many reasons, such as the following:

- These plants need radioactive "fuels" such as ^{238}U, ^{233}U, ^{239}Pu, which are pretty hard to obtain, they're not equally distributed around the world and they're not easy to handle.
- These plants produce radioactive waste which are difficult to manage and deposit. Some of these wastes have halving time of around 24000 years and they need to be stored for about 300000 years.
- The risk of accident is perceived as high by the population, as some past event (Fukushima in Japan, Chernobyl…) are still in the memories of global population.
- The availability of ^{235}U is not infinite.

That's why many countries are evaluating other alternatives to produce a large amount of energy for the base load supply.
If the process of dividing nuclei (fission) has some withdrawal as already mentioned, the inverse process, the fusion of nuclei (the process that takes place in the stars) can be the solution.

1.3 Nuclear Fusion

The basic concept of nuclear fusion is to collide two (or more) light nuclei (such as Helium, Deuterium, Tritium), to form a new nucleus with a mass lower than the total mass of the original nuclei. The difference of mass is turned into energy (in form of radiation and/or particle kinetic energy) according to the well-known Einstein's relationship:

$$E = \Delta \mathrm{m} * c^2 \tag{1.1}$$

The fusion reactions that are considered as solutions for future thermonuclear plants are the following:

$$\begin{aligned} D + T &\rightarrow {}^4He\ (3.56\ MeV) + n\ (14.1 MeV) \\ D + D &\rightarrow {}^3He\ (0.82\ MeV) + n\ (2.45 MeV) \\ D + D &\rightarrow T\ (1.01\ MeV) + p\ (3.02 MeV) \\ D + {}^3He &\rightarrow {}^4He (3.71\ MeV) + p\ (14.64\ MeV) \end{aligned} \tag{1.2}$$

To obtain a fusion reaction, two nuclei that have a natural tendency to repel each other, both being positively charged, must be brought close enough together. Therefore, a certain amount of energy is necessary to overcome this natural barrier and reach the zone close to the nucleus where nuclear forces are capable of overcoming the barrier. The probability of crossing this barrier may be quantified by the ''cross section'' of the reaction. The variation of the effective cross section of several fusion reactions as a function of interaction energy is provided for light elements in *Fig. 1.2*.

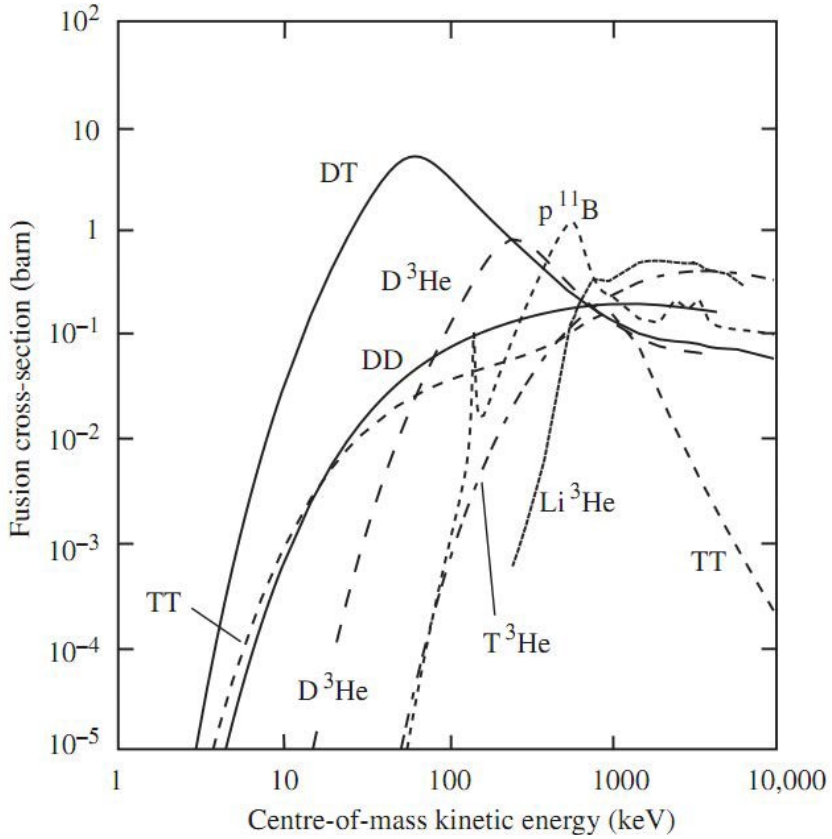

Figure 1.2: Cross section of many possible fusion reaction as function of the particle cross section. 1 barn = 10^{-28} m^2

Some considerations on these reactions can be made:

- The most desirable reaction would be the deuterium-deuterium one since this element is virtually infinite in nature. In facts, about 1 out of every 5000 hydrogen atoms in seawater are in the form of deuterium. This means our oceans contain a large amount of deuterium. In every cubic meter of seawater there are about 33 grams of deuterium.
- The deuterium-helium reaction is the most energetic one, realising 18.35 MeV per each reaction, and so it would require a lower amount of "fuel" to obtain the same amount of energy output.
- Despite these previous considerations, the deuterium-tritium reaction is the one that is considered suitable for the thermonuclear plants. This is due to the higher cross section at "lower" temperatures. For example, the D-D reaction would require a plasma temperature higher than 450-500 million Celsius, while the D-T reaction will require a plasma temperature above 100 million Celsius.

Tritium is a radioactive isotope that decays relatively quickly (it has a 12 years half-life), and so it is extremely rare in nature. This means that it must be produced appositely for the reaction (it is estimated that a 1 GW fusion reactor will require on the order of 100 to 200 kg of tritium per year).
Researchers are studying how to breed tritium in fusion reactors at the rate needed to make future power plants tritium self-sufficient.
In particular, exposing the element Lithium to energetic neutron can generate tritium,

according to the following:

$$^{6}Li + n \rightarrow He + T + 4.8\ MeV \quad (1.3)$$

In the deuterium-tritium (DT) fusion reaction, high energy neutrons are released along with helium atoms. These electrically-neutral particles escape the magnetic fields that confine the plasma and are absorbed by the blanket covering the surrounding walls.
If the blanket modules contain lithium, a reaction occurs: the incoming neutron is absorbed by the lithium atom, which recombines into an atom of tritium and an atom of helium. The tritium can then be removed from the blanket and recycled into the plasma as fuel.
Blankets containing lithium are referred to as breeding blankets. Through them, tritium can be bred indefinitely. Once the fusion reaction is established in a tokamak, deuterium and lithium are the external fuels required to sustain it, so the problem of the availability of tritium is replaced by the availability of lithium. Both of these fuels are readily available.

1.4 The challenge of thermonuclear power balance

The greatest challenge for future thermonuclear plants based on fusion regards the power balance between the useful power from the reactor and the power required by the reactions to be maintained.
Researchers are studying the conditions that permit to obtain a higher amount of energy than the amount of energy spent to maintain the reaction and to feed all the auxiliary systems.
To assess the energy balance at the reactor, a deeper knowledge in the physics of the reactions is required; the concept of cross section has already been exposed in the previous paragraph, but only in a "qualitative" way.
Let's assume, for simplicity, two spherical nuclei, N and M, with N moving at velocity v and M stationary.

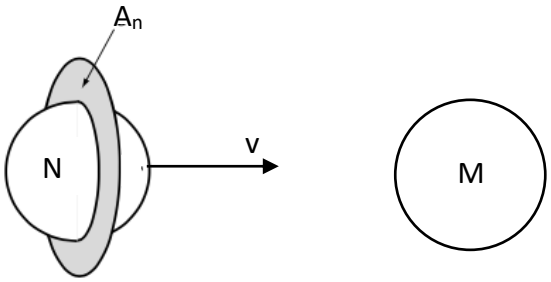

The cross section can be defined physically as follows:

$$\sigma = p_f p_t A_N \quad (1.4)$$

Where:
p_f is the probability that the reaction occurs once the incident particle N is in the energy well (inversely proportional to the kinetic energy);
p_t is the probability that the incident particle N overcomes the Coulomb barrier (0.4

MeV ford-T reactions);
A_N is the cross-sectional area of N as "seen" by the target particle M.
It is important to underline that σ:
-increases as much as the relative velocity between the two particles increases (p_t increases, high probability of tunnelling)
-decreases for high velocity v because of the limited time available for fusion reaction to occur (low p_f).
That's the reason why the cross-section curve for DT reactions in Fig.1.2 has that shape, with a maximum around 60 keV of kinetic energy.
Moving at velocity v, N covers a certain distance x and a volume:

$$V = A_N v \tag{1.5}$$

Considering, inside this volume, n_N moving particles at velocity v and n_M standing target particles, the reaction rate g (number of fusion reactions occurring in the volume in a unit of time) can be written as:

$$g = n_N n_M \sigma \tag{1.6}$$

In more generic terms, if n_1 and n_2 are the densities of two species (Deuterium and Tritium for example) and $v=|v_2-v_1|$ is the relative velocity, then:

$$g = n_1 n_2 < \sigma v > \tag{1.7}$$

Where $< \sigma v >$ is the product of the relative velocity and the cross-section averaged on the velocity distribution.

The thermonuclear power released per unit of volume is, indeed:

$$P_{th} = g Q_{th} \tag{1.8}$$

Where Q_{th} is the energy released by a single fusion reaction (in the case of D-T reaction Q_{th}=17.6 MeV as seen in *1.2*).

Considering the optimal ratio of deuterium and tritium densities (which is $n_1 = n_2 = \frac{n}{2}$), formula *1.7* can be written as:

$$g = \frac{n^2}{4} < \sigma v > \tag{1.9}$$

And finally:

$$P_{th} = g Q_{th} = \frac{n^2}{4} < \sigma v > Q_{th} \tag{1.10}$$

In a simplified way, it is possible to evaluate the power balance of a simplified reactor, with a 0-D model with sources and sinks.

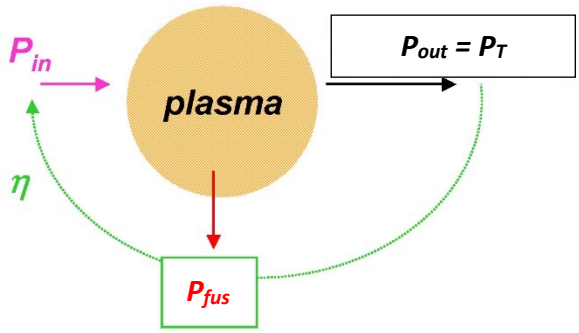

Figure 1.3. Schematic of the operation of a reactor. Source: https://it.wikipedia.org/

If plasma is in stable and in equilibrium, input and output power are balanced according:

$$P_{in} = P_{out} \tag{1.11}$$

It is possible to breakup these terms into various component, highlighting the role of different physical phenomenon, as follows:

$$P_{\alpha} + P_{n} + P_{ohm} + P_{add} = P_{n} + P_{rad} + P_{syn} + P_{con} \tag{1.12}$$

Where:
-P_{α} and P_{n} are the power associated with the alpha particle and neutrons respectively produced by the reactions;
-P_{ohm} is the power produced by the ohmic heating;
-P_{add} is the power added to the plasma with other sources;
-P_{rad} is the power lost through radiation, including the losses due to Bremsstrahlung radiation (emitted by electrons when they are accelerated), which are actually both negligible;
-P_{syn} is the power lost due to synchrotron radiation (negligible);
-P_{con} is the power lost due to imperfect plasma confinement, through convection and conduction over plasma boundary.
The power associated with neutrons P_n appears on both sides of the equation, because it is produced by the reaction, but, since neutrons are electrically neutral, they cannot be confined and so they escape from the plasma with their energy content.
Some terms can be grouped together:

$$P_{\alpha} + P_{n} = P_{fus} \tag{1.13}$$
$$P_{ohm} + P_{add} = P_{ext} \tag{1.14}$$
$$P_{syn} + P_{con} + P_{rad} = P_{T} = P_{\alpha} + P_{ext} \tag{1.15}$$

P_{fus} is analogue to P_{th} in 1.10, while P_t represents the power lost due to "transport" phenomenon and imperfect confinement, and it is evaluated in the synthetic form:

$$P_{T} = \frac{3\, n\, T\, V}{\tau_{E}} \tag{1.16}$$

Where τ_E is the confinement time of the energy (the characteristic time in which the system loses its energy) and the temperature T is expressed in [eV] and V is plasma volume.
An important factor to evaluate the sustainability of the reactions is the **energy gain factor**, defined as:

$$Q = \frac{P_{fus}}{P_{ext}} \tag{1.17}$$

This parameter allows to better understand how much energy can be produced by the reactions compared to the energy feed externally.
In particular, when:
Q=1 → The breakeven is reached: the power produced Is equal to the power consumed.
Q<1 → Power consumed is higher than the power produced.
Q>1 → Power produced is higher than the power consumed. When Q approaches values around 10, it is considered a proper situation to produce electricity to the grid.
Q→∞ → Reactor has reached the so called "ignition", meaning that the reaction is self-sustained with the energy produced by the reaction itself without the need for external power P_{ext}.
The record for Q has been chieved in 2021 by the National Ignition Facility in the US, with Q≈0.70.
ITER is planned to operate with Q=10, producing 500MW of fusion power from 50 MW of injected thermal power, while DEMO is planned to operate with Q=25, producing 2 GW of fusion power from 80 MW of injected thermal power.

External heating power is required to balance the power losses and prevent the plasma from cooling down:

$$P_{ext} = P_T - P_\alpha = \left(\frac{3\,n\,T}{\tau_E} - \frac{n^2}{4} < \sigma v > Q_\alpha\right) V \tag{1.18}$$

Where Q_α is the fraction of Q_{th} associated with the alpha particles (it does not include the energy associated with neutrons).
The condition for ignition to be achieved can be derived from this equation, since it happens, as already mentioned, when there is no need for external power (P_{ext}=0) and the power associated with the alpha particles is higher than the losses:

$$\frac{n^2}{4} < \sigma v > Q_\alpha \;\; > \;\; \frac{3\,n\,T}{\tau_E} \tag{1.19}$$

And so, finally:

$$n\,\tau_E \;\; > \;\; \frac{12\,T}{< \sigma v > Q_\alpha} \tag{1.20}$$

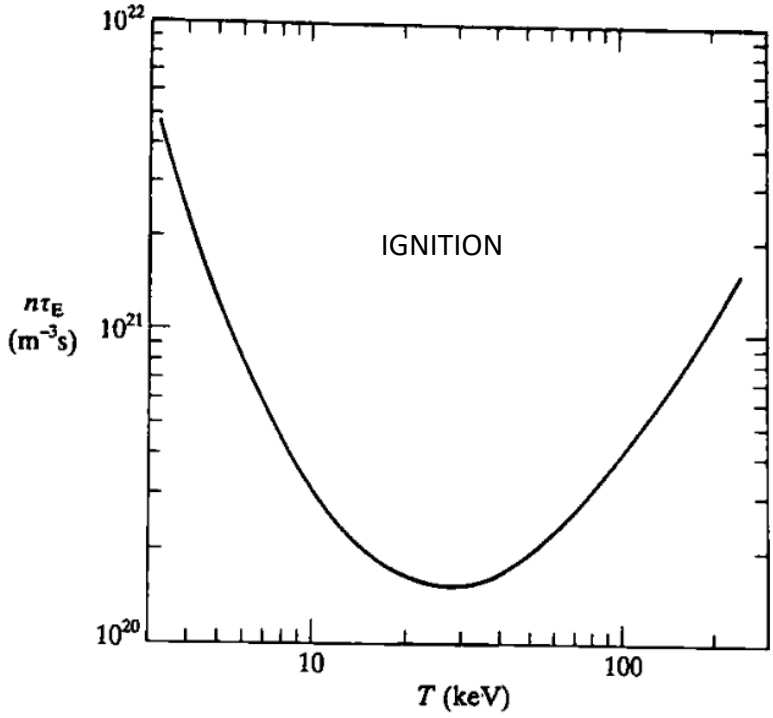

Figure 1.4. Condition for ignition based on product between n and τ as function of temperature.

As shown in *Fig.1.4*, the product $n\,\tau_E$ has a minimum at T≈30 keV, but the optimal condition (also considering the confinement time) is at lower temperature, around 10 to 20 keV, where:

$$< \sigma v > \approx 1.1 * 10^{-24}\, T^2\, \frac{keV^2 m^3}{s} \tag{1.21}$$

And being:

$$Q_\alpha \approx 3.52\ \text{MeV} \tag{1.22}$$

It is possible to write the so-called **Lawson criterion** as follows:

$$n\,\tau_E T\ >\ 3 * 10^{-21}\, \frac{keV\ s}{m^3} \tag{1.23}$$

The term at the left side of the inequality is called **triple product** or **fusion product**; this criterion gives the requirements of temperature, density, and confinement time in order to achieve the ignition condition.
For example, the reference values for ITER to satisfy this condition are:
$n = 1.5*10^{20}\ m^{-3}$
$\tau_E = 1$ s
$T = 20$ keV
It must be cleared that the Lawson criterion has purely historical value: that's because, in reality, plasma is much more stable and easier to control if there is a continuous additional heat from the outside that prevent it from cooling down.
However, it gives an idea about the order of magnitude of some parameters to be reached in a reactor, and it's also a good indicator for the technological progress achieved during the years.

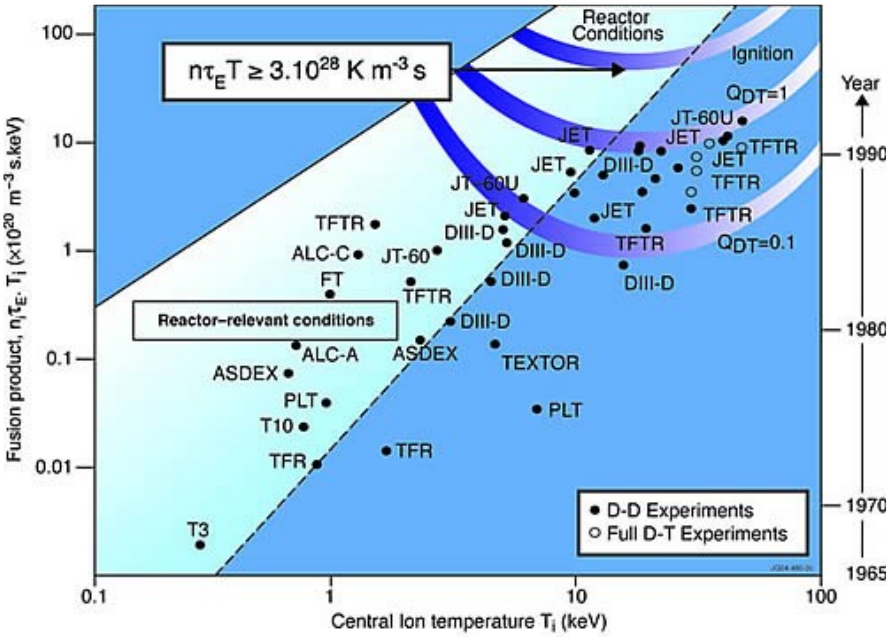

Figure 1.5. Triple product as function of temperature for different fusion experiments.

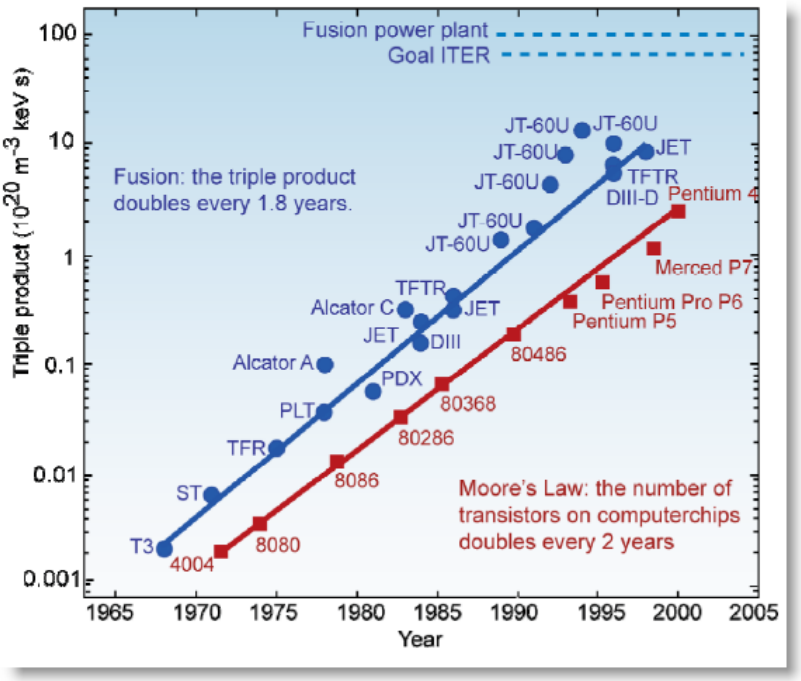

Figure 1.6. Triple product for different fusion experiments during the years.

As shown in *Fig. 1.6*, in 30 years the triple product achieved has been increased by 10.000 times. An increase by "only" six times is now needed to reach the breakeven. So far, scientists were able to achieve the required values of the three terms of the fusion product, but only one at a time separately, not all together.
The challenge is to re-create the conditions theoretically described by the Lawson criterion and to maintain them for a long time, so that the feasibility of the commercial dispatchment of electricity from fusion power plants will be proved.

Chapter 2

Tokamak configuration and DTT facility

Researchers all around the world are studying the best ways to achieve the conditions already mentioned in the Lawson criterion and to overcome engineering and technological issues like the development of structural materials withstanding severe irradiation, high temperature superconductors, tritium breeding blanket, actively cooled divertor, remote maintenance.
One of the most promising magnetic confinement configurations for future nuclear fusion power plants is the so-called Tokamak, which will be briefly presented in this chapter.

2.1 Introduction on Tokamak configuration

Confining the plasma for a sufficient time (τ_E) is one of the conditions to achieve fusion reactions, as seen in the previous chapter.
Plasma is ionized gas: the reference temperatures are above 100 million Celsius, and, as every hot gas, it has the tendency to expand (particles forming the plasma are moving at speed around 10^6 km/h).
No material can withstand contact with such energetic gas. In case of contact between the gas and the wall, the plasma would cool down, and the wall would be sputtered, increasing radiation losses in the plasma due to impurities.
Indeed, there's the necessity to find a way to confine the plasma in a certain region to avoid contact with other materials.
There are basically three ways to confine plasma in a certain region:
-Gravitational confinement: that's what happens in stars. The incredibly high masses of stars create a gravitational force able to confine plasma inside them. However, this condition is not replicable on earth.
-Inertial confinement: it's based on the use of lasers that initiates nuclear fusion reactions by compressing and heating targets filled with fuel. Energy is deposited in the target's outer layer, which explodes outwards. This produces a reaction force in the form of shock waves that travel through the target, compressing and heating it.
-Magnetic confinement: since plasma is formed by electrically charged particles, it is possible to deviate their trajectory to keep them in a certain region by creating a proper magnetic field.
This last option is considered the most promising configuration for future thermonuclear power plants.
A **Tokamak** is a machine that confines a plasma using magnetic fields in a donut shape that scientists call a torus.

The Tokamak configuration was proposed for the first time in 1950 by two soviet scientists, Andrej Sacharov and Igor Tamm; its name is a russian acronym for *TOroidal KAmara MAgnit Katushka*, which means toroidal chamber with magnetic coils.

2.2 Tokamak magnetic field system

According to the Lorentz force law, a particle of charge q, moving with a velocity v in a magnetic field B experiences a force:

$$F = q\, v \times B \tag{2.1}$$

This force depends on the angle θ between the velocity of the particle and the magnetic field.
It can be written also:

$$F = q\, v\, B\, \sin\theta \tag{2.2}$$

F is maximum when v and B are perpendicular (sen(90°)=1), and it's minimum (null) when they're parallel (sen(0°)=1). The direction of F depends on the charge of q, according to the right-hand rule.
Three types of magnetic field are used:
-**Toroidal field B_ϕ**: generated with toroidal coils, it allows to generate a field directly around the symmetry axis of the torus, constraining charged particles to move in that direction.
-**Vertical field B_V**: generated with poloidal coils, it generate a force opposing to the centrifugal force and it allows to control the plasma position, preventing from collision with walls.
-**Poloidal field B_θ**: as plasma is a conductor, it is possible to induce a current in the plasma itself to generate a poloidal field; this field avoids the drift of particles, ensuring plasma equilibrium.

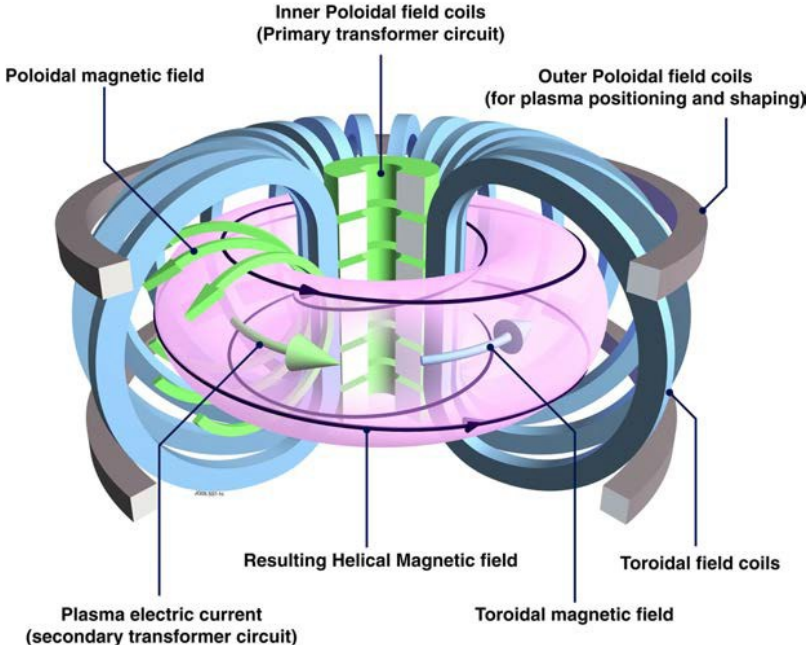

Figure 2.7. Scheme of a Tokamak reactor

In a tokamak, as initial condition deep vacuum is created by using vacuum pump.
Plasma current accension happens by following these steps:
-current is generated inside the toroidal field coils;
-a small amount of gas is immitted (generally hydrogen or its isotopes);
-current is immitted inside the central solenoid, generating a flux inside tokamak core: it represents the primary of a transformer of which the torus represents the secondary;
-current in the primary is rapidly dropped to low values, causing the generation of an electromotive force. Neutral atoms are ionized, a discharge is created with more and more electrons;
-gas is no more neutral, but it has become plasma: at this point the electric current, via Joule effect, heats up plasma at really high temperature (a few million degrees).
In reality, toroidal field coils have not a circular shape, but a D-shape: this solution permits to keep almost null bending moments and shear stresses on the coils.
At the end, the trajectory of plasma particle will follow a "banana" shaped trajectory, which is considered an optimal situation for controlled fusion reactions.

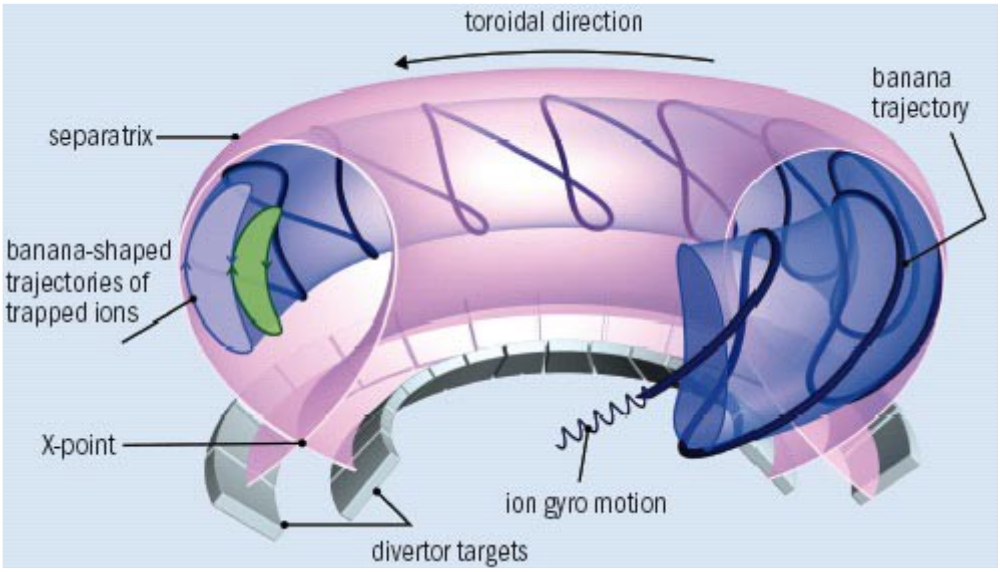

Figure 2.8. Banana-shaped trajectory of trapped ions

2.3 Cryostat

The magnetic system is crucial for the operation of the machine, since it allows to control the plasma operation.
In general, the higher the magnetic field generated, the better is the control on plasma confinement; anyway, there are limitations due to the power losses associated with the resistivity of the coils materials.
In a fusion reactor, the Joule heating losses in copper coils would be unacceptable.
That's why superconducting magnets will be used in future power plants.
Superconductivity is defined as the property of different elements and alloys to lose their electrical resistivity completely when cooled to very low temperature below a certain value named critical temperature (T_C).

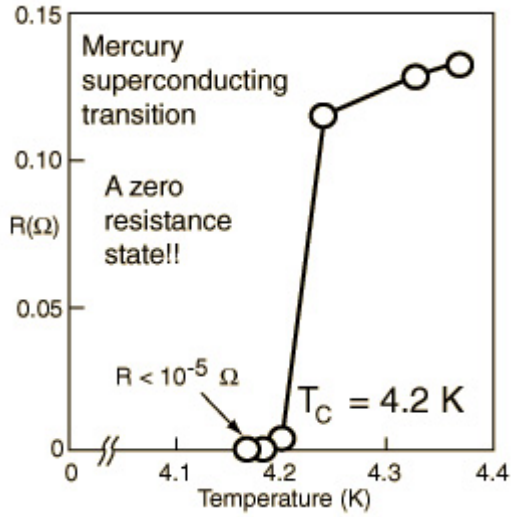

Figure 2.9. Resistivity of mercury at cryogenic temperature

In 1911 Onnes, a dutch physician, cooled mercury at liquid mercury temperature (@ 4.2 K).
Its resistance suddenly almost disappeared (its values dropped from 0.12 to 10^{-5} Ohm).
This new dissipation-free state of matter was called superconductive state.
It happens in metals, but also in metal alloys.

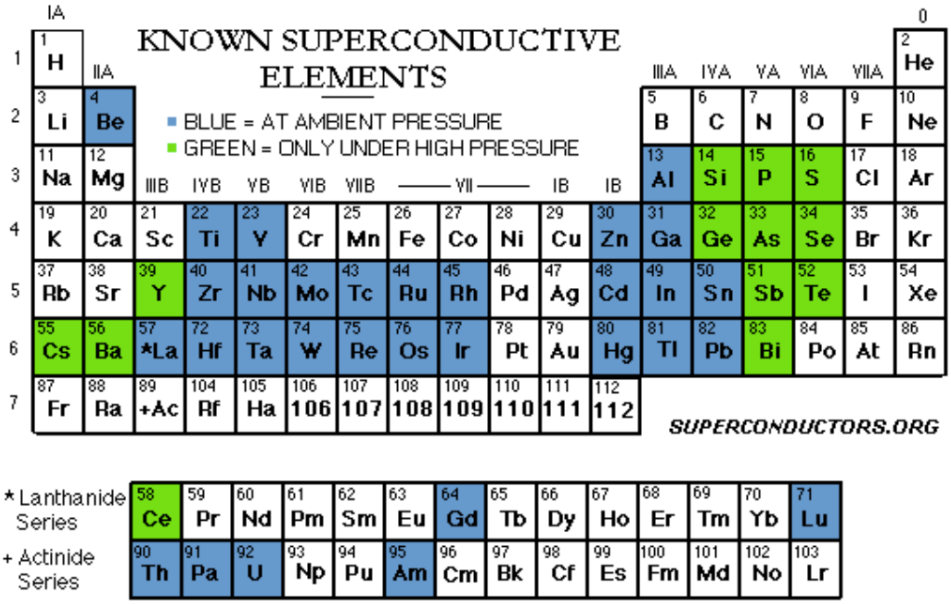

Figure 2.10. Periodic tables showing the superconducting elements.

Following the discovery of high-field superconductivity in the late 1950s, superconducting **wires** for magnet construction were produced in industry and offered for sale within a remarkably short space of time. By 1961 small magnets were being made from 1/4 mm diameter wires of **niobium zirconium**, a ductile alloy. This was quickly followed by **niobium tin (Nb3Sn)**, an intermetallic compound with excellent superconducting properties but so brittle that it could not be fabricated by conventional wire-drawing processes. […] **Niobium titanium (NbTi)** wires were first produced in 1965 and this ductile alloy has since become the standard "work-horse" of

superconducting magnet construction, mainly because it is relatively easy to fabricate and may be co-processed with copper.

This physical property allows to generate very high magnetic fields by introducing large currents (tens of kA) without excessive losses by Joule effect.
Superconductor for magnetic system must:
-be able to carry large currents with high magnetic field (~68kA for Toroidal Field Coils TFC, ~40kA for Central Solenoid CS);
-have high mechanical strength;
-have quench protection (avoid transition from cryogenic to normal condition due to heat propagation).
To maintain these cryogenic conditions for the magnetic field system, a vacuum chamber is needed: this component is called **cryostat**.
The cryostat is a vacuum vessel having a very large volume (ITER cryostat ~16000 m^3) designed to be evacuated to a base pressure of 10^{-4} Pa.
The main function of the cryostat is to provide the vacuum environment to avoid excessive thermal loads being applied by gas conduction and convection to the components that are being operated at cryogenic temperatures, such as the superconducting magnet systems (but also thermal shields etc.).
The cryostat has penetrations to allow the passage of all the systems that are required to operate and maintain the tokamak.

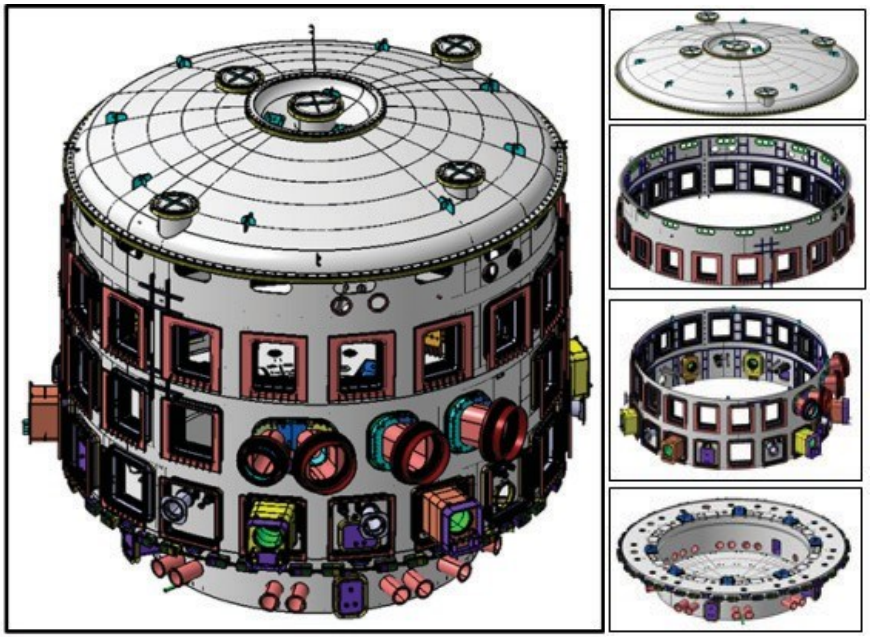

Figure 11. ITER cryostat scheme composed by four sections.

It is a single wall fully welded stainless steel cylindrical chamber with internally vertical and toroidal ribs. It has top dome shape lid and bottom flat head.
In the following table, the main overall parameters of ITER cryostat are shown as an example.

Items of parameter	Number & unit
The cryostat outside diameter	28.54 m
The cryostat height	29.25 m
Wall thickness	40 mm - 180 mm
Number of sections	4
Main cylinder shell thickness	50 & 60 mm
Material of Construction	Dual Mark 304L/304
Toroidal resistance	> 10 μΩ
Design base pressure	1*10^-4 Pa
Required leak rate of completed cryostat	≤ 1*10^-4 Pa/(m3s)
The cryostat surface rea	~3400 m2
Interior free volume	~8500 m3
Interior total volume	~16000 m3
Mass	
Top lid	656 ton
Upper cylinder	600 ton
Lower cylinder (+TCPH)	809 ton (+214 ton)
Base section	125 ton
Total mass	3500 ton

Table 2.1. Parameter of ITER cryostat

The pedestal ring is the platform where the magnet and the vacuum vessel supports stand on. It is supported by eighteen sliding bearings installed on the concrete crown wall support and is integrated with the pit floor.
The skirt support, which is installed to a stage of the bio-shield, supports the upper cryostat. It allows radial movement of the cryostat shell in case of helium and water spillage event inside the cryostat. The support lugs, which are installed on the outer periphery of the cryostat and are locked toroidally with the mating lugs embedded in bio-shield, are designed to confine the cryostat and the tokamak from horizontal movement during seismic events.

2.4 Vacuum Vessel

Along with the magnet system, the cryostat hosts another crucial component for fusion reaction: the **Vacuum Vessel** (VV).
The vacuum vessel is one of the main components of the tokamak, with the purpose of giving a physical confinement to the plasma and keeping the required level of vacuum needed for the operation of the machine. It also improves radiation shielding and plasma stability, it acts as the primary confinement barrier for radioactivity, and it provides support for in-vessel components such as the blanket and the divertor, which will be presented in a moment.

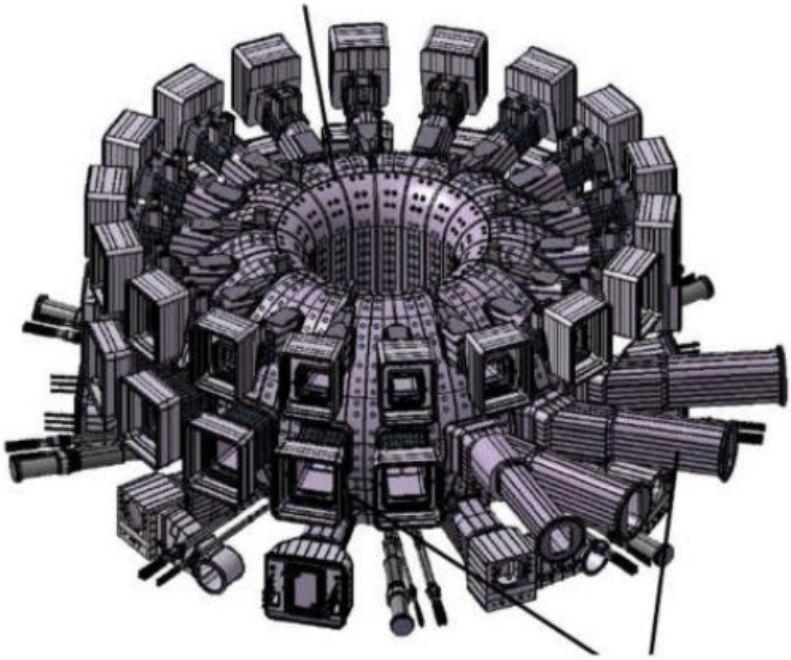

Figure 2.12.ITER vacuum vessel with ports.

In ITER, forty-four openings, or **ports**, in the vacuum vessel provide access for remote handling operations, diagnostics, heating, and vacuum systems. (Neutral beam injection will take place at equatorial level, for example, while on the lower level, five ports will be used for divertor cassette replacement and four for vacuum pumping.)
The ITER VV has a toroidal double-walled stainless steel (316L(N)-IG) structure divided into nine sectors with an angle of 40◦ in the circumferential direction. The volume between the external and internal shells of each sector is designed to allow the circulation of the cooling water delivered by the VV Primary Heat Transfer System (VV PHTS). One single cooling loop per sector removes the heat deposition due to nuclear heating.
The inner wall presents the so-called plasma facing components, including the **blanket** and the first wall, and the **divertor**.
The first wall can be part of the blanket or a separate component. It has to be designed accordingly to the expected thermal flux that it has to withstand, which vary according to the position considered (thermal loads expected: 1-4.7 MW/m^2).

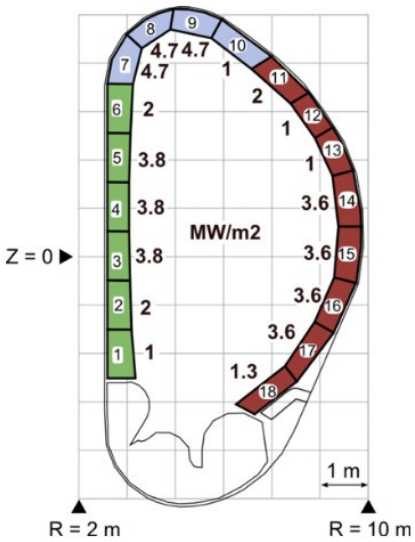

Figure 2.13. Poloidal cross section of the ITER First Wall with expected heat loads.

The blanket is a modular component (440 modules in ITER, 1x1.5m, 4.6 tons each) that covers completely the inner walls of the VV, in order to:
-protect the steel structure and the superconducting TFC from the heat and high-energy neutrons;
-generate Tritium (hence the term "breeding blanket") thanks to neutrons that, being electrically neutral, are not influenced by the magnetic field (they are not confined) and extract Tritium (purging);
-host the neutron kinetic energy conversion into utilisable heat, (transferred to heat transfer fluid) that, in a fusion power plant, will be used for electrical power production.
In the bottom region of the VV, another crucial component is placed: the divertor.
It is composed by 54 ten tonnes "cassettes" with a supporting in stainless steel and it has mainly two tasks:
-Extracts ash produced by the fusion reaction, so to minimize plasma contamination;
-Protects the surrounding walls from thermal and neutronic loads.
The heat flux sustained by the ITER divertor vertical targets is estimated at 10 MW/m² (steady state) and 20 MW/m² (slow transients).
Tungsten, with the highest melting point of all the metals, has been chosen as the armour material following an international R&D effort, encouraging experimental results, and successful prototype testing.

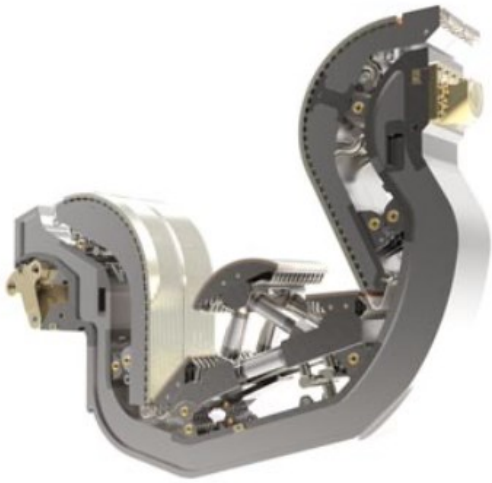

Figure 2.14. ITER divertor cassette

ITER divertor is actively cooled with water flow at 10 m/s, with 100°C inlet temperature and 150°C outlet temperature.
The inner and outer vertical targets are positioned at the intersection of magnetic field lines where particle bombardment will be particularly intense in ITER. As the high-energy plasma particles strike the vertical targets, their kinetic energy is transformed into heat and the heat is removed by water.

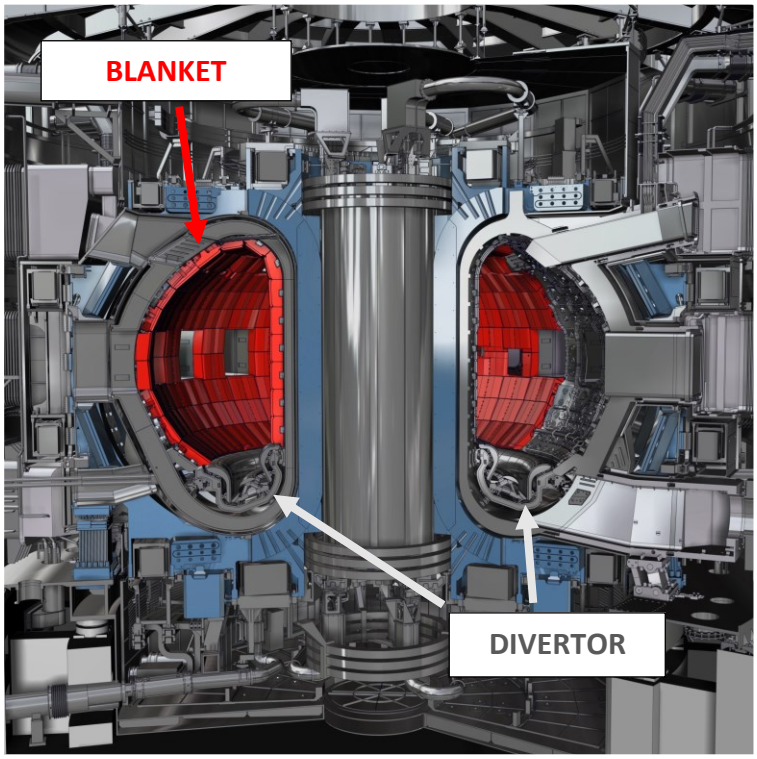

Figure 2.15. ITER Plasma facing components

2.5 DTT facility: role and description

In the previous paragraphs, some of the main component of a nuclear fusion power plant have been briefly presented. In addition to those, there are a lot of smaller components, including diagnostics instruments, auxiliary machines, tubes etc.
Each one of these components must be studied in detail in order to match as much as possible the condition in a plant during the operation.
In this sense, in the international community the urgency for a research effort on the plasma exhaust issue and on the divertor is now broadly recognized, in particular in the *European Fusion Roadmap*.
That's where the **DTT facility** takes place. Held in Frascati (Rome, Italy), the Divertor Tokamak Test facility is an experimental project which has a great relevance in EUROfusion research program. The organizations and institution which co-operate for the project are ENEA in collaboration with ENI, Consorzio RFX in Padua, Consorzio CREATE in Naples, Universities of Rome Tor Vergata, University of Tuscia, Milan Bicocca, Turin Polytechnic university, CNR, INFN, and CETMA, together in Consorzio DTT.
Following the guidelines described within the European Fusion Roadmap, the DTT facility has been charged with the challenge to test the science of tokamak **alternative divertor concepts** under integrated physics and technical conditions that can reliably be extrapolated to DEMO. In a magnetic fusion device, the divertor, as already seen, is the system where energy and particles, transported out from the plasma, are collected.
In order to comply with the material, the power flowing to the divertor must be 10 MW/m^2.
The baseline solution to the exhaust issue consists in a metal divertor operating in a plasma fully detached condition. However, as widely illustrated within the European Fusion Road Map, the baseline solution might not fit the needs of DEMO and of a future reactor. The plasma exhaust issue needs therefore to be solved with great urgency and strength in order not to cause delays to the development of fusion. In this effort a key aspect will be the availability of DTT scenarios, with high-performance core plasma properties consistent with relevant edge and SOL (Scrape-Off Layer) parameters.
Testing the alternative divertor configurations in different scenarios will provide the whole set of information needed to choose the right solution for DEMO.
This tokamak has to carry out a number of scaled divertor experiments, under integrated physics and technical conditions that can reliably be extrapolated to DEMO.
DTT should therefore have the possibility of testing different divertor magnetic configurations and technologies, including liquid metal divertor targets, and other promising solutions to cope with the power exhaust problem.

2.6 DTT main parameters

The relatively high toroidal field (B_T = 6 T) will give the possibility to achieve plasma performances (mainly measured by the ratio between power and major radius of about 15 MW/m), not far from those in DEMO.
The present design of the DTT facility is based on a superconducting tokamak with a double layer stainless steel vacuum vessel with major radius R=2.11 m, minor radius

a=0.64 m and aspect ratio A=3.3, corresponding to a plasma volume of 28 m3. The on-axis maximum toroidal field is B_T=6 T, and the maximum discharge duration allowed by the power supplies and the superconducting coils is 100 s. The maximum plasma current in the single null reference scenarios is Ip=5.5 MA, with an additional auxiliary power P_{tot}=45 MW.
The design choices meet, even within the limits of machine size and cost, the need to create Scrape-Off Layer and heat exhaust conditions similar to those of DEMO. *Table 2.2* shows the main data for the comparison between DTT, ITER and DEMO.

	DTT	ITER	DEMO
R (m)	2.19	6.2	9.1
a (m)	0.70	2	2.93
A	3.13	3.1	3.1
I_p (MA)	5.5	15	19.6
B (T)	6.0	5.3	5.7
Heating P_{tot} (MW)	45	120	460
P_{sep} /R (MW/m)	15	14	17
l_q(mm)	0.7	0.9	1.0
Pulse length (s)	100	400	7600

Table 2.2. DTT, ITER and DEMO parameters compared.

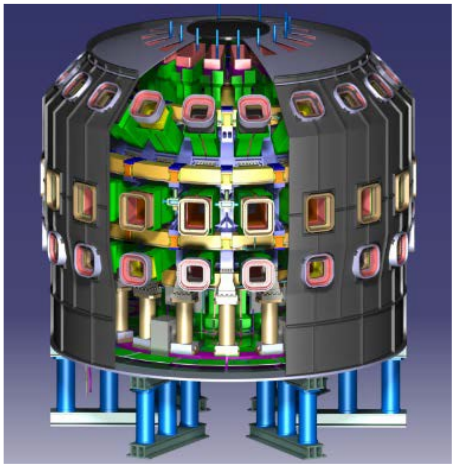

Figure 2.16. Artistic view of DTT

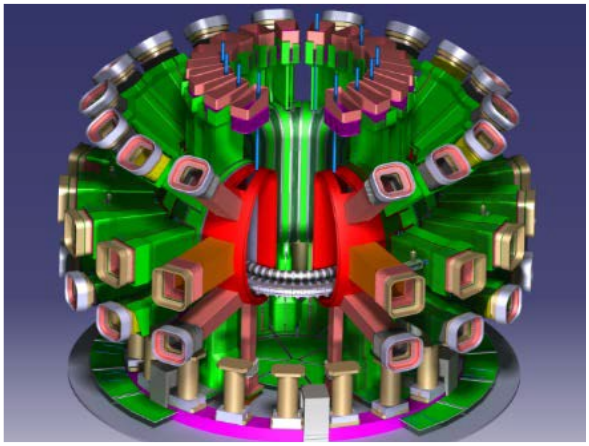

Figure 2.17. Artistic view of DTT mechanical structure

2.7 DTT operational states

In the project design phase, the material and geometric choices are taken according to the foreseen thermal and mechanical loads.
These loads depend on the operational status of the machine.
In DTT, the operations are classified in:
-**Long Term Maintenance (LTM)**: are those operations in which the interlock systems grant safety on classified areas (also by means of keys), few systems are required to be operative and ready and these ones do not impact the human safety, no power is delivered to the Tokamak.
-**Short Term Maintenance (STM)**: are those operations in which some power goes to the plant, Toroidal Magnetic Field could be on, some laser could be on and for this reason the access to some of the classified areas shall be restricted by the working groups.
-**Pulsed Operation (PO)**: are those operations in which also ECRH (Electron Cyclotron Resonance Heating), ICRH (Ion Cyclotron Resonance Heating) or NBI (Neutron Beam Injection) sources, High Voltage, high magnetic fields, lasers, B_2H_6 toxic could be injected in to the Hall and the VV so the access to the classified areas shall be forbidden, the sequence includes the dwell time before the next Plasma Operation State (POS). Between two POS the access to the classified areas comes back to be restricted (when the radiation monitoring gives the acknowledgment).
LTM includes:
-Install/remove components in the Hall;
-Remote Handling Operation;
-Open Vacuum/N_2;
-Install/remove components in VV;
-**Baking (BAK).**

STM includes:
-Glow Discharge Cleaning (GDC): VV cleaning by glow discharge;
-Boronization (BOR);
-Standard Standby (STS): this state covers the start-up, evacuation, tokamak cooldown, standby overnight and during weekends with magnets de-magnetized, **regeneration of cryopumps**, short term maintenance activities and tokamak warm-up;
-Calibration of special diagnostics (CAL);
-Toroidal Field Magnet charge/discharge (TFM).
PO includes:
-**Plasma Operation State (POS):** any test pulse with or without plasma or ICRH, ECRH or NBI;
-Electron Cyclotron Wall cleaning (EWC);
-Ion Cyclotron Wall cleaning (IWC);
-Dwell time (DWE): phase between two sequence of POS states in which closure operations will be performed (recover vacuum, cooldown in Vessel Coils etc...).

Two of these operational states deserve a brief description since, as will be shown in the next chapters, they present thermal loads that differs from the other operational states.

Baking
It is the process of cleaning the VV. This is a necessary operation since a lot of molecules will accumulate inside the vessel either buried in the near surface of the plasma-facing components, trapped in layers of plasma-deposited material, or "adsorbed" (deposited) on their surfaces: fuel molecules, particles from the erosion of materials, oxygen, etc. even trace quantities of material from the manufacturing process for the in-vessel components. Removing these contaminants is extremely important to achieving high performance in a Tokamak, as too many impurities released from the walls during the operation will pollute the plasma, causing dilution of the fusion fuels and plasma energy losses through photonic radiation.
This is possible by heating the VV walls to detach impurities from it.
Even if it seems contradictory, the cooling water system, during baking operation, will provide hot water (200-240°C instead of around 100°C in the normal operation) to heat up to 200-240°C the VV and other components (blanket, first wall and divertor).
In this way, those molecules move freely inside the VV until they're evacuated by the vacuum pumps.
DTT will be able to perform baking in two different ways:
-**Strong baking** (S-Bak) at the commissioning and at the start of campaign in LTM (foreseen 1 per year typically);
-**Light baking** (L-Bak) during the STM (foreseen 1 per week typically with ramp-up time for reaching above systems temperatures in maximum 24 hours).
Technical differences between the two scenarios will be presented in the following chapters.

Regeneration of cryopumps
It is the process of realising the gas evacuated from the VV and captured by the cryopumps; it is considered an operation of STS.
As in the case of baking, this process is held by heating up the considered component, in this case the cryopump.
More precise value will be presented in the next chapters.

Chapter 3

Cryogenic, electrical and cooling penetrations for the DTT VV: Port number 5

In a Tokamak, the vacuum vessel shall provide several openings in order to permit the insertion of all the components for the operation, such as diagnostic systems, auxiliary systems, remote handling, vacuum systems, services and so on.
These openings in the VV are called **ports**, and they give access to the vacuum vessel from the atmospheric pressure side.

3.1 Vacuum Vessel and ports

As already seen in previous chapters, the DTT VV will have a double walled D-shaped poloidal section, and a toroidal configuration.
This torus will be divided into 18 sectors in the toroidal direction, with an extension of 20°: each section will present 5 penetrations, designed according to their requirements.
Each port will be numbered from 1 to 5 clockwise from the top to the bottom, following the D-shaped curve, as in the following representation.

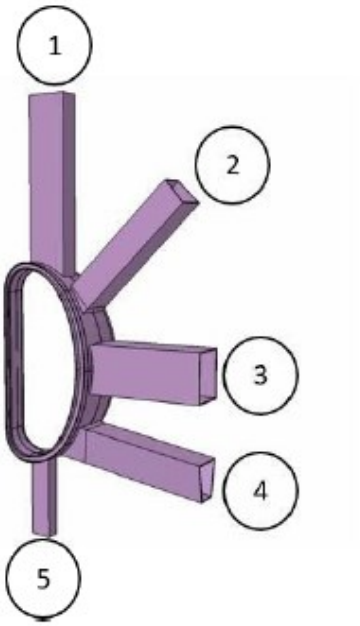

Figure 3.18. Typical 20° Vacuum Vessel section with ports numbered.

The requirements for these 5 ports can be summarized as follows:
-Port #1: it is mainly assigned to remote handling operations required for maintenance of inboard segments of the First Wall, fuelling and routing of cooling pipes of VV and

First Wall.
-Port #2: it is aligned to the centre of the plasma so that it can house properly the ECRH antennas (only in 4 out of 18 sectors). It will house also some other diagnostics.
-Port #3: it is called also equatorial port. It will house diagnostic systems, ECRH and ICRH antennas. This port allows the remote handling operations for the outboard segments of the FW.
-Port #4: it will be aligned with a possible divertor exit path to ease the access for RH maintenance or its decommissioning.
-Port #5: it will be mainly devoted to diagnostics, pumping and fuelling. Its tasks and components will be better presented in this chapter.
The analysis that will be carried out with this thesis work will vert on **port number five.**

3.2 VV and Ports Geometry

The main geometrical parameters have already been defined, but there is still a lot of work in progress to select the optimal dimensions of each single component of DTT. As it stands, in the current configuration, the thicknesses of the inner and outer shell of the double walled VV are set equal to 15 mm.
The overall external dimensions of the VV are reported in Fig. 3.2. The maximum height is equal to 3940 mm, with a radius of 1265mm at the inboard side and of 3400 mm at the outboard side.

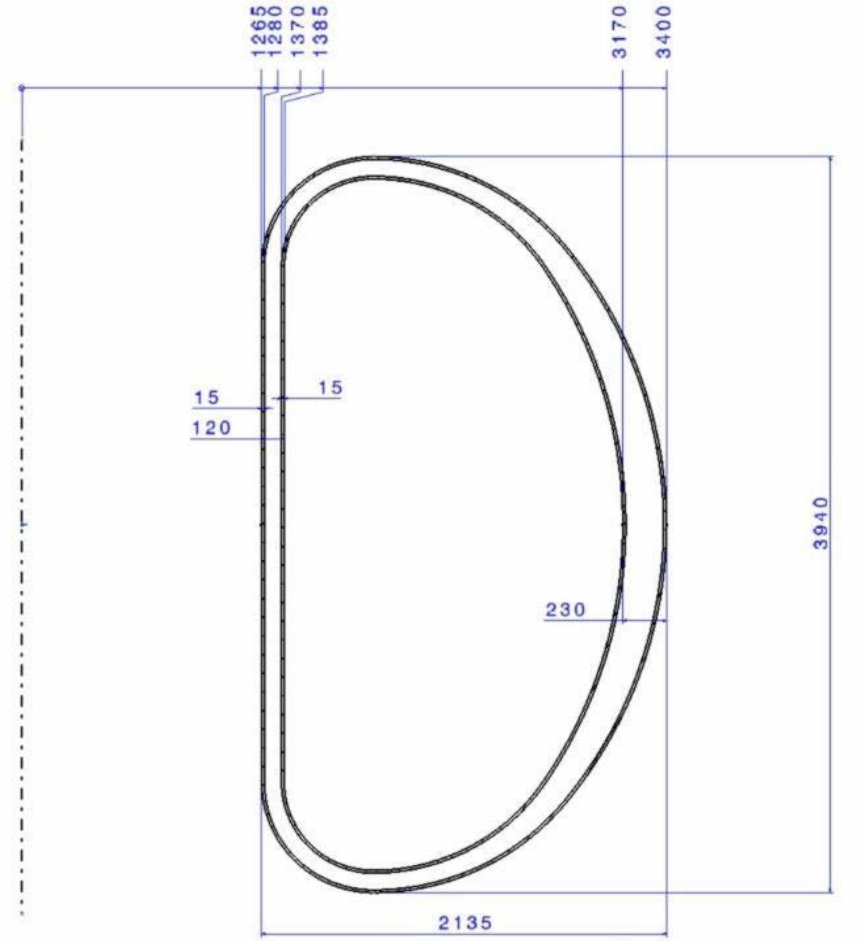

Figure 3.19. Vacuum vessel D-Shaped poloidal section

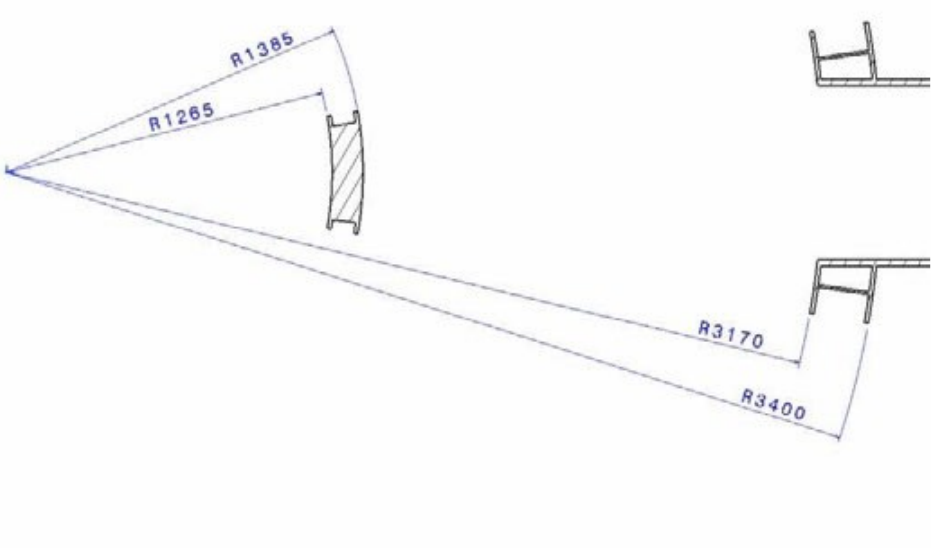

Figure 3.20. Vacuum vessel radial dimensions

A crucial aspect for the performances is the choice of the material. Influence on performance, fabrication characteristics, mechanical strength at operating temperature, chemistry properties, and cost are the criteria considered in the choice. Compared with other possible candidates, **AISI 316L(N) stainless steel** has good mechanical properties, good chemistry properties, which are well-known.
As already seen, water will flow in the region between the two walls of the VV: this structure will include 10mm thick ribs that will draw the path for the fluid.
The dimensions of access ports are reported in Fig. 3.4.
Port number five have an almost triangular shaped cross section. It extends from the base of the cryostat to the bottom of the VV.

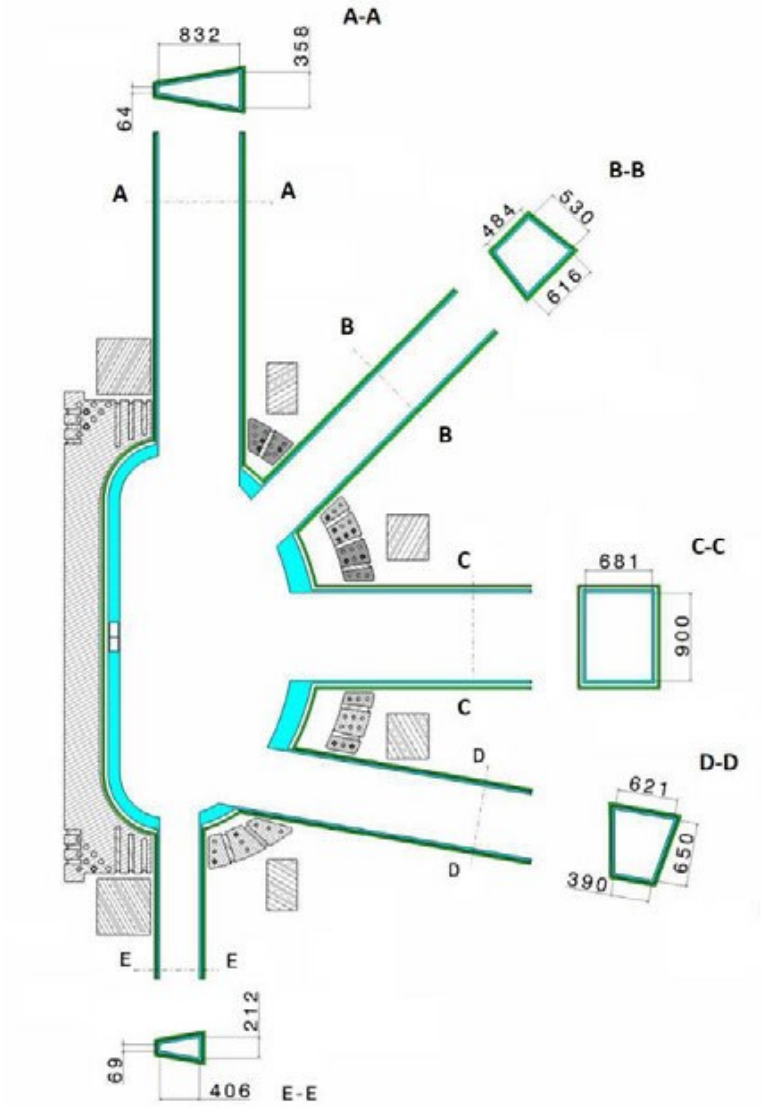

Figure 3.21. VV ports dimensions.

Each port is connected to the cryostat through a bellow.
This is a crucial element from the mechanical point of view since it is designed to compensate for the thermal dilatation of the port, for the relative displacements between the cryostat base and the VV and for other mechanical stresses that could lead to damage on the structure.

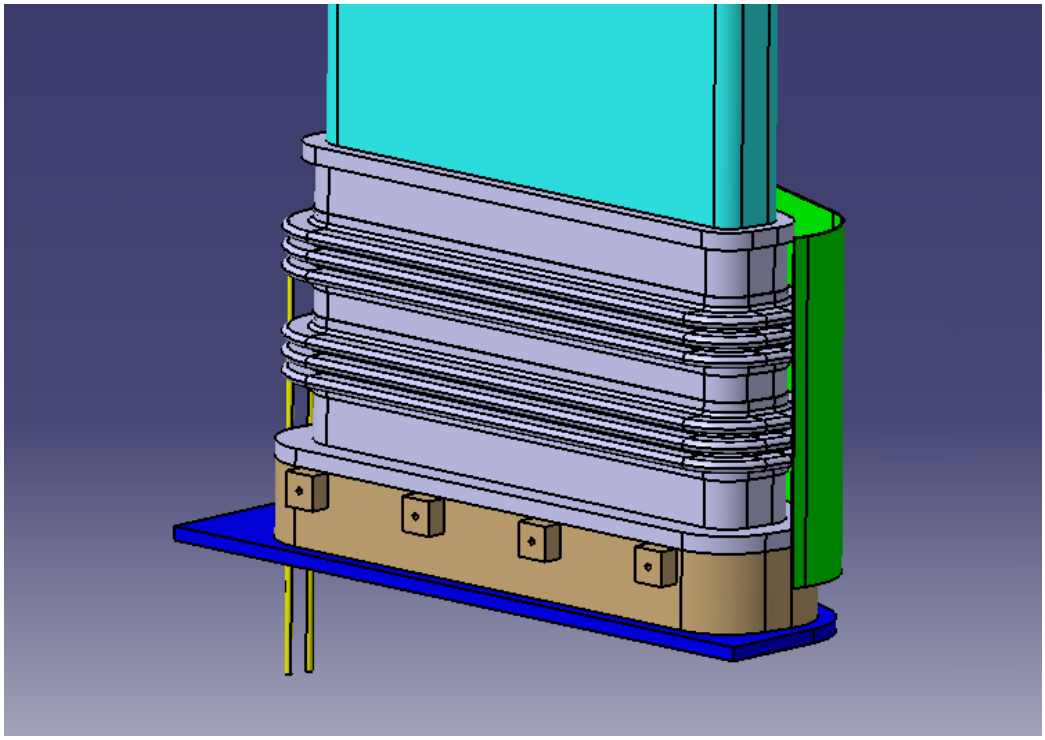

Figure 3.22. Port 5 bellow.

The bellow presents some convolution that are still in phase of study from the geometrical point of view, and so this component will be simplified schematically in the simulations.

3.3 Port #5: role and components

In the previous pages, a brief description of the tasks of each port has been carried out. Being the subject of the analysis, port #5 deserves a more detailed description, including a presentation of the components that are part of the port.
Fig. 3.6 shows a section of a typical port #5 (in the next pages, it will be shown that not all the 18 port #5 present the same components). Port 5 bellow will not appear in this representation since, as already said, it will be simplified in the simulations.

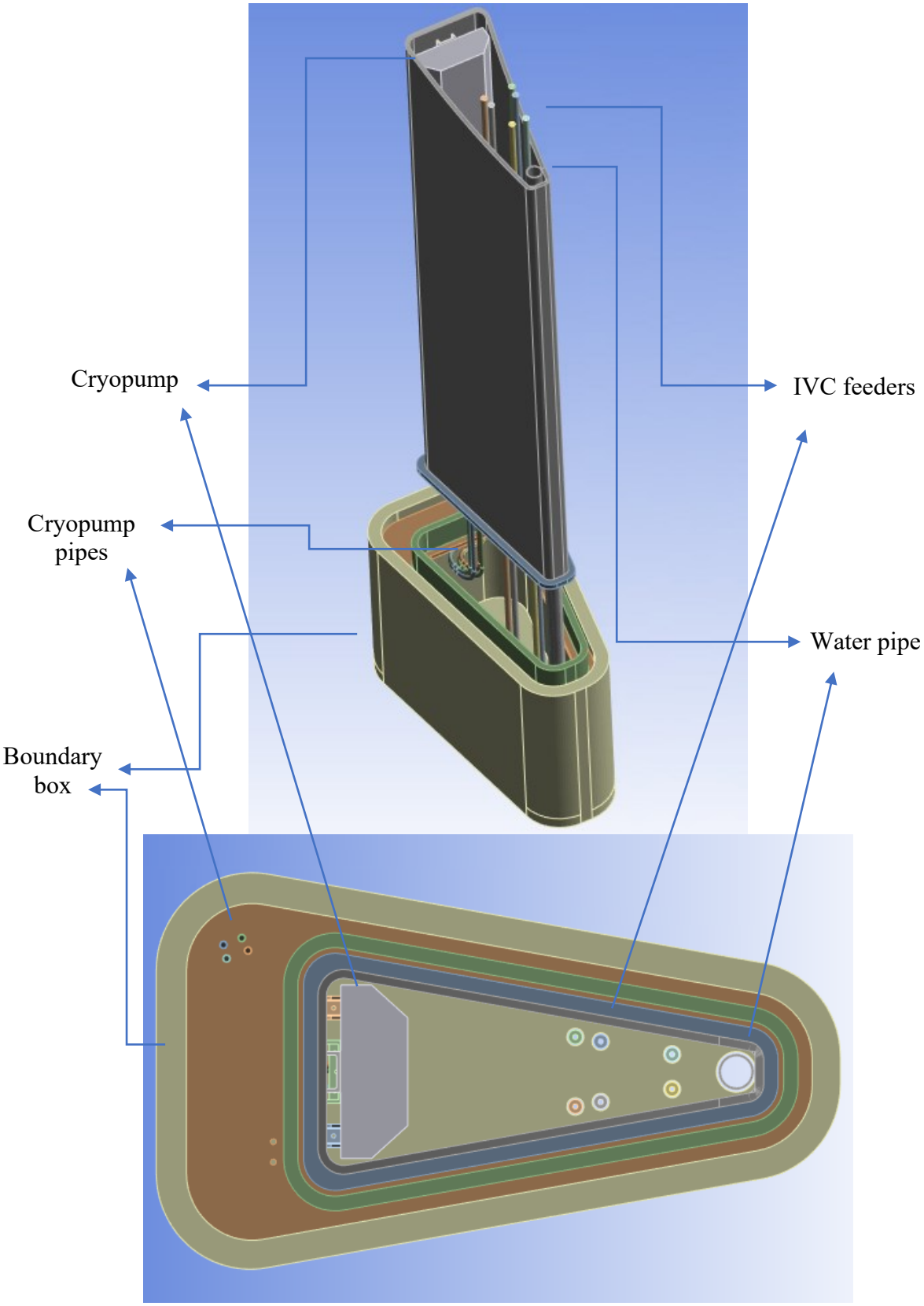
Cryopump
IVC feeders
Cryopump pipes
Water pipe
Boundary box

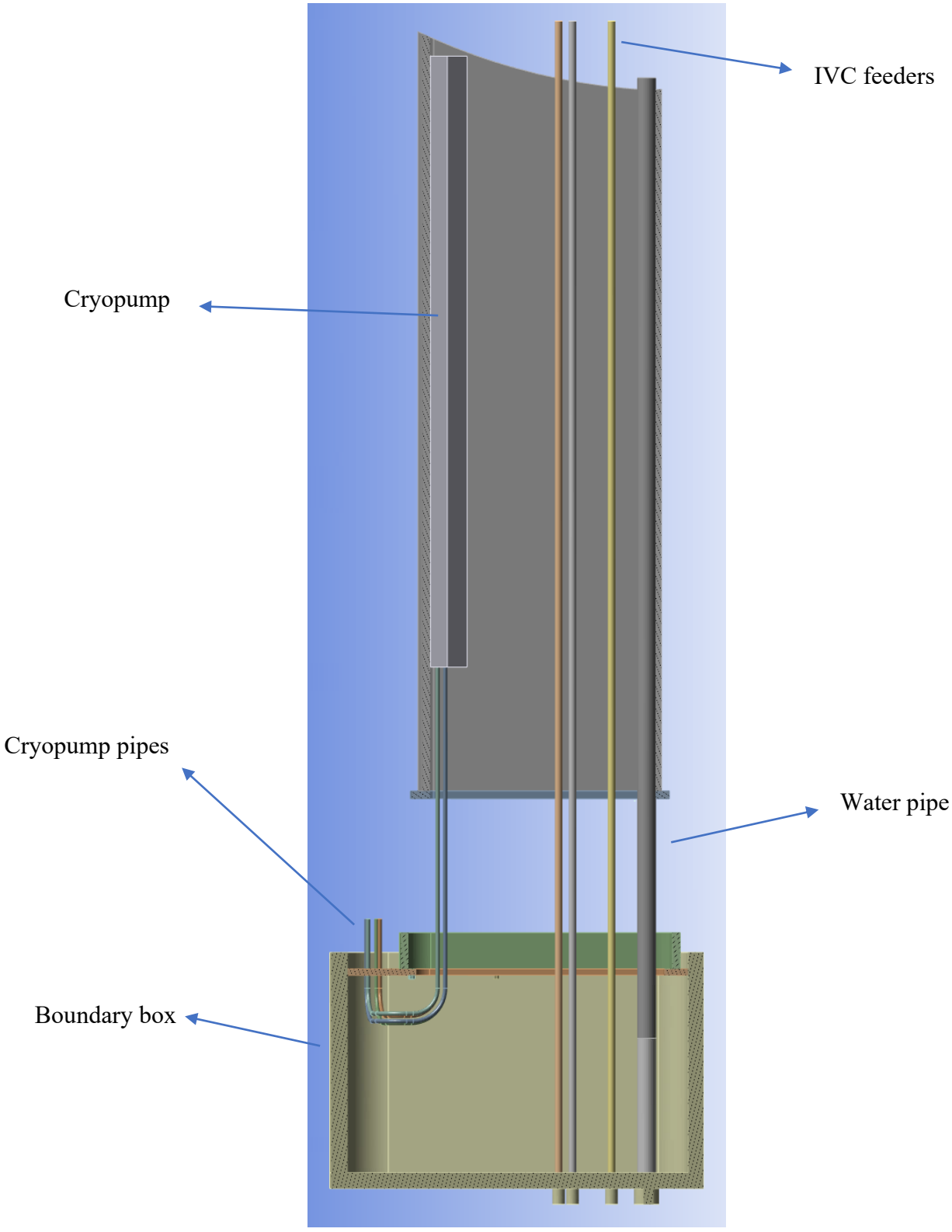

Figure 3.23. Port 5: isometric and top view, side section.

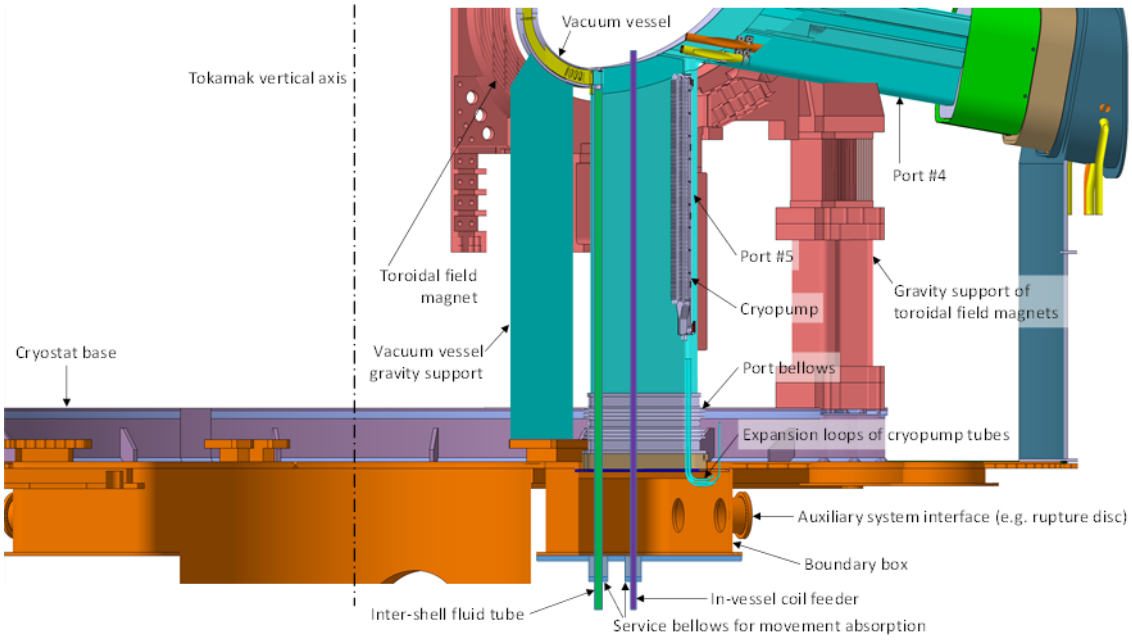

Figure 3.7. Port 5 and cryostat configuration

-Cryopump
The most important and typical element of port #5 is the cryopump with its cryopanels. Cryopumps are responsible for the divertor pumping operations; they will be better described in the next paragraph.
Cryopumps are fixed to the lateral surface of the port thanks to two welded inserts on the surface of the port.
A vertical guide is installed in the port to make easier the initial installation of the cryopump inside the port.
The cryopump is alimented through two inlet and two outlet pipes.

-Water inlet pipe.
The water flowing inside the double walled VV is alimented through this pipe.
During the normal operation, water at the inlet will flow at 60°C with a mass flow rate assumed to be equal to 20 kg/s.

-IVC feeders.
Inside the Vacuum Vessel, in the region close to the divertor, some coils are expected to be installed. These are called In Vessel Coils (IVC). The number of coils to be installed is still to be confirmed: in the last few months 4 coils were planned, but now it seems that 3 coils are enough. Their role is to stabilize vertically the plasma, to improve the radial control during breakdown and to improve the radial control the magnetic configuration in the divertor region and strike point sweeping.
These coils will be electrically fed with six conductors (three pairs) through port #5, schematized in *Fig.3.6* as pipes. The IVC are symmetric components, and so only a couple of conductors is sufficient to fed them: this means that only one out of the 18 port#5 will present these feeders.
In reality, these copper conductors will present an internal cavity with water flowing as coolant, and an insulant layer and a stainless-steel layer covering it.
There is the necessity to install a bellow at the extremity of each feeder (and also at the

extremity of the water pipe) in order to compensate for the thermal dilatation that they will suffer.
-Generic Interfaces
On the lateral face of the port, some other interfaces will be installed, which are not shown in the figures above. These inserts allow to install some other devices and components in the machine. They work as generic supports for other devices. Not really interesting for this work.

3.4 Cryopump

The divertor cryopump is installed to evacuate neutralized hydrogen or deuterium fuel, seeding gases (N_2, Ar). The cryopump system is separated into 9 identical units and located inside port #5.
The cryopump assembly comprises the inlet thermal shields (163 chevron-baffles cooled at 80 K to allow the incoming particles to thermalize) which are blackened and connected via cooling tubes, the 80 K panel on the rear side, which is electropolished, and the charcoal coated 4 K panels. Pumping takes place at the baffles (for heavier species), and the panels (for the lighter species).
The location of the cryopumps is an important aspect to mention; in the Japanese *JT-60SA* experiment, for example, the cryopumps are installed directly under the divertors in the VV. Anyway, in DTT, which is a smaller machine, there isn't enough space in that region, and so it has been decided to move the cryopumps inside the bottom vertical ports.
This choice implies some considerations on the design selection of the cryopumps.
Port #5, in fact, has a pretty low cross section area, which penalizes the performances of the pump.
One of the parameters influencing the performances of a cryopump is the conductance: it is defined as:

$$C = \frac{Q}{\Delta p} \quad [\frac{l}{s}] \tag{3.1}$$

Where Q is the gas flow rate evacuated, and Δp is the pressure difference between the two extremities of the pipe element considered (in this case, the port itself).
This parameter is highly influenced by the geometry of the pipe element, and in particular by the cross-section area: the smaller this area, the lower the value of the conductance.
To compensate for this disadvantage, these cryopumps must have an high pumping capacity to be able to properly evacuate the gases from the VV
That's the reason for the important length of the cryopumps, which cover almost entirely the length of the port.
In the next figures, the cryopump is shown in detail.

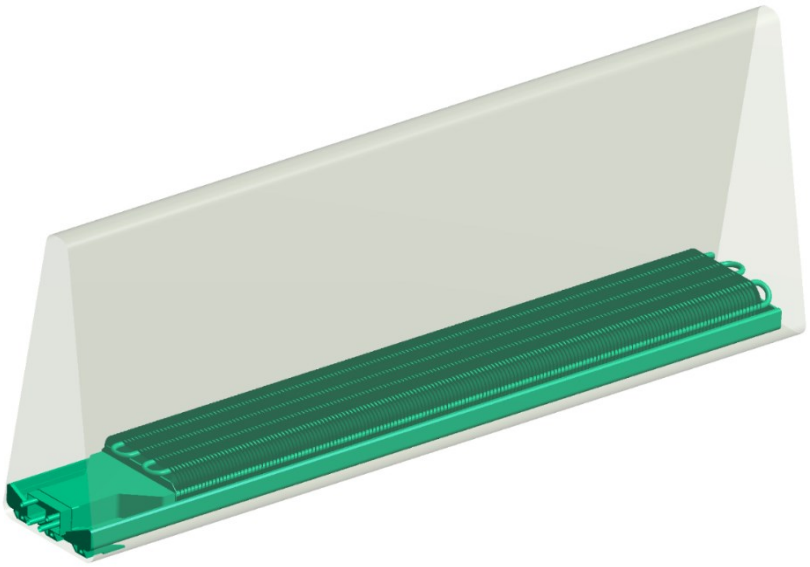

Figure 3.8. Representation of the cryopump inside the port.

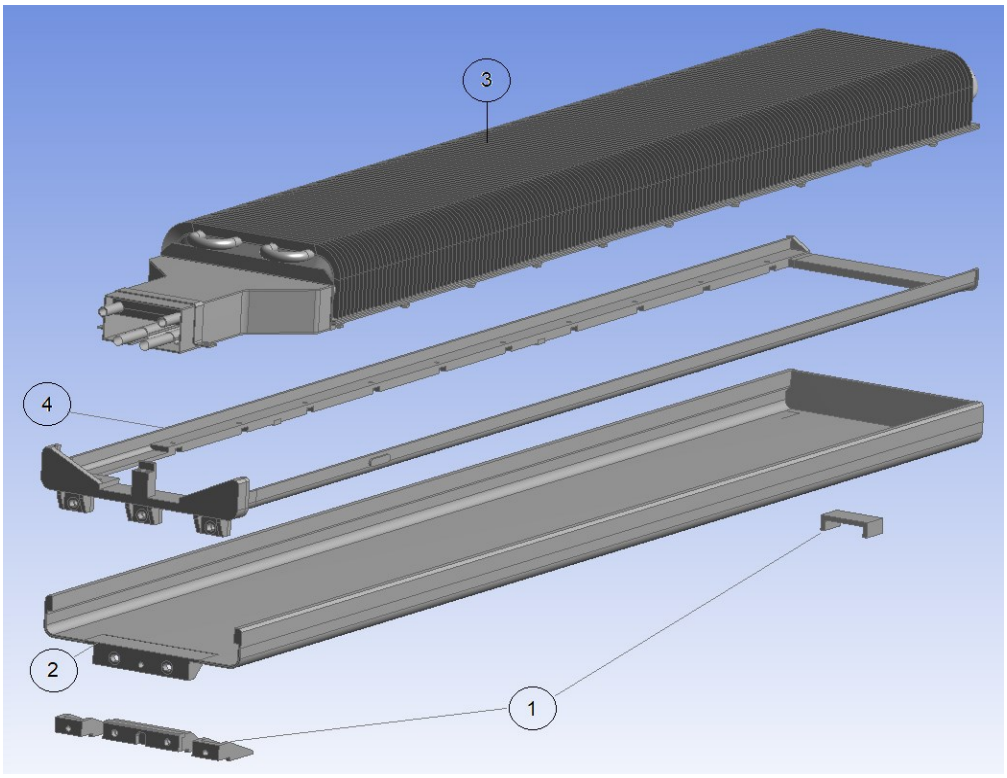

Figure 3.9. Components of the cryopump

1:Fixations welded to the inner wall of the vertical port.

2:Frame-tray as “Guide rail” for the frame and heat protection (hot Port wall).

3:Cryopump (total assembly) with bolts connected to the frame.

4:Frame with sliding in the tray and fixed at the end (Frame-Tray).

The material chosen for the cryopumps is **AISI 316L** (let's remember that the material for the VV and ports is AISI 316LN, which, compared to AISI 316L, has a different chemical composition that implies a lower magnetic permeability after welding and higher mechanical properties, which are not required for the cryopumps).
Cryopumps also present an electrical and thermal insulation layer (green layer in *Fig. 3.10*) that allows to keep the cryogenic temperature. The material chosen as insulant is **Torlon 4203**.

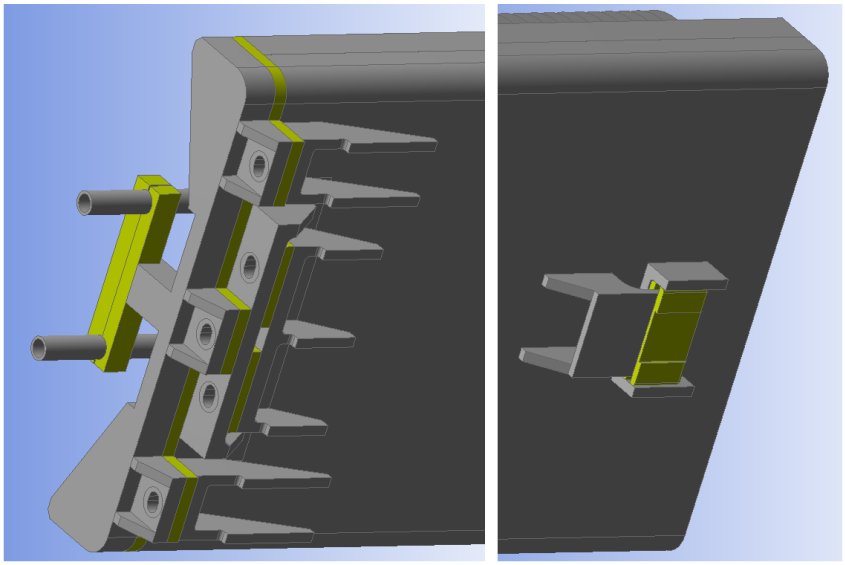

Figure 3.10. Cryopump supports.

The top fixation is designed so that the cryopump is electrically insulated in respect to the port. Knowing this, it's not so important to evaluate the electrical potential of the cryopump since, even if some current path will pass through the screws by-passing the insulation layer, these paths are likely to be short.
That's an important assessment in the electromagnetic analysis, since electromagnetic forces must be evaluated in the mechanical stresses study.

A description of the cryopumps has been carried out. Anyway, a specific finite element model analysis (FEM) has already been assessed by other researchers, in a preliminary detailed design analysis.
For this reason, the cryopump will be schematically simplified in the following simulations, since it is not requested a high level of detail for this component, but only the effects of its presence inside the port.

3.5 Boundary box

Underneath the extension of port #5, directly in contact with the bottom disk of the cryostat base, a boundary box will be installed.
Its role is to be a partition and an interface between the vacuum of the VV and the atmosphere: through this volume it will be possible to have access to the pumping groups and all other auxiliaries present in that region of the machine.
This box is closed in his bottom side with a flange, where the feeders and water pipe's bellows will be installed.

The next figures are useful to give an idea of this component from a functional point of view; the real geometry will be different, since it is expected that each boundary box will host two ports #5. Anyway, for the purposes of this work, this geometrical approximation is acceptable. What is important is the axial dimension of the box, since it will determine also the length of the auxiliaries and hence their displacements.

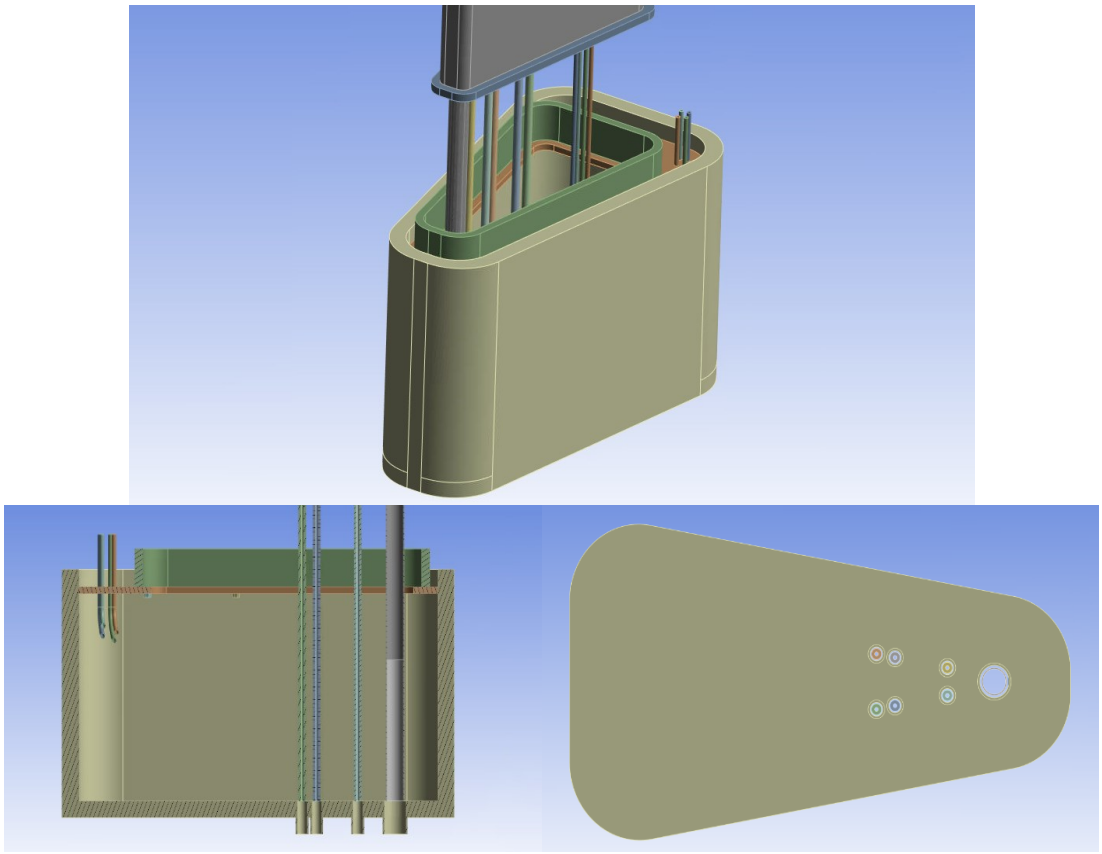

Figure 3.10: Boundary box: isometric view, side section, and bottom view.

The feeders and the water pipe are connected to the vacuum vessel on one side, and to the boundary box through the bellows on the other. Since the boundary box is directly connected to the cryostat base, these components will suffer for the relative displacement between VV and the cryostat base. That's the reason why bellows are necessary in this configuration.
An exception can be made for the cryopump pipes.
Their geometry and material (AISI 316L, the same of the cryopump itself), in fact, is studied in such a way that a bellow is not necessary for their displacements.

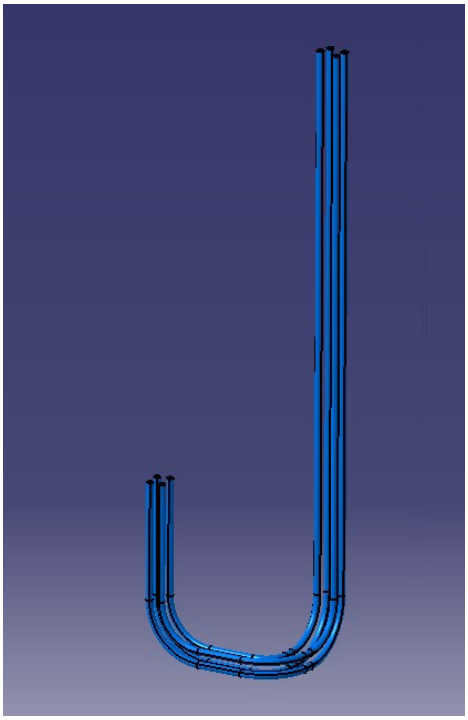

Figure 3.11: Cryopump pipes.

When these tubes cool down and contract, what happens is that the tubes tend to move upwards, leading to a flexion of the horizontal portion of the tube itself, similarly to a bent shelf with weights on top.
Hence a displacement is imposed to the horizontal stroke of the tube (colored in orange in the following scheme), which takes a shape similar to the green one.
The longer is this horizontal portion of tube, the softer the deformation will result.
That's because the displacement is constant, since it depends on the thermal expansion coefficient, and so the longer this portion is, the lower the slope will be.
Here's the reason why this horizontal "arm" must be long: this configuration allows the tube to deform in his length without the need to install a bellow.
This solution could not be feasible in the case of the feeders, since, being made in copper and stainless steel, they're too rigid and could not bend in the same way as the cryopump pipes.

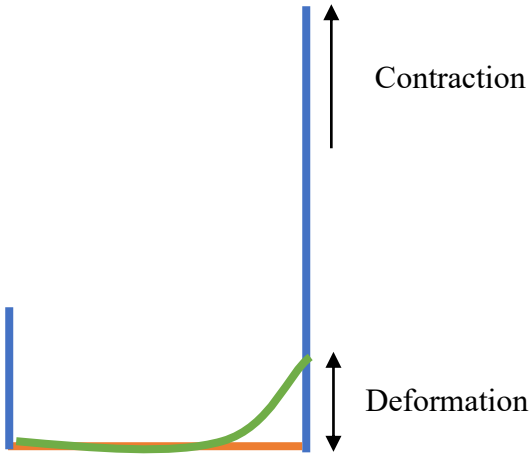

Chapter 4

Simulation analysis: input data and assumptions

A finite element model (FEM) analysis will be carried out to study the behaviour in different operative conditions of all the components of port #5.
The software chosen for the simulations is Ansys: this engineering software developed by Ansys Inc., is used to simulate computer models of structures, electronics, or machine components for analysing the strength, toughness, elasticity, temperature distribution, electromagnetism, fluid flow, and other attributes.

4.1 Geometrical simplifications and assumptions

Ansys is a very precise and reliable software; anyway, some simplifications are still necessary in order to make the model less heavy and easier to run.
In the following paragraph, all the geometrical simplifications assumed will be presented.
Let's remember that DTT will present 18 sectors, and so 18 port #5. One every three port #5 has actually only function of gravity support (GS) for the vacuum vessel, and so they're not considered in this analysis.
Each port #5 may or may not feature the components presented before. In the following table, the layout of the 18 sectors is shown.

SECTOR -->		1	2	3	4	5	6	7	8	9
Port 5 (or GS)	Cooling tubes	1 VV inlet		1 VV inlet		1 VV inlet	(GS)	1 VV inlet		1 VV inlet
	In-vessel coil feeders			(GS)			(GS)	2 IVC3 2 IVC4 2 IVC5	2 IVC3 2 IVC4 2 IVC5	(GS)
	Pumping panels	1 cryo	1 cryo	(GS)		1 cryo	(GS)	1 cryo	1 cryo	(GS)

SECTOR -->		10	11	12	13	14	15	16	17	18
Port 5 (or GS)	Cooling tubes		1 VV inlet	(GS)	1 VV inlet		1 VV inlet		1 VV inlet	(GS)
	In-vessel coil feeders			(GS)			(GS)			(GS)
	Pumping panels	1 cryo	1 cryo	(GS)	1 cryo	1 cryo	(GS)	1 cryo	1 cryo	(GS)

Table 4.3. Layout of the 18 port 5.

There is no reason to repeat the simulation for each different configuration of port 5. So, the choice is to evaluate the worst case, where all the components are present inside the port: the model considered is essentially the port of sector 7.

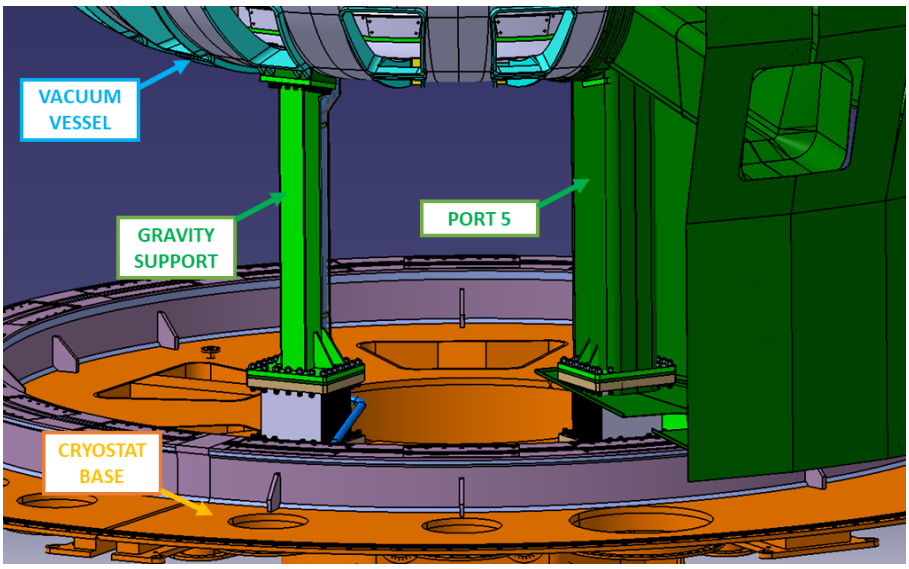

Figure 4.24. Cryostat configuration: gravity support and port 5

-Cryopump

As already mentioned in Chapter 3, a preliminary detailed FEM analysis of the cryopump has already been carried out by other researchers.
Let's consider that the cryopump presents more than 160 chevron baffles 1 mm thick. Indeed, using the real geometry of the cryopump would end up making the model a lot heavier, and the mesh would result difficult to be generated in a proper way.
A possible solution would be to consider simply a rectangular shell element, with the same dimensions of the cryopump, positioned tangent to the supports on the lateral surface of the port: in this way, the conduction thermal exchange would results pretty precise, even if simplified.
To better analyse also the irradiation exchanges, it is possible to "give a volume" to this shell element by introducing also the dimensions orthogonal to the shell. In this way, the effects of the presence of the cryopump inside the port is close to the actual one.
Note that, when this volume is generated in Ansys, the mass of the object will be calculated by the software, consistently with the assigned material; consequently, the thermal capacity is given too.
Anyway, since the cryopump temperature, as it will be presented, is one of the

conditions imposed in the model, the thermal capacity doesn't play any role in the final results.

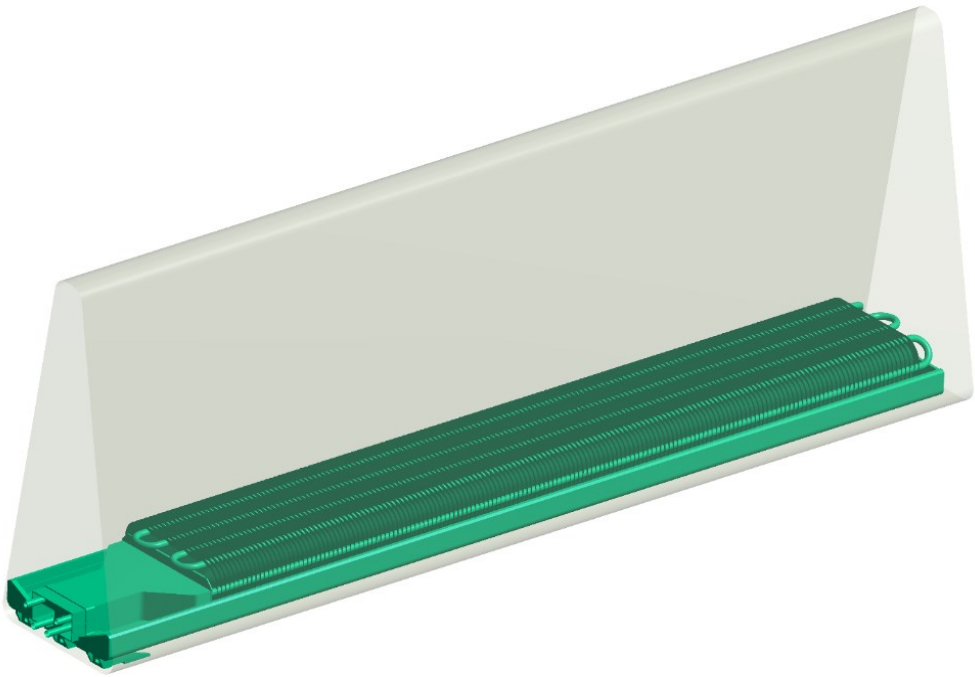

Figure 4.25. Real cryopump

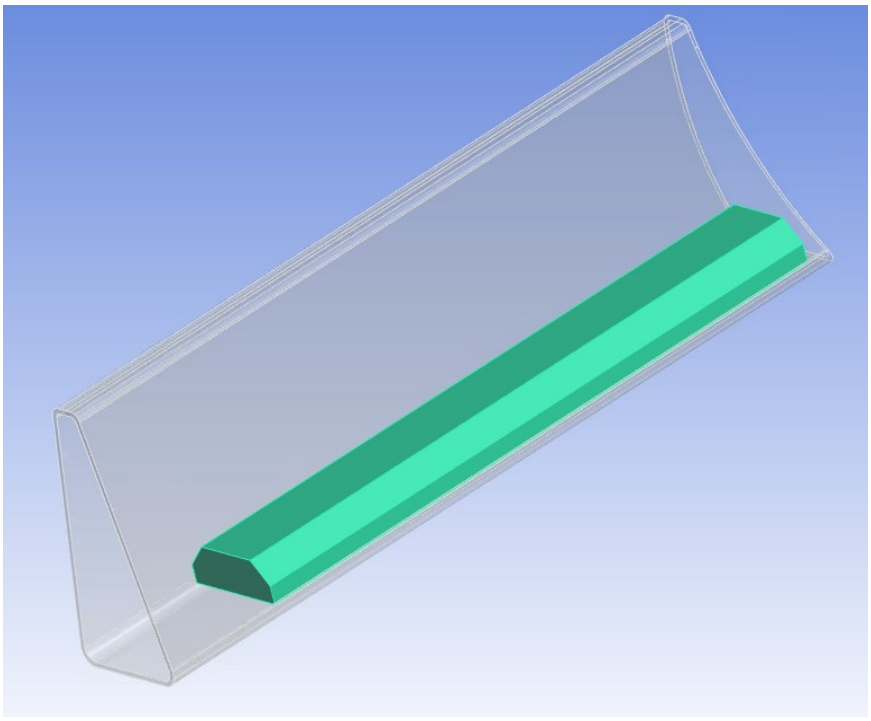

Figure 4.26. Simplified cryopump

-IVC Feeders

Fig.4.4 shows the cross section of the feeders for the IVC.
As can be seen, they have a multilayer configuration, with water flowing inside the cavity at the center.

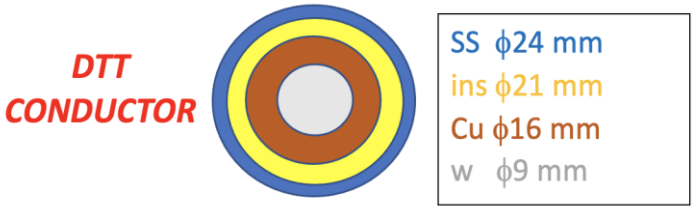

Figure 4.27. Schematic cross section of IVC feeders.

The external diameter is equal to 24mm, while the internal diameter is 9 mm.
The external layer is made of stainless steel and the internal layer is made of copper, with an insulation layer (Teflon) between the two layers.
In the following analysis, the most important material parameter for the feeders is the thermal expansion coefficient, since it will determine the deformation and stresses on the feeders.
Copper and stainless steel have the same thermal expansion coefficient:

$$\alpha = 1.7 * 10^{-5} \quad [\frac{1}{^{\circ}C}] \tag{4.1}$$

This means that they have the same behaviour in terms of displacements.
As regards the insulating layer, on the other hand, even if it has a different thermal expansion coefficient and therefore expands less, in reality it will be bound by the copper and steel at least in the bent areas. In fact, it will not be able to flow freely between the two layers like a fluid, and having a very low mechanical stiffness, it will dilate and change its characteristics to "chase" the expansions of copper and steel, which are the materials that impose the expansions being more rigid.
For these reasons, it is acceptable to consider the feeders as tubes of homogeneous material with external diameter equal to 24mm and internal diameter equal to 9mm, with water flowing inside the cavity.

-Bellows

These components have already been presented in the previous chapter.
In the model 8 bellows are present: one for the lateral surface of the port, one for the water pipe and one for each single feeder (6 in total).
Their geometry isn't defined yet: one of the purposes of this analysis is to select the right bellow based on the results.
Bellows will be selected from catalogues of two different constructors: *BOA Group* and *Witzenmann*.
Ansys allows to simulate the behaviour of a generic spring element by connecting two different parts and giving a spring rate as input data.
The model, indeed, won't present the geometry of the bellows, but only a graphical representation of a spring connecting the two extremities considered.
These bellows will undergo deformations in all three dimensions (axial, toroidal, poloidal), but with different stiffnesses. To simulate this behaviour, at every connection

three springs element are defined, one per each direction, and an APDL command snippet is added to the model: element *Combin14* is assigned to the springs. In this way, it is possible to assign a different stiffness in the three directions.
From Ansys help page: Combin14 is a spring element that *"has longitudinal or torsional capability in 1-D, 2-D, or 3-D applications. The longitudinal spring-damper option is a uniaxial tension-compression element with up to three degrees of freedom at each node: translations in the nodal x, y, and z directions. No bending or torsion is considered. The torsional spring-damper option is a purely rotational element with three degrees of freedom at each node: rotations about the nodal x, y, and z axes. No bending or axial loads are considered*.".
Right away the APDL command implemented are presented:

```
!COMBIN LUNGO X POLOIDALE


ET,_sid,14
!*
KEYOPT,_sid,1,0          !Linear Solution (default)
KEYOPT,_sid,2,1          !KEYOPT(2)=1   :        1-D longitudinal spring-damper (UX degree of freedom)


R,_sid,666,0,0,, !Spring constant - damping coefficients
```

```
!COMBIN LUNGO Y TOROIDALE


ET,_sid,14
!*
KEYOPT,_sid,1,0          !Linear Solution (default)
KEYOPT,_sid,2,2          !KEYOPT(2)=2   :        1-D longitudinal spring-damper (UY degree of freedom)


R,_sid,233,0,0,, !Spring constant - damping coefficients
```

```
!COMBIN LUNGO Z ASSIALE


ET,_sid,14
!*
KEYOPT,_sid,1,0          !Linear Solution (default)
KEYOPT,_sid,2,3          !KEYOPT(2)=3   :        1-D longitudinal spring-damper (UZ degree of freedom)


R,_sid,508,0,0,, !Spring constant - damping coefficients
```

These commands are assigned to the spring element according to the direction of deformation considered.
Damping effects aren't considered, and so damping coefficients are null.
The values of the spring constants in the code are referred to the case of the port bellow.
Port bellows for DTT are custom built: geometrical parameters and spring coefficients are given to the constructor that realizes the custom bellow. The following values are chosen mainly based on the expected displacements, on the number of cycle required and on the imposed pressure difference.
In the case of port #5, the given parameters are:

2: bellows inner poloidal size [mm]	3: bellows inner toroidal size [mm]	2: bellows outer poloidal size [mm]	3: bellows outer toroidal size [mm]	bellows building length [mm]	1: bellows axial spring rate [N/mm]	2: bellows poloidal spring rate [N/mm]	3: bellows toroidal spring rate [e] [N/mm]
780	360	920	500	450	508	666	233

Table 4.2. Port bellow parameter

Based on the nominal diameter and on the pressure where it will be installed (vacuum inside the cryostat), the chosen bellows for the feeders and the water tube from *Witzenmann* catalogues are the following:

UNIVERSAL EXPANSION JOINTS FOR LOW PRESSURE WITH WELD ENDS

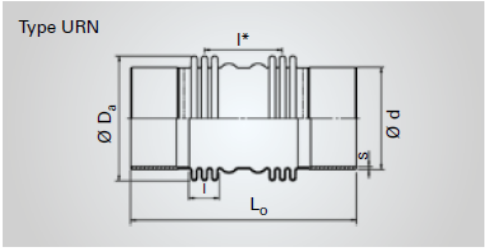

Nom-inal dia-meter	Axial Movement absorption Nominal	Type URN 01...	Order number standard version	Overall length	Weight approx.	Centre-to-centre distance of bellows	Weld ends	
							outside diameter	wall thickness
DN	$2\delta_N$	–	–	L_0	G	l*	d	s
–	mm	–	–	mm	kg	mm	-	mm
50	56	.0050.056.0	425696	480	1.4	257	60.3	4
65	83	.0065.083.0	425697	520	2.2	279	76.1	4
80	95	.0080.095.0	425698	530	2.6	280	88.9	4
100	119	.0100.119.0	425699	550	3.4	291	114.3	4
125	144	.0125.144.0	425700	550	4.2	286	139.7	4

Bellows			Nominal movement absorption[1)] at 1000 load cycles		Spring rate		
outside diameter	corrugated length	effective cross-section	angular	lateral	axial	angular	lateral
D_a	l	A	$2\alpha_N$	$2\lambda_N$	c_δ	c_α	c_λ
mm	mm	cm^2	degree	mm	N/mm	Nm/deg	N/mm
89	63	46	41	154	37	0.9	1.6
107	81	68.7	49	197	28	1.1	1.5
121	90	89.1	49	196	26	1.3	1.8
148	99	137	49	203	24	1.8	2.4
174	104	187	49	204	18	1.9	2.5

Figure 4.5. Characteristics of bellows for services

For the water tube, which has a diameter of 60mm, the bellow with a nominal diameter of 125mm is chosen. This bellow can be installed through welding and can absorb up to 144mm of movement in the axial direction (72mm of compression and 72mm of elongation).
For the feeders, which have a diameter of 24mm, the bellow with a nominal diameter of 65mm is chosen. It can absorb up to 83mm of movement in the axial direction (41.5mm of compression and 41.5mm of elongation).
Spring rate (stiffness) is given for the axial and lateral (poloidal and toroidal) directions, and an angular spring rate is given too. Anyway, there is a correlation between angular and lateral movement given by:

$$C_a = C_{lat} * l^{*2} * \frac{\pi}{360} * 10^{-3} \quad [\frac{Nm}{deg}] \tag{4.2}$$

Where l* is the centre-to-centre distance of bellows.
Indeed, angular and lateral spring rates are two different coefficients representing the same behaviour.

-Services supports
The last simplification of the model regards the supports of feeders and water tube. These components will be fixed to the port wall by using some “collar” supports. This means that feeders and water tube are free to expand or compress along the axial direction, but they will follow the displacements of the port in the other two directions.

Three supports will be installed to the closest wall along the length of each feeder, and each support is designed so that it will host two feeders.
For the water pipe, two supports are expected to be installed, one at the top of the port and one close to the flange connecting the port to the bellow.
To allow for an easy installation of these supports, it is important to consider a different installation height of each couple of supports, in order to prevent clutter problem in phase of fixing by bolt.
For this reason:
-the three supports of feeders #1 and #2 are installed at a distance from the top of the port respectively of 175mm, 925mm and 1675mm.
- the three supports of feeders #3 and #4 are installed at a distance from the top of the port respectively of 375mm, 1125mm and 1875mm.
- the three supports of feeders #5 and #6 are installed at a distance from the top of the port respectively of 625mm, 1375mm and 2125mm.
Similarly to the case of the bellows, in Ansys the supports aren't modelled geometrically.
Anyway, their presence can be considered in other ways.
After generating the mesh of the model, a constraint equation is set between the nodes of the feeders at the height described before and the nodes of the closest wall at the same height. These constraint equations impose a constant distance between these nodes in the directions orthogonal to the axis of the tubes, leaving only one degree of freedom, the axial one. Rotations are prevented too.
In this way, the tubes are forced to follow the movement of the port but they're free to compress or expand along the axial direction.

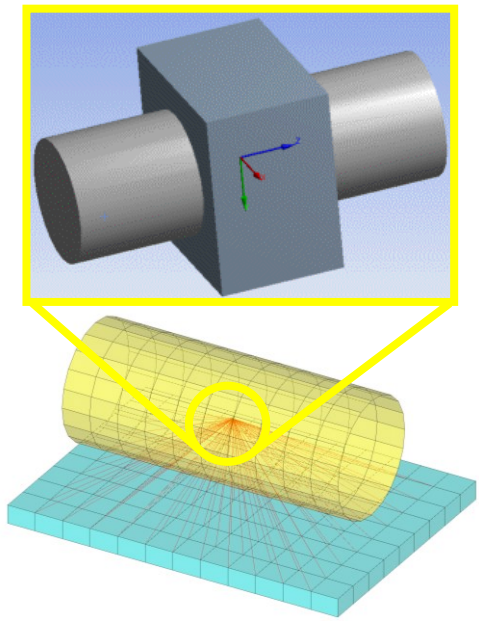

Figure 4.6. Support model

4.2 Operative cases and Materials

-Operative conditions
The operative scenarios of DTT machine have been described in paragraph 2.7.
The normal load case can be summarised in three different phases:
-Standard operation (plasma on);
-Regeneration of cryopump;
-Baking (strong/light).
However, in the design phase, some possible accident must be hypothesized, to consider a certain safety margin.
For example, the possibility of an **earthquake** to occur during the lifetime of the machine must be considered, since the stresses that it would cause to it are relevant.
Another possible cause of accident is the **leakage of water or helium** due to breakage of an in-vessel component such as in-vessel coil, first wall, divertor, pipes…
Because of this break up, some water evaporates inside the vacuum vessel; as well as wetting the first wall, this leakage leads to a pressurization of the VV:
If the leakage continues, pressure keeps on rising up to a maximum value of 1.2 bar absolute: at this point, some valves and a rupture disk intervene to limit the pressure inside the VV.
Being directly connected to the VV, port#5 will have the same internal pressure.
In this scenario, the pressure inside the port is 1.2 bar, while the external pressure is null (vacuum inside the cryostat).
Service bellows, in standard operation, will be subjected to the ambient pressure on one side, and to vacuum on the other; during this event, instead, they will still be subjected to ambient pressure on one side, but on the other side they will be subjected to a pressure of 1.2 bar, and this may lead to a different deformation of the bellow.

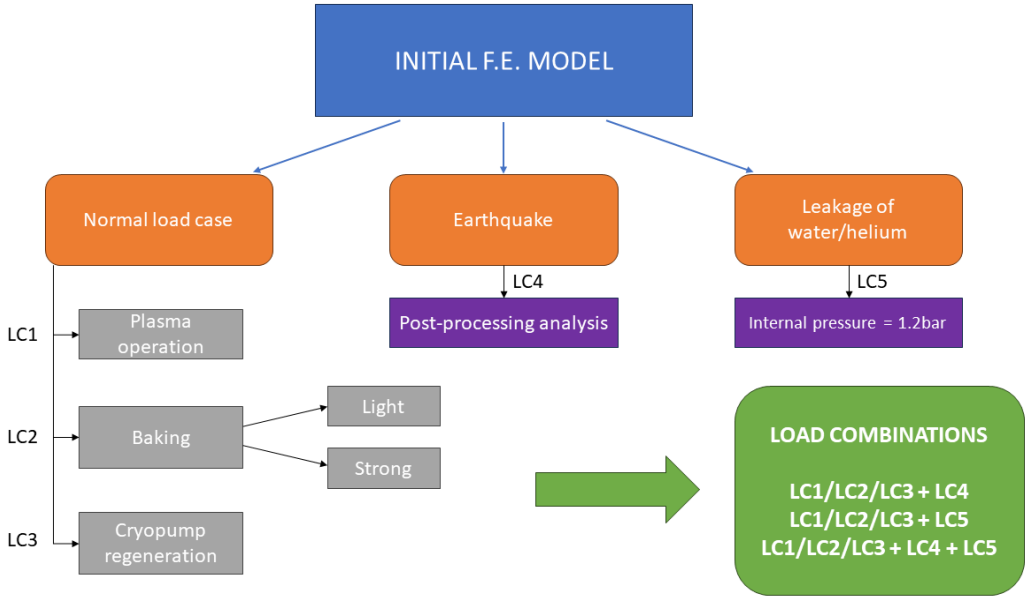

Figure 4.7. Combination of load cases

To each scenario corresponds a certain safety coefficient for the design.
Worst scenarios may lead to serious damage to the machine, but the chance of them

happening is very low.
Safety coefficients are lower for these scenarios because, in case of severe accidents, a certain damage to the machine is acceptable since the priority is the safety of people and workers in the proximity of the structure.
On the other hand, during normal load cases, safety coefficients must be higher in order to guarantee a certain operative margin to prevent damage to the machine.

-Materials

Considering the approximation described in the paragraph on the feeders material, the model present only three different materials:
-Stainless Steel AISI 304
-Stainless Steel AISI 316L
-Stainless Steel AISI 316LN
Stainless Steel 316L and 316LN differs only on a different magnetic permeability after welding. For the purpose of this work, this difference is negligible.
In the following table, the main thermal characteristics of SS304 and SS316L are shown:

	Stainless Steel AISI 316L	**Stainless Steel AISI 304**
Thermal Conductivity (W/(m*K))	16	16.2
Thermal Expansion Coefficient (1/K)	1.72E-05	1.73E-05

Table 4.3. Material Properties @Room Temperature

The chemical composition for these two materials is the following.
Stainless Steel AISI 316L: 12% Ni, 17% Cr, 2.5% Mo, 2% Mn, 1% Si, 0.03% C max, Rem. Fe
Stainless Steel AISI 304: 8 to 12% Ni, 18 to 20% Cr, 2% Mn max, 1% Si max, 0.03% C max, Rem. Fe
Thermal expansion coefficient is the most important parameter for this analysis, since it determines the thermal displacements of the components; it is almost equal for the two materials.
To study the cryopump pipes behaviour, it is useful to have some information about the mechanical properties of AISI316L.
It's yield strength is given in the following graph as function of temperature:

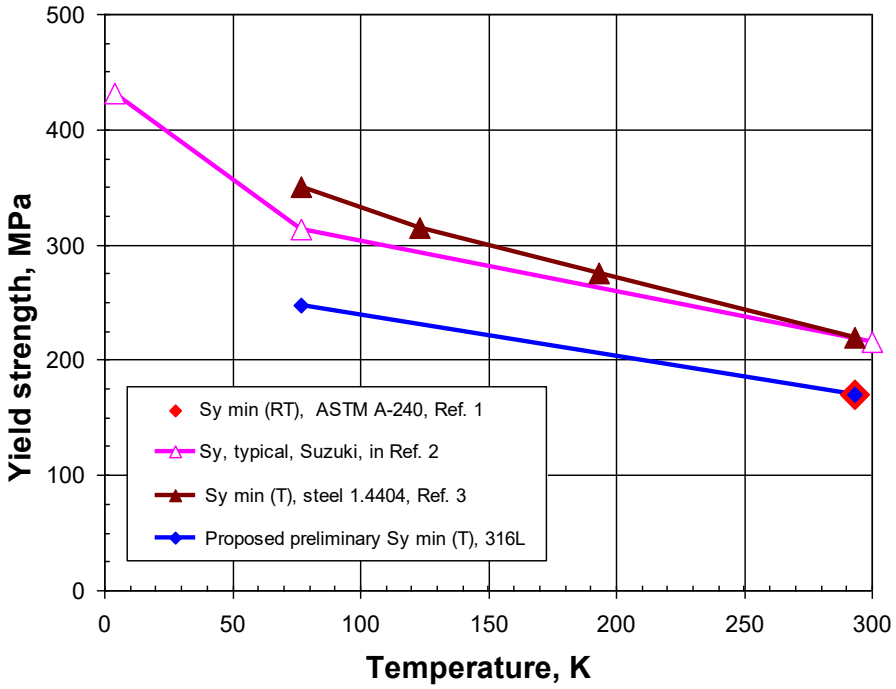

Figure 4.8. AISI316L Yield Strength vs Temperature

These properties will be used to verify the adequacy of the cryopump pipes shape.

4.3 Mechanical analysis set-up

Superposition principle

Let's start looking in detail to what happens to the port when the machine is in one of the three operative conditions mentioned.

This analysis aims to evaluate in particular the relative displacements between the cryostat base and the Vacuum vessel. The general rule used in this study is to keep fixed the elements below the port bellows (cryostat side) and evaluating the displacements of the other components with this reference (let's remember that the tubes are connected to the port surface through the constraint equation, representing the supports, and to the boundary box between spring, representing the bellows).

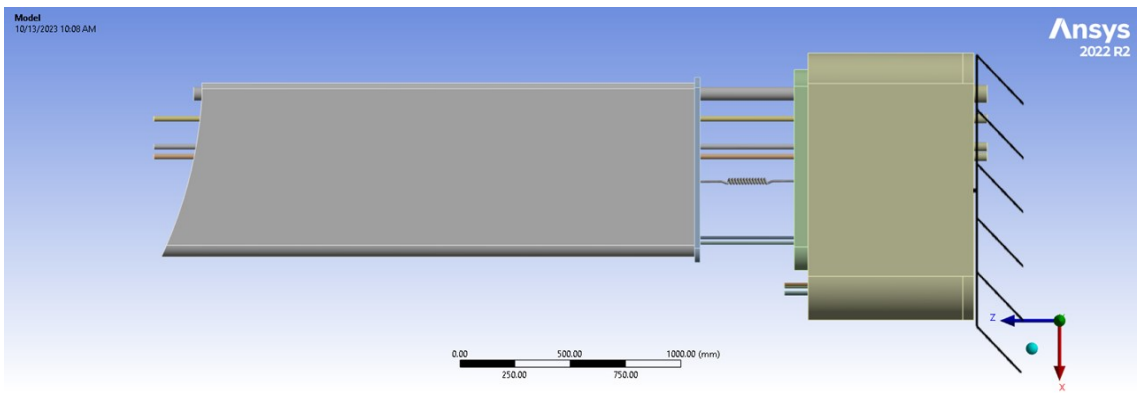

Figure 4.9. Mechanical constraint: fixed joint at boundary box

This movements can be studied through the combination of displacements of different origins: the superposition principle is used.
-The first component is the **expansion of the port** due to its temperature.
As will be shown, at each operative condition corresponds a different temperature profile of the port duct. Thie inner surface of the port duct is heated up due to the contact with the VV, whereas the external side is cooled by the Thermal Shield at about 80K. The overall increase in temperature implies a dilatation of the port itself, which is imposed downwards towards the cryostat, since on the other side the vacuum vessel prevents this dilatation: this leads to a contraction of the port bellow.
This dilatation is evaluated through FEM analysis.

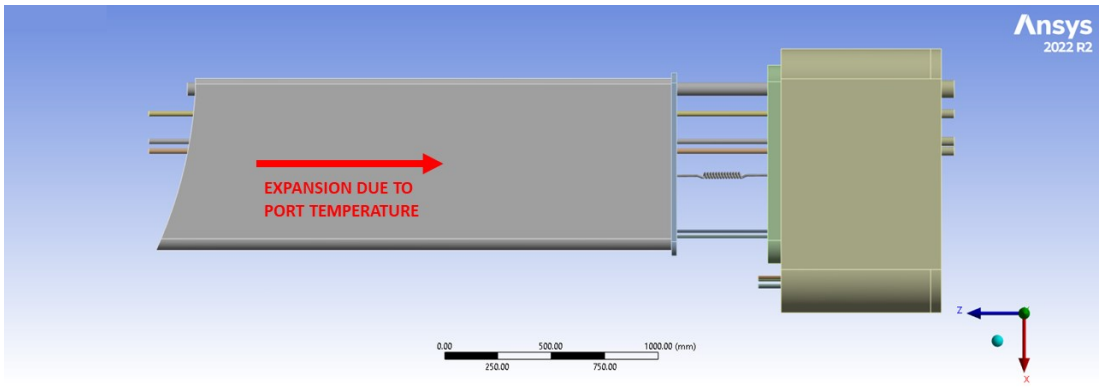

Figure 4.10. Direction of the port expansion due to its temperature

-The second component is the **expansion of the gravity support** (GS).
As already mentioned in *Table 4.1*, the vacuum vessel is supported by six gravity supports, that are positioned in the same location of port #5 in six of the 18 sectors of the machine (see *Fig.4.1*).
Being in contact with the Vacuum Vessel, the GS will expand because it heats up. Since it is rigidly installed to the cryostat base (no bellows), the effect of this expansion is a movement upwards of the entire vacuum vessel. This displacement is obviously seen also by port #5.

This dilatation can be evaluated through the following equation:

$$z_{disp\ GS} = l_{GS} * \alpha_{GS} * \Delta T \quad [mm] \tag{4.3}$$

Where:
l_{GS} is the length of the gravity support;
α_{GS} is the thermal expansion coefficient of the GS material (AISI 316LN);
ΔT is the temperature difference between the average temperature of the GS and the reference temperature (ambient temperature = 20°C).

-The third component is the **expansion of the vacuum vessel**.
Vacuum vessel is a double-walled structure: hot water flows inside the inner-shell between the two walls, heating up homogeneously the vessel.
The VV will expand symmetrically in respect to its axis, leading to:
-a compression of the port in the axial direction;
-a displacement on the poloidal direction towards the external of the machine;

-no movement on the toroidal direction, since the displacement is symmetrical in this direction.
VV is made of AISI316LN, and so the material properties are given in *Table 4.3*.
The poloidal displacements can be evaluated with eq.4.3 by replacing l_{GS} with the radius of the VV (calculated at the axis of the port) and ΔT with the temperature difference between the VV uniform temperature and the reference temperature (20°C).

The axial displacement, on the other hand, is given by:

$$z_{disp\_VV} = \left(r_{port} * \cos(90° - \theta_{pol}) * \frac{\pi}{180°} - h_{flange} * \sin(90° - \theta_{pol}) * \frac{\pi}{180°}\right) * \alpha_{VV} * \Delta T \ [mm] \quad (4.4)$$

Where:
r_{port} is the radius of the VV calculated at the axis of the port;
θ_{pol} is the poloidal orientation (θ_{pol}=0° for port 5);
h_{flange} is the height of the port flange in respect to the cryostat base;
ΔT is the temperature difference between the VV uniform temperature and ambient temperature.

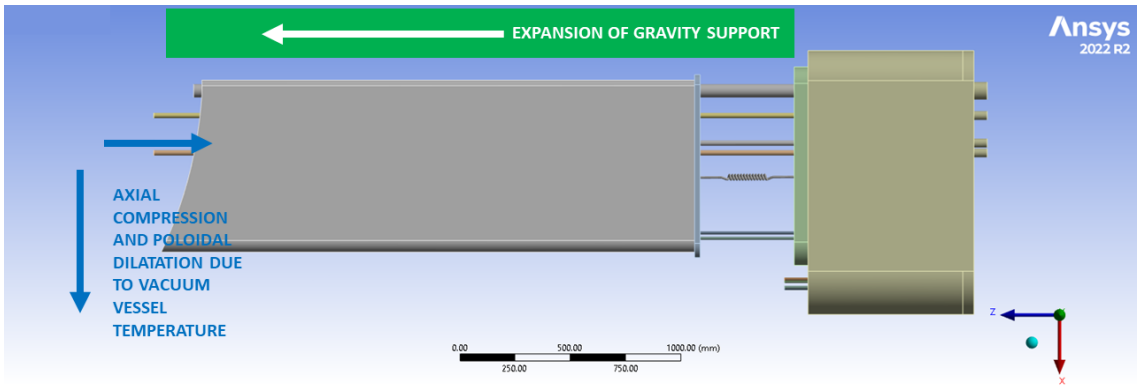

Figure 4.11. Displacement due to VV and GS expansion

-The fourth component is the **displacements due to seismic event**.
The seismic studies have been carried out through past analysis by *LT Calcoli*, a society working in the field of numerical analysis.
They evaluated the relative movements between the cryostat and the vacuum vessel by fixing the cryostat side and letting free the VV, in the case of an earthquake causing a maximum acceleration equal to 0.567 g (05.56 m/s^2).

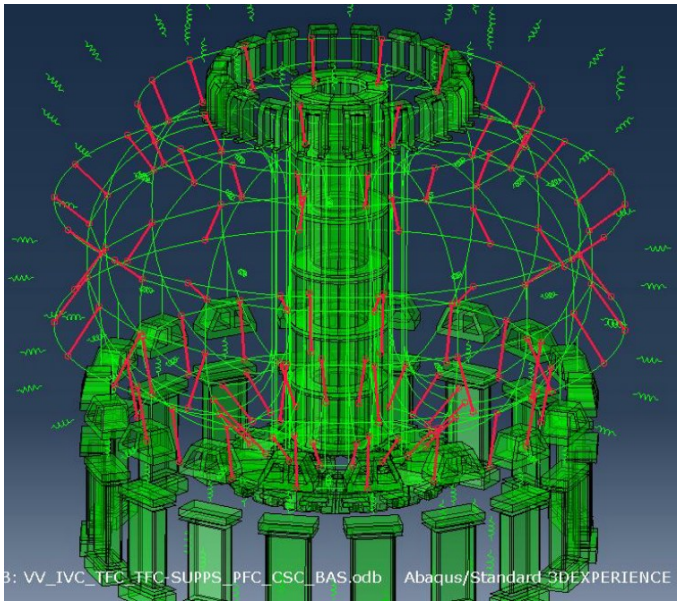

Figure 4.12. Acceleration spectrum during seismic event. Courtesy of LT Calcoli

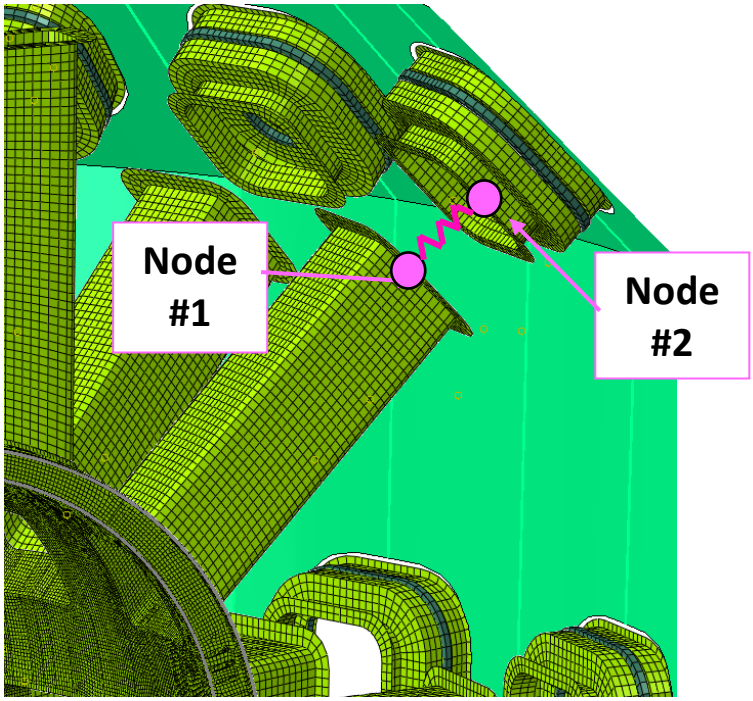

Figure 4.13. FEM Model. Courtesy of LT Calcoli

Following the same principle, the seismic load will be considered by imposing a relative displacement to the components above the bellows.
In particular, the displacements are shown in the following table:

1: Axial (±) [mm]	2: Poloidal (±) [mm]	3: Toroidal (±) [mm]
0.5	9.8	10.3

Table 4.4. Seismic displacements

Only the displacement acting in the same direction of the other effects are considered.

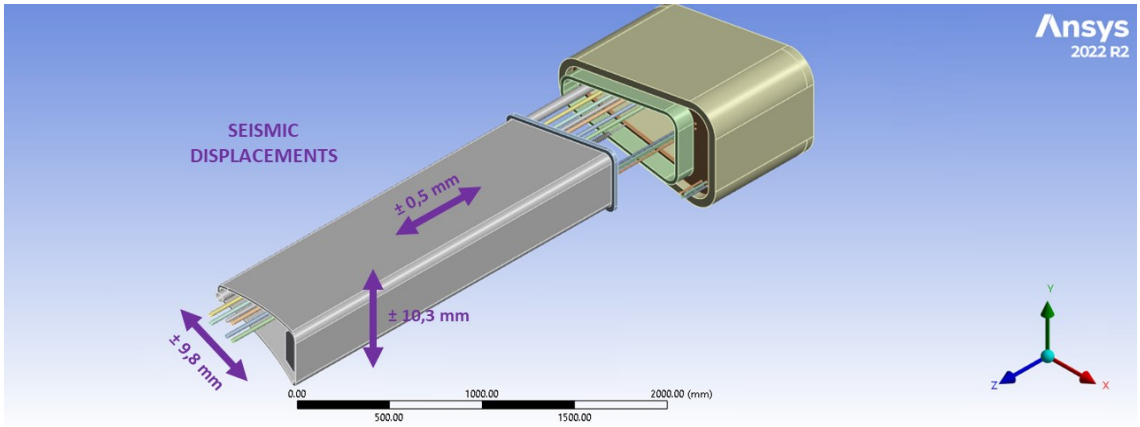

Figure 4.14. Displacements due to seismic event

-The fifth, and last, component is due to the **ingress of liquid inside the vacuum vessel**.
This condition regards, in this analysis, exclusively the service bellows.
The pressure inside the port is set at 1.2 bar: service bellows will experience this pressure, instead of null pressure, at the port side, while it will experience the atmospheric pressure on the other side.

4.4 Temperature set-up

The temperature of the components plays a major role in the mechanical analysis.
The port surface heats up due to the contact with the VV, while the tubes (feeders and water pipe) are heated up by the fluid flowing inside them.
The temperature considered as input in the model are the following:
- Port surface temperature;
- In-Vessel coil fluid temperature: T_{in} and T_{out}
- First Wall water (flowing inside the pipe)
- Cryopump Helium
- Cryopump baffle
- Cryopump panels

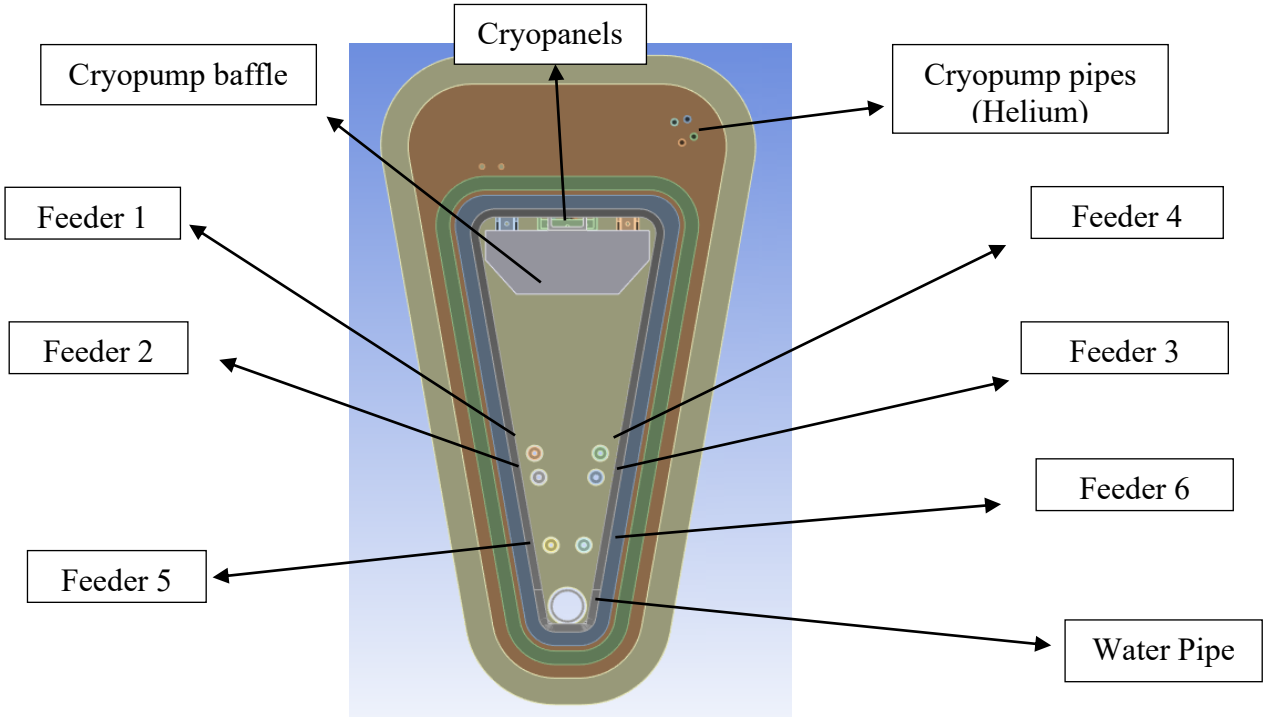

Figure 4.14. In-port components and feeders numbering

Fig.4.14 shows the configuration of the component inside the port, and gives a number to distinguish one feeder to the others.
For the sake of simplicity, the cryopanels temperature is assigned to the back surface of the simplified cryopump, while the baffle temperature is assigned to the front surfaces.
The in-vessel coil fluid enters from a feeder, flows inside the IVC and goes out through another feeder: indeed, there are 3 "inlet" feeders and 3 "outlet" feeders.
Feeders number 2, 4 and 5 are inlet feeders (T_{in}), while feeders number 1, 3 and 6 are outlet feeders (T_{out}).

-Port surface temperature
The temperature of the port duct varies along the length of the port from the VV temperature to the cryostat (ambient) temperature with a certain profile.
The profile temperature of the port surface has been studied for port #4 by *EUROfusion* (report *DIV-IDTT.S.11-T002-D003_Assessment of baking operating state for vacuum vessel & ports, [16]*).

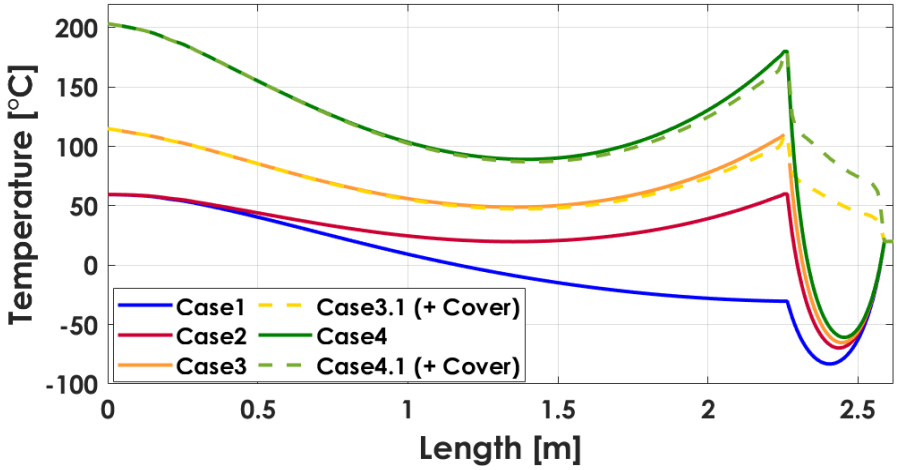

Figure 4.15. Port 4 surface profile temperature at different load cases [16] [EUROfusion DIV-IDTT.S.11-T002-D003]

Fig.4.15 shows the profile temperature of port 4 at different load scenarios.

Case #	State
1	POS
2	POS (HEATER ON)
3	L-BAK
4	S-BAK & CRYOPUMP REGEN.

Table 4.4. Load cases and data used to evaluate port4 surface temperature.

The reference case for plasma operation state (POS) at port 5 is case 1 of the previous figure, since case 2 describe a scenario with heaters installed on the port surface working to avoid condensation problems. It's unlikely that heaters will work during plasma operation in port #5, since they would penalize the performance of the cryopump.
Case 1 is an acceptable reference for the port temperature of port #5; obviously, the profile must fit the different length between port 4 and 5, and so it will be normalized on the length of port 5.
For example, *Fig.4.16* shows how this temperature profile is applied at the port surface.

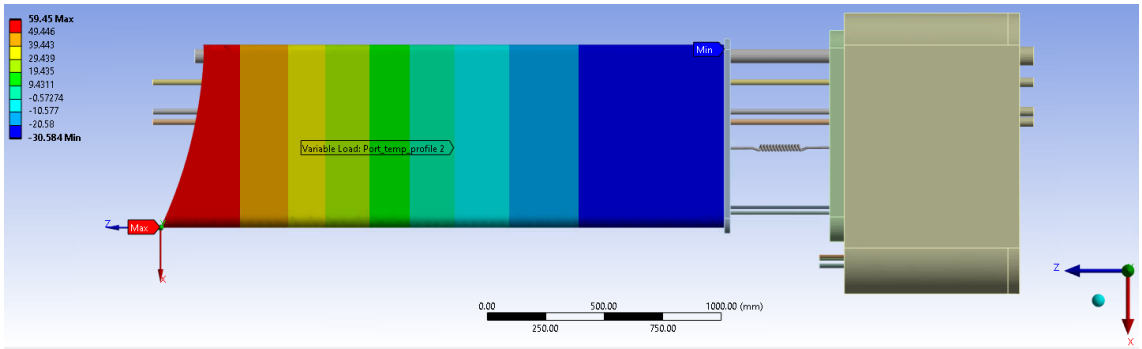

Figure 4.16. Temperature profile of inner port duct surface, Input

4.5 Summary of the input for each case

In the following chapter, a brief summary of all mechanical and thermal input is held.

-Normal Operation (POS)
Port surface temperature profile: Case1 in *Fig.4.14*.
In-Vessel coil fluid temperature: T_{in}=25°C, T_{out}=110°C
First Wall water: 80°C
Cryopump Helium: -268.65°C
Cryopump baffle: -193.15°C
Cryopump panels: -268.65°C

Displacements due to VV and GS expansion:

	Normal Operation
Cryostat temperature (°C)	20
VV temperature (°C)	60
Average temperature (°C)	40
ΔT (average-ambient) (°C)	20
ΔT (VV-ambient) (°C)	40
Axial Dilatation (mm)	0.928
Axial compression due to VV expansion (mm)	-0.126
Poloidal Expansion (mm)	1.472
Axial displacement (mm)	0.802

-Light Baking (L-Bak)
Port surface temperature profile: Case 3 in *Fig.4.14*.
In-Vessel coil fluid temperature: T_{in} = T_{out} =110°C
First Wall water: 130°C
Cryopump Helium: -173.15°C
Cryopump baffle: -173.15°C
Cryopump panels: -173.15°C

Displacements due to VV and GS expansion:

	L-Baking
Cryostat temperature (°C)	20
VV temperature (°C)	110
Average temperature (°C)	65
ΔT (average-ambient) (°C)	45
ΔT (VV-ambient) (°C)	90
Axial Dilatation (mm)	2.088
Axial compression due to VV expansion (mm)	-0.283
Poloidal Expansion (mm)	3.313
Axial displacement (mm)	1.805

-Strong Baking (S-Bak)
Port surface temperature profile: Case 4 in *Fig.4.14*.
In-Vessel coil fluid temperature: $T_{in} = T_{out} = 200°C$
First Wall water: 200°C
Cryopump Helium: -173.15°C
Cryopump baffle: -173.15°C
Cryopump panels: -173.15°C
Displacements due to VV and GS expansion:

	S-Baking
Cryostat temperature (°C)	20
VV temperature (°C)	200
Average temperature (°C)	110
ΔT (average-ambient) (°C)	90
ΔT (VV-ambient) (°C)	180
Axial Dilatation (mm)	4.177
Axial compression due to VV expansion (mm)	-0.566
Poloidal Expansion (mm)	6.626
Axial displacement (mm)	3.611

-Cryopump Regeneration
Port surface temperature profile: Case 4 in *Fig.4.14*.
In-Vessel coil fluid temperature: $T_{in} = T_{out} = 200°C$
First Wall water: 240°C
Cryopump Helium: -173.15°C
Cryopump baffle: -173.15°C
Cryopump panels: -173.15°C

Displacements due to VV and GS expansion:

	Cryopump Regeneration
Cryostat temperature (°C)	20
VV temperature (°C)	200
Average temperature (°C)	110
ΔT (average-ambient) (°C)	90
ΔT (VV-ambient) (°C)	180
Axial Dilatation (mm)	4.177
Axial compression due to VV expansion (mm)	-0.566
Poloidal Expansion (mm)	6.626
Axial displacement (mm)	3.611

Chapter 5

Results of the analysis

In the following pages the results of the FEM analysis are reported.
The goal of the analysis is to evaluate:
-the displacement of the components;
-how the bellows reacts to the displacements;
-the deformation and stresses on the cryopump pipes;
-the adequacy of the actual configuration and position of the in-port component.

5.1 Normal State Operation (POS) - RESULTS

The daily operation scenario, during DTT experimental time, shall be 10 hours per day, 4 days per week.
POS is the most frequent scenario: for this reason, even if it's not the most severe condition, it is important to understand how port #5 and its components behave during normal operation.
Given the low temperatures presented in the previous chapter, the displacements due to thermal expansion aren't expected to be large, with the exception of the cryopump pipes, inside which Helium flows at 4.5K.
The results for the POS will be presented following, step by step, the superposition principle presented in chapter 4.

RESULTS: DISPLACEMENTS DUE TO PORT AND COMPONENTS TEMPERATURE
The first component is the displacement due to the temperature of the port and its components only (VV and gravity support displacements are not considered yet).
Fig.5.1 shows the total deformation due to the thermal expansion (and compression) of port 5.

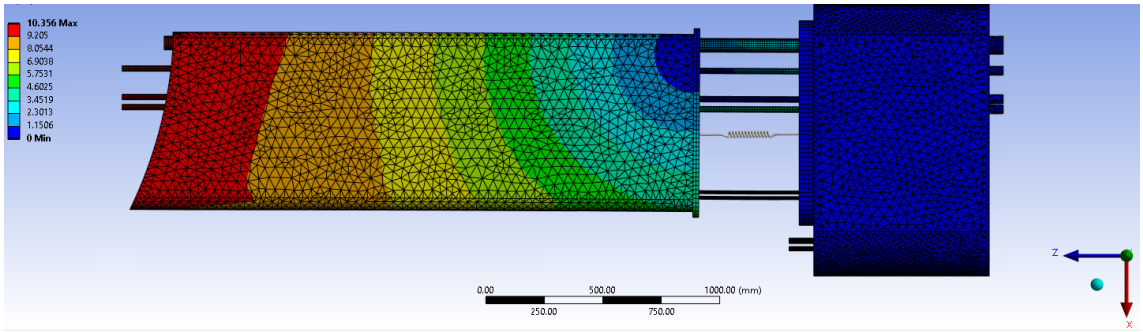

Figure 5.28. Total deformation due to temperature

To better understand this figure, let's analyse the directional displacement:

Displacements along X axis (POLOIDAL DIRECTION):

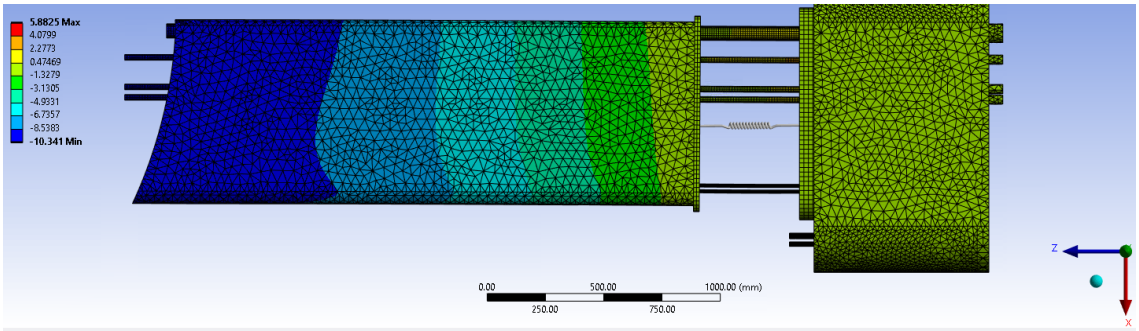

Figure 5.29. Directional deformation due to temperature (X axis)

Displacements along Y axis (TOROIDAL DIRECTION):

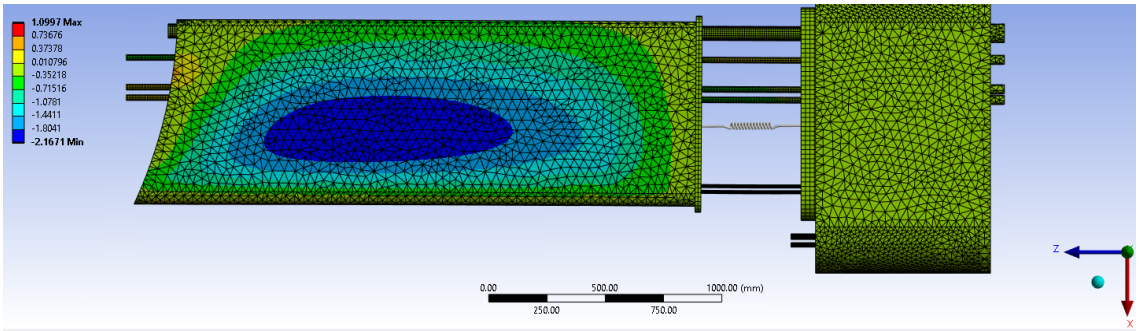

Figure 5.30. Directional deformation due to temperature (Y axis)

Displacements along Z axis (AXIAL DIRECTION):

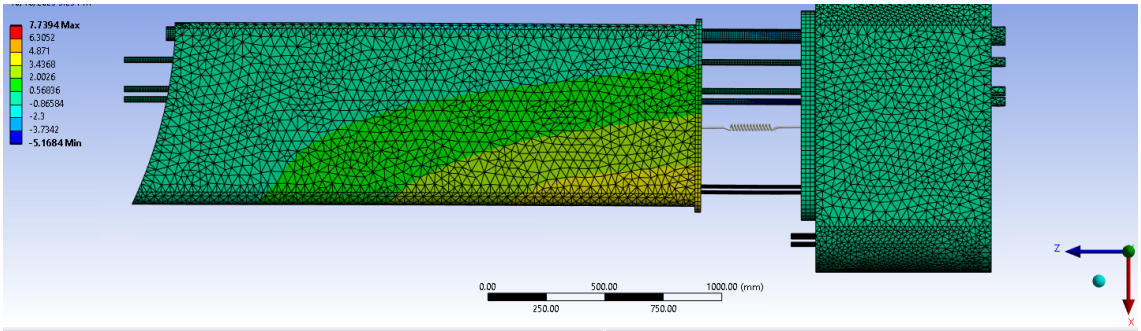

Figure 5.31. Directional deformation due to temperature (Z axis)

These results, taken alone, aren't so significant, since during the real operation the displacements due to VV and GS expansion occurs. Anyway, it is possible to make some considerations:
-along the poloidal direction, port moves towards the central axis of the machine;
-along the toroidal direction, displacements are small, due to the high symmetry of the

machine and the port;
-along the axial direction, port moves towards the cryostat base, compressing the bellow (it will be more evident on the other operative cases, in which the port temperature is higher).

RESULTS: DISPLACEMENTS DUE TO PORT COMPONENTS TEMPERATURE + VACUUM VESSEL AND GRAVITY SUPPORT DISPLACEMENTS

The second component is relative to the displacements due to Vacuum Vessel and Gravity Support thermal expansions.
In the following figures, these results are already combined with the results seen before.

Total deformations:

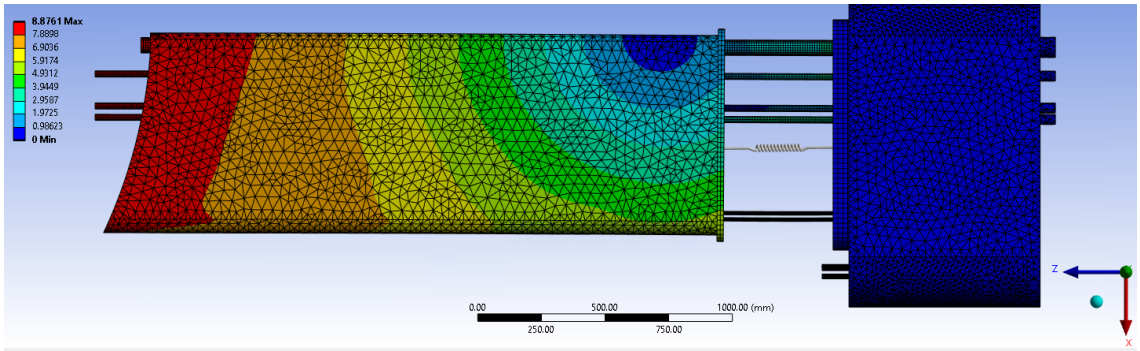

Figure 5.32. Total deformations due to port temperature + VV and GS expansions

Again, let's look at the directional displacements.
Displacements along X axis (POLOIDAL DIRECTION):

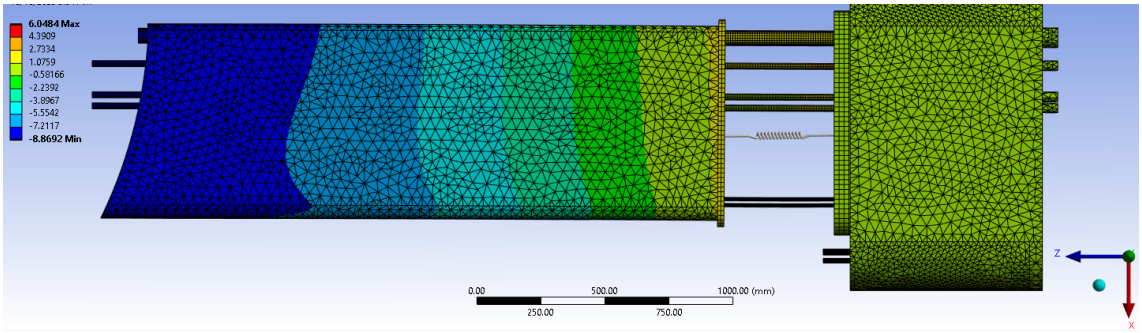

Figure 5.33. Directional deformations due to port temperature + VV and GS expansions (X axis)

The largest displacement occurs at the top of the port surface: in that region, the displacement is equal to -8.869mm (negative sign means that the movement is toward the central axis of the torus).

Displacements along Y axis (TOROIDAL DIRECTION):

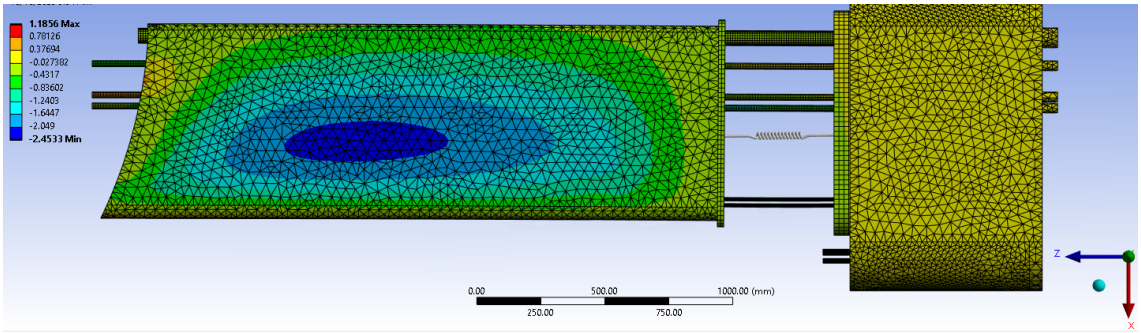

Figure 5.34. Directional deformations due to port temperature + VV and GS expansions (Y axis)

Displacements along Z axis (AXIAL DIRECTION):

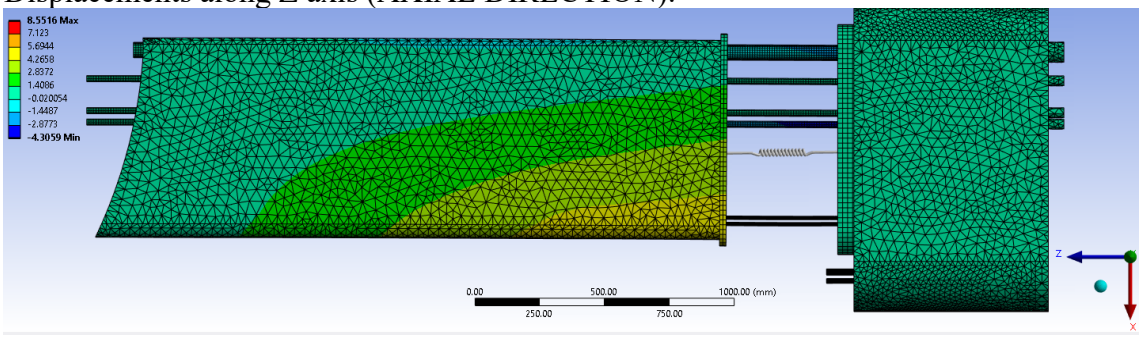

Figure 5.35. Directional deformations due to port temperature + VV and GS expansions (Z axis)

The largest displacement in the axial direction occurs at the cryopump pipes, with a deformation equal to 8.552mm.
Fig. 5.9 shows a detail of the region inside the boundary box where this displacement occurs.

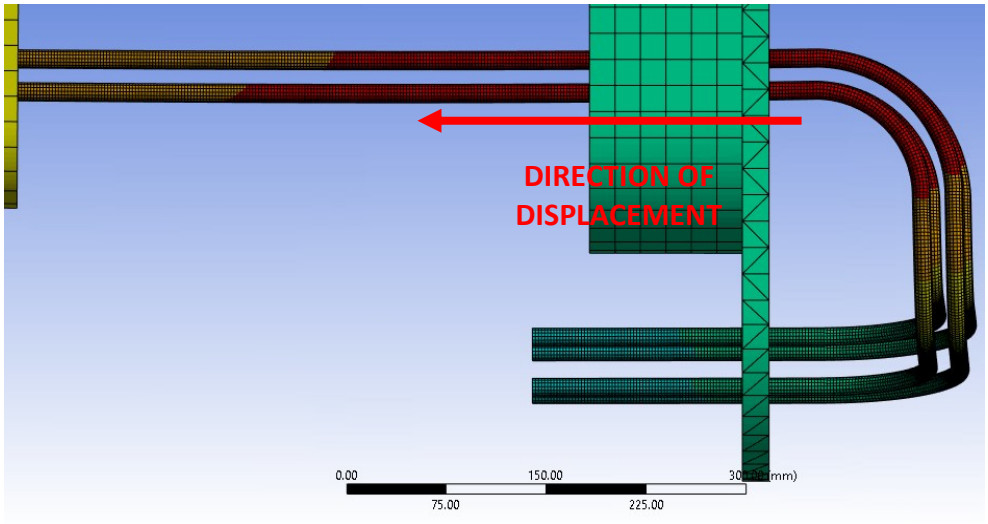

Figure 5.36. Deformation of the cryopump pipes during POS

This deformation is due to the cryogenic temperature of the helium flowing inside the pipes.
As seen, their shape is studied so that they can deform with a certain freedom, avoiding

the need to install a bellow. The FEM analysis confirms this behaviour. In the next pages, a brief mention to the mechanical resistance of the pipes will be presented.

RESULTS: DISPLACEMENTS DUE TO PORT COMPONENTS TEMPERATURE + VACUUM VESSEL AND GRAVITY SUPPORT DISPLACEMENTS + EARTHQUAKE

The last component to add to the results is the displacement due to seismic event. The values presented in *paragraph 4.3*, and recalled here in *Table 5.1*, of the seismic loads are intended as ranges of values: this means that, for example, the maximum poloidal displacement due to earthquake will be +9.8mm (toward the external region of the machine) and -9.8mm (towards the central axis of the torus).

1: Axial (±) [mm]	2: Poloidal (±) [mm]	3: Toroidal (±) [mm]
0.5	9.8	10.3

Table 5.4. Displacements between VV and cryostat due to seismic event

Anyway, only the values acting in the same direction of the other components are considered.

Total deformation:

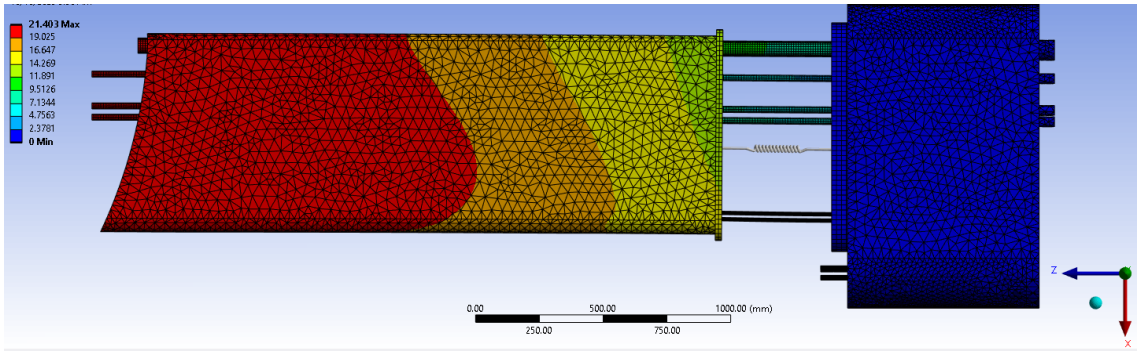

Figure 5.37. Total deformation during POS in case of earthquake

Largest displacement occurs at the top of port surface (21.403mm).

Displacements along X axis (POLOIDAL DIRECTION):

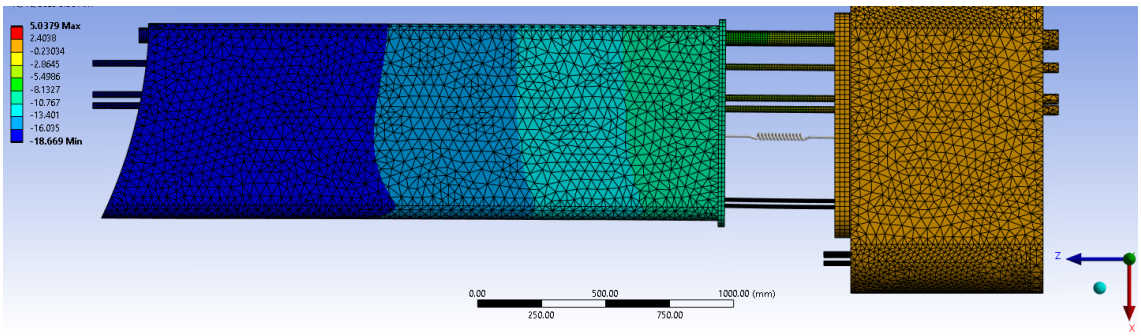

Figure 5.13. Displacements during POS in case of earthquake along X axis

Largest displacement occurs at the port surface (-18.669mm).

Displacements along Y axis (TOROIDAL DIRECTION):

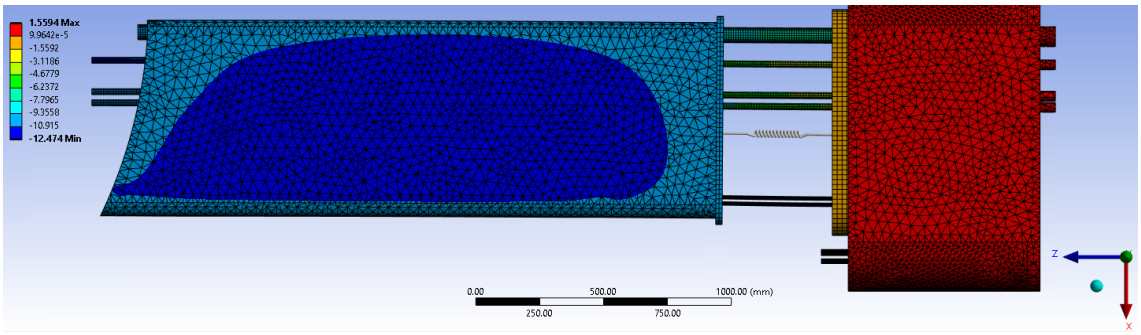

Figure 5.15. Displacements during POS in case of earthquake along Y axis

Largest displacement occurs at port surface (-12.474mm) and at feeder #2 (11.256mm).

Displacements along Z axis (AXIAL DIRECTION):

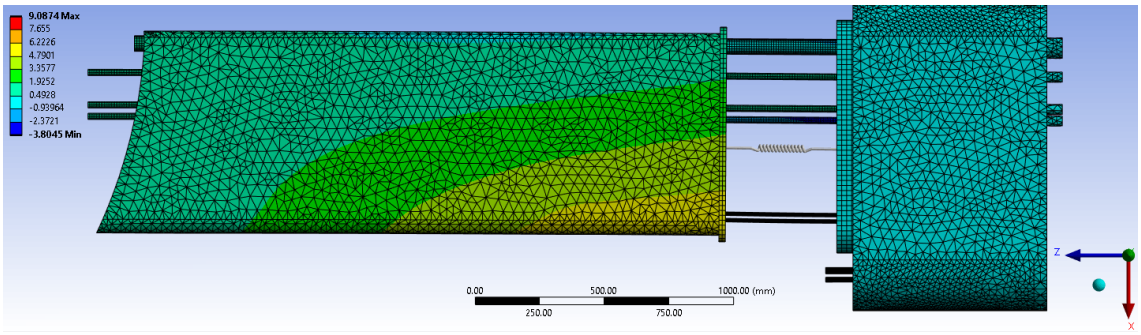

Figure 5.16. Displacements during POS in case of earthquake along Z axis

Largest displacement occurs at cryopump pipes 9.087mm.

Earthquakes have little impact on the axial direction (±0.5mm), but the same cannot be said for the other directions:
-displacements along the toroidal direction are small in the normal operation but can be important during a seismic event;
-displacements along the poloidal direction, which are already important during the normal operation, are accentuated even more.

5.2 Light Baking (L-BAK) - RESULTS

Light baking is an “intermediate” load case between the normal operation and the strong baking/cryopump regeneration.
Indeed, the results of this scenario aren’t that much interesting for the purposes of this work, but they will still be presented, even if in a summarized form.

RESULTS: DISPLACEMENTS DUE TO PORT COMPONENTS TEMPERATURE + VACUUM VESSEL AND GRAVITY SUPPORT DISPLACEMENTS

During light baking, as shown in the previous chapter, all the input temperature are higher in respect to those in the POS case.
For this reason, larger displacements are generally expected during L-Bak than during POS.

Total deformation:

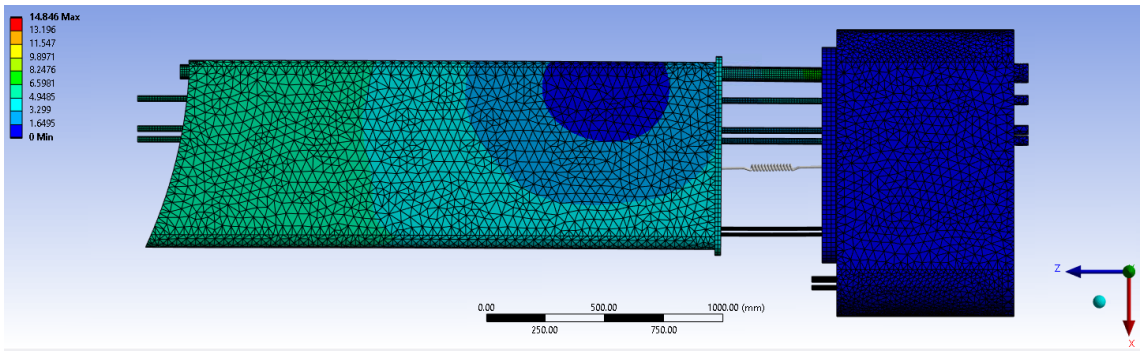

Figure 5.18. Total deformation during Light Baking

In fact, the largest displacement (14.846mm) is higher than in the POS case (8.8761mm).

The largest displacement in the poloidal direction (X) occurs at the extremity (cryostat side) of the water pipe (14.142mm).

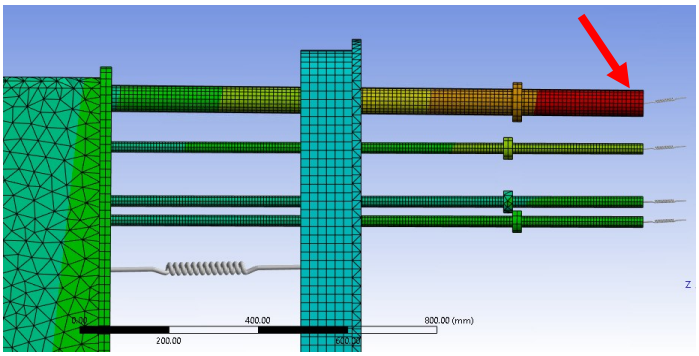

Figure 5.19. Largest poloidal displacement – detail

Toroidal displacements are still lower than 2mm for all the components, while the axial displacements are actually smaller than in the case of POS (*Fig.5.8*).

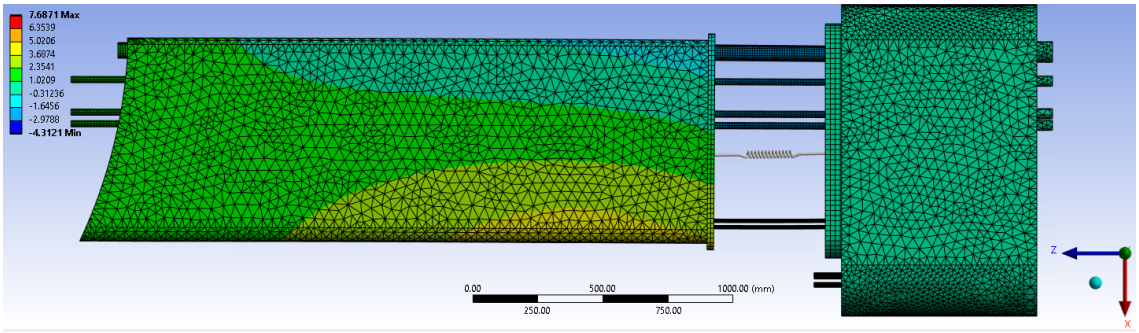

Figure 5.20. Displacements during L-Bak along axial direction

This happens because, in the POS scenario, the average port duct temperature is pretty low (8.90°C) compared to the L-Bak scenario (76.6°), while the difference between the GS temperature in the two scenarios is smaller (40°C vs 65°C).
Let's remember that the port displacements due to its temperature and due to the GS expansion have opposite directions; during POS the gravity support expansion plays a major role, while during L-Bak the two effects counterbalance each other more.
In any case, the largest displacement occurs at the cryopump pipes (7.687mm).

RESULTS: DISPLACEMENTS DUE TO PORT COMPONENTS TEMPERATURE + VACUUM VESSEL AND GRAVITY SUPPORT DISPLACEMENTS + EARTHQUAKE

Even in the case of an earthquake, during light baking the largest displacement occurs at the bottom of the water pipe.

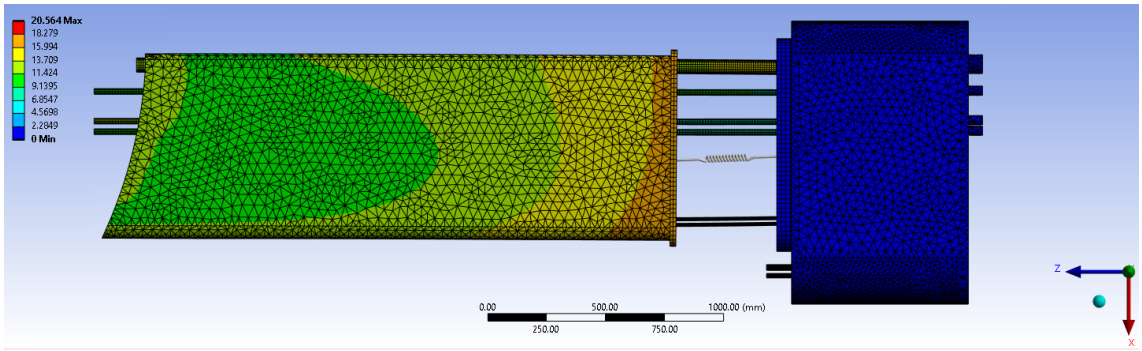

Figure 5.21. Total displacement during L-Bak in case of seismic event

Another component suffering an important displacement is feeder #5, reaching a deformation of -16.273mm along X.
Feeder #2 is particularly solicited on the toroidal direction (11.684mm) while the cryopump pipes are still the most solicited on the axial direction (8.212mm).

5.3 Strong Baking (S-BAK) - RESULTS

During strong baking VV is heated up to 200°C: the port temperature is higher than in the previous cases, and so are the fluid temperatures (IVC fluids, FW water).
In this scenario, the thermal displacements are expected to be larger than in POS or L-Bak.

RESULTS: DISPLACEMENTS DUE TO PORT AND COMPONENTS TEMPERATURE

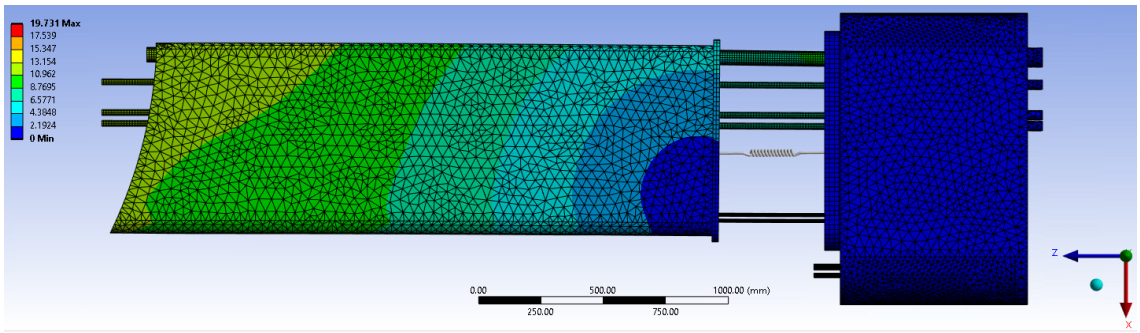

Figure 5.22. Displacement due to their temperature during S-Bak

If *Fig.5.22* is compared with *Fig. 5.1*, it is immediately evident the effect of the higher temperature during strong baking: the largest displacement (occurring at the water pipe) is almost double than in the normal operation.
Fig.5.23 shows the displacements due to port and components temperature along z axis: in respect to *Fig. 5.4*, here it is more evident the movement of the port flange toward the cryostat, compressing the port bellow, in particular in the light blue region.

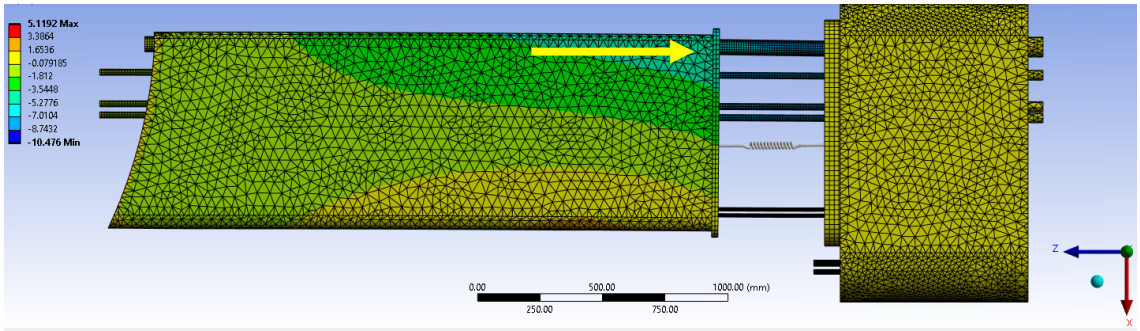

Figure 5.23. Displacement due to temperature during S-Bak along Z axis

RESULTS: DISPLACEMENTS DUE TO PORT COMPONENTS TEMPERATURE + VACUUM VESSEL AND GRAVITY SUPPORT DISPLACEMENTS

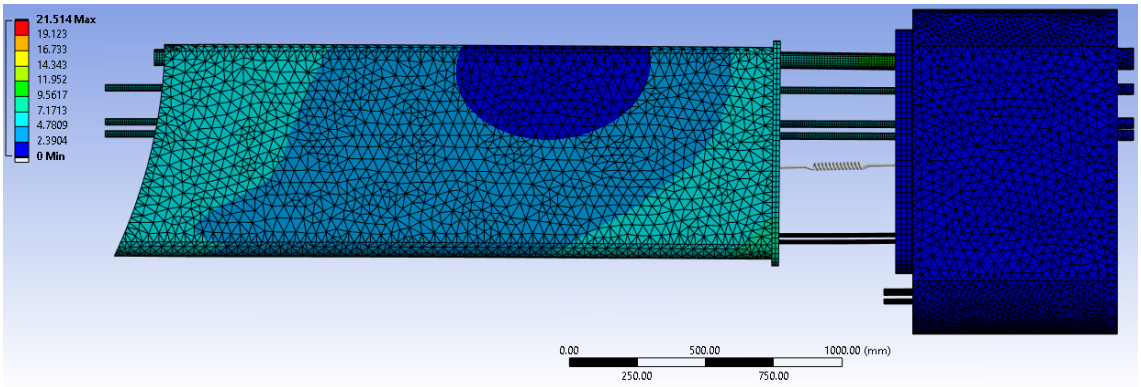

Figure 5.24. Total displacements during S-Bak

The largest directional displacements are respectively:
-Poloidal→ water pipe (20.379mm)
-Toroidal → port surface (-2.106mm)
-Axial → cryopump pipes (8.788mm)

RESULTS: DISPLACEMENTS DUE TO PORT COMPONENTS TEMPERATURE + VACUUM VESSEL AND GRAVITY SUPPORT DISPLACEMENTS + EARTHQUAKE

Similarly to the case of L-Bak, the largest displacement along the poloidal direction occurs at the water tube (25.632mm); another component suffering an important displacement along this direction is feeder #6 (-15.591mm).

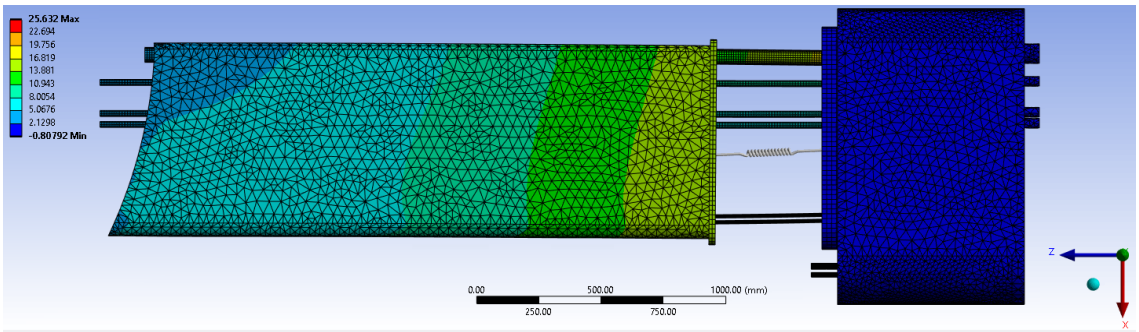

Figure 5.25. Displacements during S-Bak in case of seismic event (X axis)

In the toroidal direction the largest displacement occurs at the port surface (-12.177mm).
In the axial direction the largest displacement occurs at the cryopump pipes (9.3013mm); feeder #3 suffers an important displacement too (-7.3635mm).

5.4 Cryopump Regeneration - RESULTS

Out of all the 4 cases studied, cryopump regeneration is the most severe scenario, given the high temperature of the components.
It is actually similar to the strong baking scenario: the only difference, as seen in Chapter 4, is the first wall water temperature, equal to 240°C instead of 200°C.
Indeed, results similar to that case are expected.

RESULTS: DISPLACEMENTS DUE TO PORT COMPONENTS TEMPERATURE + VACUUM VESSEL AND GRAVITY SUPPORT DISPLACEMENTS

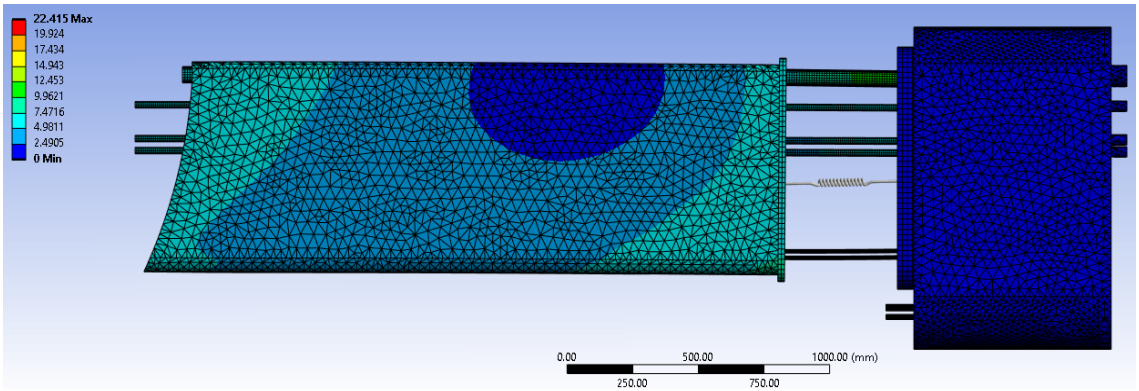

Figure 5.26. Total displacements during Cryopump regeneration

The largest directional displacements are respectively:
-Poloidal→ water pipe (20.472mm)
-Toroidal → port surface (-1.822mm)
-Axial → water pipe (8.790mm) / cryopump pipes (-8.764mm)

RESULTS: DISPLACEMENTS DUE TO PORT COMPONENTS TEMPERATURE + VACUUM VESSEL AND GRAVITY SUPPORT DISPLACEMENTS + EARTHQUAKE

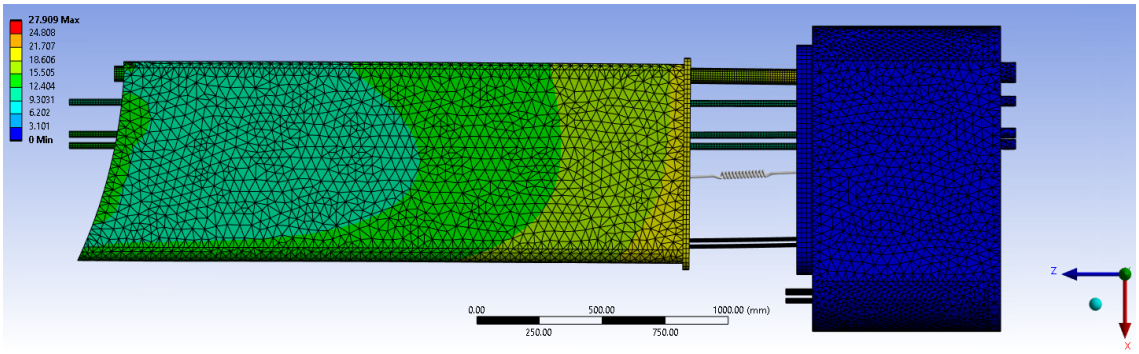

Figure 5.27. Total displacements during cryopump regeneration in case of seismic event

The largest directional displacements are respectively:
-Poloidal→ water pipe (25.824mm) / feeder #6 (-15.596mm)
-Toroidal → port surface (-12.122mm)
-Axial → water pipe (-9.326mm) / cryopump pipes (9.302mm)
Except for the toroidal one (the maximum displacement during S-Bak is equal to -12.177mm), these are the largest displacements registered.

5.5 Bellows results

As seen, bellows are modelled as 3D springs with different stiffness on the three directions.
There are 8 springs in total: 1 port bellow, 6 feeder bellows, 1 water pipe bellow.
Table 5.2 summerizes the main characteristics of the selected bellows:

	Feeders bellow	Water pipe bellow	Port bellow
Nominal diameter (mm)	65	125	-
Axial stiffness (N/mm)	28	18	508
Poloidal stiffness (N/mm)	1.5	1.9	666
Toroidal stiffness (N/mm)	1.5	1.9	233
Maximum deformation (mm)	± 41.5	± 72	TBC

Table 5.2.Main characteristics of selected bellows

Let's see how they behave in the standard scenario (Normal state) and in the most severe scenario (Cryopump Regeneration).

NORMAL OPERATION
During normal operation (plasma), port bellow suffers the following deformations:
POLOIDAL X: 1.440 mm
TOROIDAL Y: -0.166 mm
LONGITUDINAL Z: 3.718 mm

The feeder bellow suffering the largest displacements is number 5:

POLOIDAL X: 6.048 mm
TOROIDAL Y: -0.355 mm
LONGITUDINAL Z: -4.326 mm
These values are much lower than the maximum deformation allowed by the chosen spring (41.5mm) → OK

Water pipe bellow suffers the following deformations:
POLOIDAL X: 5.435 mm
TOROIDAL Y: -0.188 mm
LONGITUDINAL Z: -2.301 mm
These values are much lower than the maximum deformation allowed by the chosen spring (72mm) → OK

CRYOPUMP REGENERATION
During cryopump regeneration, port bellow suffers the following deformations:
POLOIDAL X: 6.586 mm
TOROIDAL Y: -0.135 mm
LONGITUDINAL Z: 1.573 mm

The feeder bellow suffering the largest displacements is, again, number 5 (but is close to feeder 6):

POLOIDAL X: 8.230 mm
TOROIDAL Y: -0.094 mm
LONGITUDINAL Z: -7.085 mm
These values are much lower than the maximum deformation allowed by the chosen spring (41.5mm) → OK

Water pipe bellow suffers the following deformations:
POLOIDAL X: 20.464 mm
TOROIDAL Y: -0.828 mm
LONGITUDINAL Z: -8.725 mm
These values are much lower than the maximum deformation allowed by the chosen spring (72mm) → OK

5.6 Liquid Ingress Scenario

In the previous results, the scenario described in *Chapter 4* related to the possible ingress of liquid (water/helium) inside the VV has not been considered.

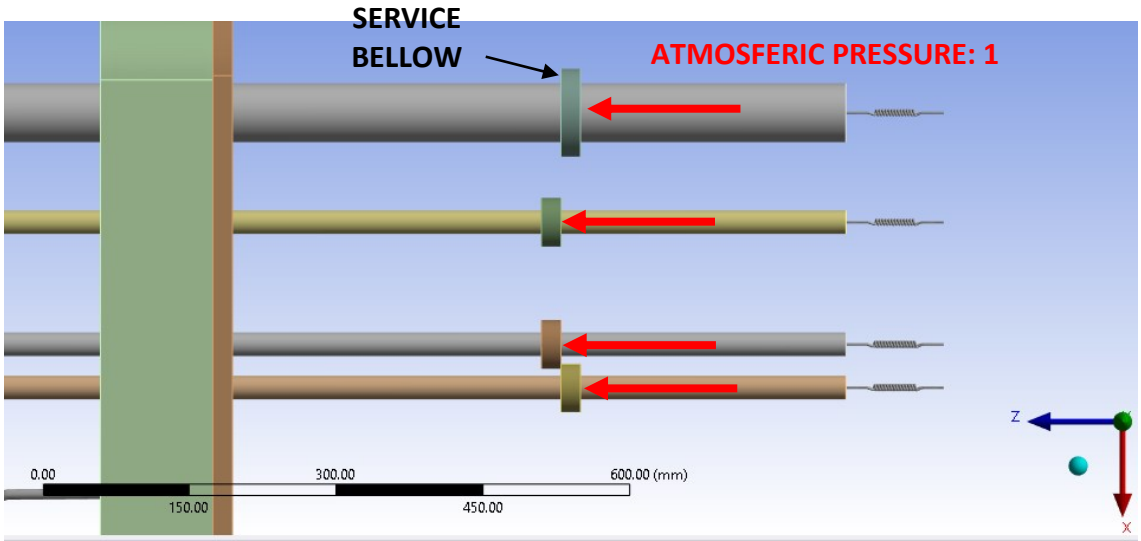

Figure 5.28. Pressure effecting service bellows in standard operation

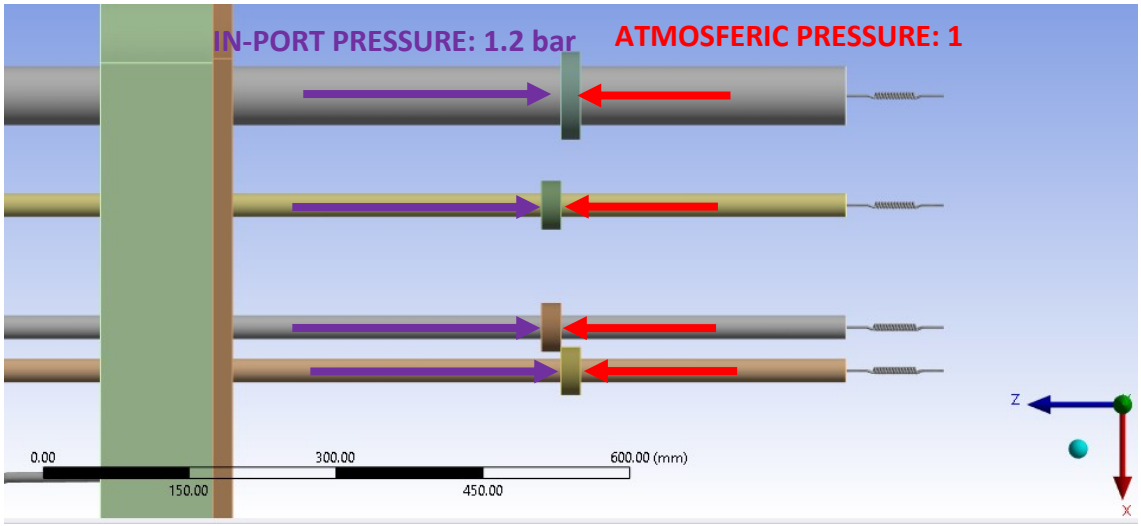

Figure 5.29. Pressure effecting service bellows in case of liquid ingress

Analysis has shown that this contribution is negligible for the purpose of this work. For example, in the case of the water pipe during cryopump regeneration, the difference between the spring axial displacements is just equal to -0.02554mm when the pressure inside the port is 1.2 bar and when there is vacuum. This means a difference equal to 0.36% in respect to the original axial displacement during cryopump regeneration (-7.111mm).

5.7 Cryopump Pipes

In all the different operating conditions, the largest displacement along the axial direction (Z direction) occurs at the pipes feeding helium to the cryopump.
As seen, their shape is studied so that they can deform with a certain freedom, avoiding the need to install a bellows also for these components.
Being made in Stainless Steel AISI 316L, anyway, their elasticity isn't very large. So, it is important to evaluate the stresses generated on the pipes to verify if they can bear such elongation.

The largest stress occurs with the largest displacement: that's the case of Cryopump regeneration + seismic event, when the displacement is equal to 9.302mm.
In this case, the maximum value of Von-Mises stress is equal to 292.21 MPa.

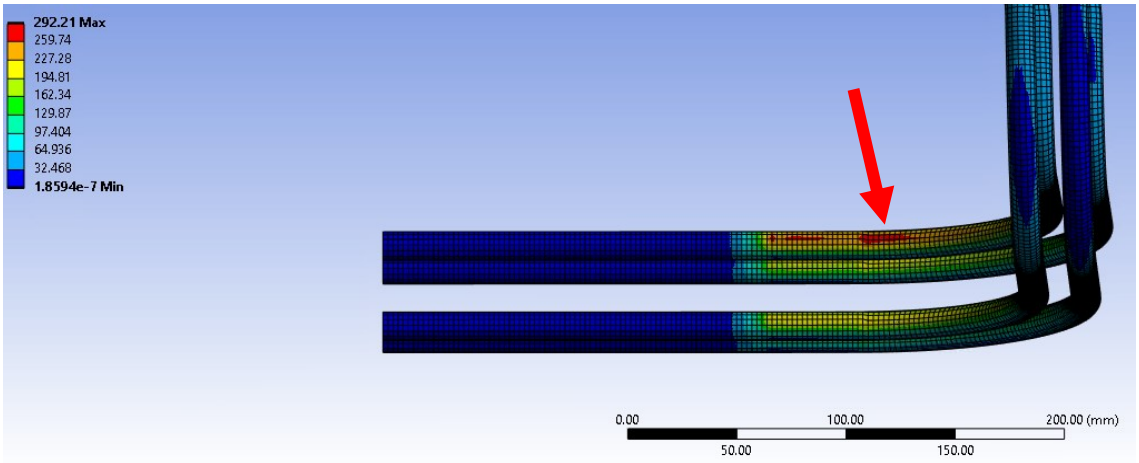

Figure 5.30. Stresses on cryopump pipes during Cryopump regeneration in case of earthquake

During cryopump regeneration without earthquake, the maximum stress is equal to 255.82MPa.

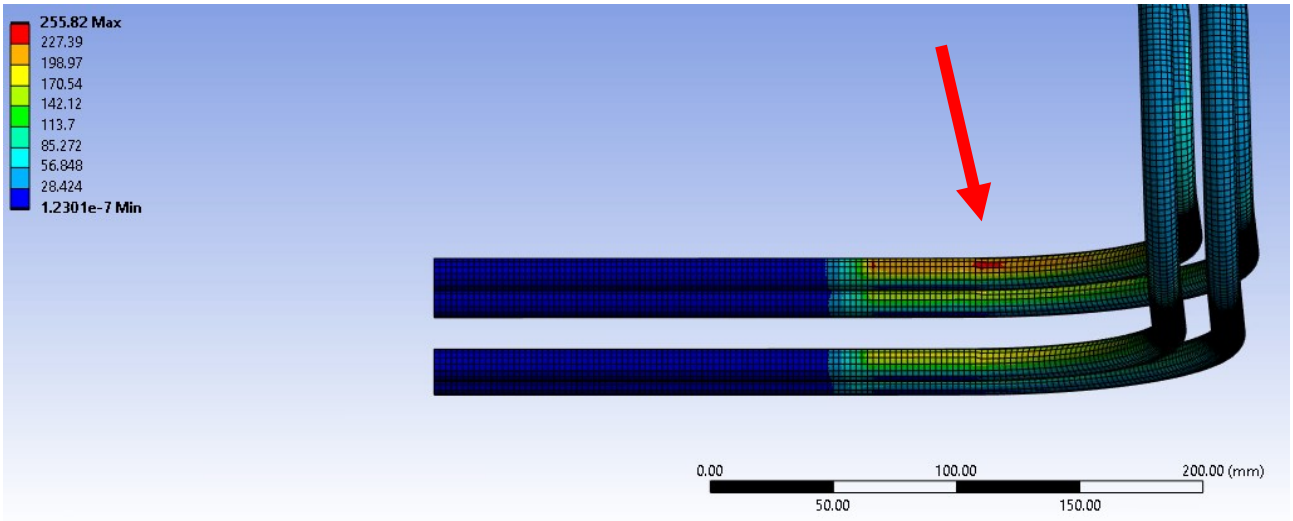

Figure 5.31. Stresses on cryopump pipes during Cryopump regeneration

Let's recall the graph shown in *Fig. 4.10* relative to the yield tensile strength S_y of stainless steel AISI316L.

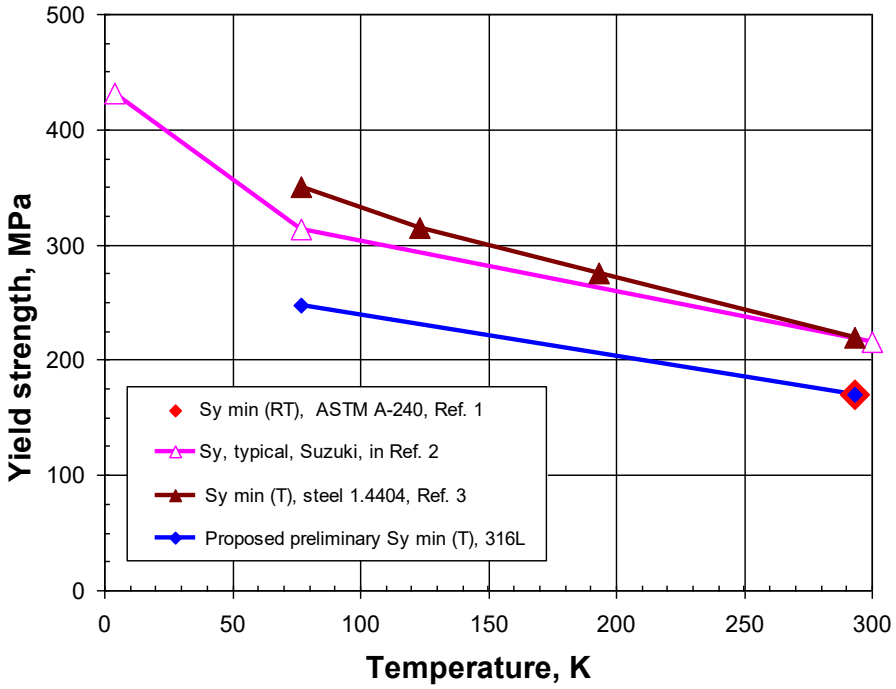

Figure 5.32. AISI316L Yield tensile strenght VS Temperature

During cryopump regeneration, Helium is fed to the cryopump at 100K, and so the pipes temperature is 100K.
At this temperature, the proposed preliminary S_y min (*Source: ITER Material Book*) is:

$$S_{y\ min} = 247\ MPa \tag{5.1}$$

The FEM analysis has shown that the stresses generated on the cryopump pipes are higher than this value.

$$S_{max} > S_{y\ min} \tag{5.2}$$

The preliminary check is, indeed, not passed.
However, we are confident that is possible to evaluate and design a new path for the tubes in order to satisfy the structural integrity of these components.
More detailed analysis will be carried out on this topic in the future.

5.8 Feeders' configuration

The actual configuration of the feeders' position inside the port and the design of the cryostat flanges must be modified.
This is due to the presence of the bellows which are bulky.
In the actual configuration, feeders are "coupled" by the supports and the minimum distance between them is 21mm.
This distance is not compatible with the installation of 65mm nominal diameter bellows.
Considering the corrugation of the bellows, they have an external diameter of 107mm.

This means that the minimum distance between the feeders must be at least equal to 107mm, but possibly a little higher than that, to simplify their installation and management.

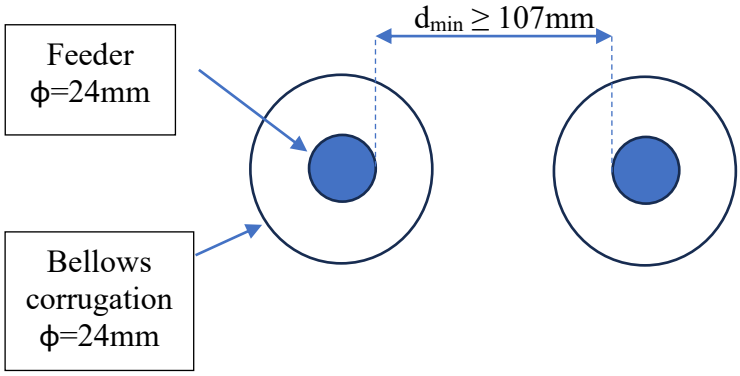

Chapter 6

Conclusions

In this thesis, activities for the design and the analysis of the present configuration of cryogenic, electrical and cooling penetration for the DTT vacuum vessel has been carried out.

Lots of researchers are working daily on DTT project to evaluate the best configuration achievable, to specify design and manufacturing requirements, and to follow up the ongoing procurements with the Industry, so that this experiment will be able to give DEMO the most reliable results as possible.
Within this framework, starting from a geometric model, a work of collecting and cross-referencing data was necessary to obtain the latest and most updated configuration and data to be used in the developed model for the design and analysis of the services penetrating through the lower vertical port (identified as #5). It is not excluded that, in future, some other changes will be made in this data, implying that the model should be re-verified.

The proposed configuration for port five includes:
-Custom bellows for port duct → the particular shape of the duct requires custom. bellows to be used to compensate for the displacements occurring during the operation;
-Commercial bellows for services → based on the services dimensions and expected displacements, two commercial bellows have been preliminary identified: 125mm nominal diameter bellow for the water tube, 65mm nominal diameter for the feeders.
-Expansion loop for cryogenic tubes → the u-shaped cryopump pipes are designed so that they can be deformed without the need for bellows.

The analysis highlighted some interesting results.
The most solicited components are:
-the water pipe, in particular in the poloidal direction, reaching a maximum displacement on this direction equal to 25.8mm during cryopump regeneration in case of seismic event;
-the cryopump pipes, in particular in the axial direction, reaching a maximum displacement on this direction equal to 9.3mm during cryopump regeneration in case of seismic event, and a generated yield stress equal to 292MPa, which is larger than the proposes minimum yield for stainless steel AISI 316L (247 MPa) at the tube operation temperature of 100K.

Out of the two possible cases of accident identified in *Paragraph 4.2*, seismic event is largely the worse scenario. While the liquid ingress inside the VV leads to negligible differences at the bellows (ex. Water pipe bellows compresses only by 0.36% during cryopump regeneration in case of liquid ingress), seismic event analysis has shown large differences in the components' displacements. For example, during normal operation (POS), a seismic event leads to a maximum displacement more than doubled

in respect to the same scenario without earthquake.
The preliminary choice of the service bellows has shown a good compatibility with the FEM results.

All this results, and all the other results collected from this analysis, will be used to better understand the behaviour of port #5 in different load cases, and they can be used for future studies.

6.1 What's next?

The results in *Chapter 5* have highlighted some issues in the actual design of port #5. In the next future, starting from these results, some changes can be brought to the components' design, in order to satisfy the identified requirements.

First of all, there is the need to change the geometry of the cryostat flanges where the service bellows will be installed.
Knowing the external diameter of the bellows to be installed depending on the calculated movements, it is possible to update the design of the cryostat flanges.
In second place, minor changes to the cryopump pipes path are necessary. With the actual configuration, stresses on the material are too high, and so a review of this expansion loops is required. This change is not considered critical given the large available envelop to draw the new path.
It is also possible to start with an evaluation study regarding the feasibility of the construction of custom bellows, given the specific requirements obtained with this thesis: 1.0 bar as maximum pressure difference applied from the external side, 2000 cycles, maximum compensation movements as calculated in Section 5.

Then, some other work can be held in parallel.
For example, there are other possible cases of accident during the operation that should be evaluated. One of this is the case of plasma disruption.
Plasma disruption occurs when an instability grows in the plasma to the point where there is a rapid loss of the stored thermal and magnetic energy. This rapid loss can also accelerate electrons to very high energy (so-called "runaways"). The disruption mitigation system has to protect the plasma-facing components against the heat and forces that arise during the disruption, and at the same time it must tame the runaway electrons that—if generated—could lead to melting of the first wall and leaks in the water-cooling circuits. As a consequence of these events, the loss of coolant accident has also been analysed.
Another possible accident to be evaluated is the case of vertical displacement event. Vertical displacement events are major disruption events that occur in elongated tokamaks when vertical stability control is lost due to a failure of the control system or other off-normal occurrences. These events cause large currents to flow in the vessel and other adjacent metallic structures and they produce large loads with relative displacements, in particular among the vacuum vessel, the penetration services, and the cryostat ports.
Another work that can be held is a comparison between the results obtained in this thesis, related to port #5, to those relative to port #3.

Port#3 develops on the equatorial plane of the machine. It can be interesting to notice the different behaviour of port #5 and port #3 with the same operating regime.
The analysis on port#3 is under development and has been carried out in parallel with this work: all the assumptions, data, and logical process coincide to those presented in the previous chapter, and so the results can be compared coherently without discrepancies in the working method.

Bibliography

1. E. Acampora, R. Albanese, R. Ambrosino, A. Castaldo, P. Innocente, V. P. Loschiavo, *Conceptual design of in-vessel divertor coils in DTT*, Fusion Engineering and Design, Volume 193, 2023

2. I. Sekachev, M. Meekins, C. Sborchia, G. Vitupier, H. Xie, C. Zhou, *The Cryostat and Subsystems Development at ITER*, Physics Procedia, Volume 67, 2015

3. Magaud, Philippe et al. "*Nuclear Fusion Reactors.*" (2004).

4. R. Albanese et al 2017, *DTT: a divertor tokamak test facility for the study of the power exhaust issues in view of DEMO*, Nucl. Fusion 57 016010

5. L.A. Artsimovich, *Tokamak devices*, 1972 Nucl. Fusion 12 215

6. A. Fasoli, *EUROfusion, un paradigma unico di integrazione europea per realizzare il sogno della fusione*, Enea Magazine, EAI 2019-006

7. Hokyu Moon et al., *Evaluation of the functional acceptability of the ITER vacuum vessel*, 2023 Nucl. Fusion 63 016003

8. Jeffrey Freidberg, *Plasma Physics and Fusion Energy*, Cambridge University Press, 2007

9. M.N. Wilson*, Superconducting magnets,* Clarendon Press, 1987

10. https://www.iter.org/

11. https://www.energy.gov/

12. https://it.wikipedia.org/wiki/

13. https://euro-fusion.org/

14. *World Energy Outlook 2022*, International Energy Agency

15. J. Wesson, D. J. Campbell, *Tokamaks, Fourth Edition*, Oxford Science Publications

16. G. Barone, M. Dalla Palma, *Assessment of baking operating state for vacuum vessel & ports*, Deliverable DIV-IDTT.S.11-T002-D003, ENEA

17. R. Martone, R. Albanese, F. Crisanti, P. Martin, A Pizzuto, *Divertor Tokamak Test facility Interim Design Report*, ENEA, 2019

18. S. Holger, *Preliminary detailed design of the DTT divertor pumping system,* Deliverable DIV-IDTT.S.03-T004-D001, EUROfusion

19. R. Ambrosino, "*DTT - divertor tokamak test facility: A testbed for DEMO*," Fusion Engineering and Design, vol. 167, p. 112330, 2021

20. G. Di Gironimo et al., *The DTT device: Advances in conceptual design of vacuum vessel and cryostat structures,* Fusion Engineering and Design 146 (2019)

21. G. Di Gironimo et al., *The DTT device: First Wall, vessel and cryostat structure,* Fusion Engineering and Design 122 (2017)